THE
PHYSICAL REVIEW

A journal of experimental and theoretical physics established by E. L. Nichols in 1893

SECOND SERIES, VOL. 66, NOS. 9 AND 10 NOVEMBER 1 AND 15, 1944

The Absorption of Gamma-Radiation in Copper and Lead

J. M. CORK AND R. W. PIDD
University of Michigan, Ann Arbor, Michigan

(Received September 2, 1944)

The absorption coefficients for the gamma-rays emitted by certain activated elements have been accurately measured in copper and lead. The energies of the gamma-rays used, have all been determined by use of the beta-ray spectrometer. These gamma-rays are as follows: 1.14 Mev from zinc 65, 1.30 Mev from cobalt 60, and 1.38–2.85 Mev from sodium 24. The absorption coefficients for zinc and cobalt are in close agreement with the calculated values of Heitler. For the high energy component of the sodium radiation, values of 0.285 cm^{-1} and 0.405 cm^{-1} were obtained for the absorption coefficients in copper and lead, respectively. These values are more than ten percent less than the Heitler values. Since absorption in copper at this energy is due almost entirely to Compton scattering it is indicated that the Klein-Nishina formula is not completely valid.

THE absorption of gamma-radiation in matter has been the subject of many investigations. On passage through matter, the over-all absorption may be attributed to the combination of three effects, namely, the Compton effect, the photoelectric effect, and the production of electron pairs.

The absorption due to Compton scattering has been formulated[1] by Klein and Nishina. Experimental observations,[2] usually by counting ejected positrons in a Wilson chamber, have substantiated the theoretical calculations[3] for pair production. The contribution of the photoelectric effect to the absorption coefficient has been variously estimated.[4] The combination of these effects to obtain the total absorption coefficient has been fully discussed[5] by Heitler. The values as proposed by him in the energy range 1 Mev to 5 Mev for copper and lead are collected in Table I. These same values are shown graphically for lead in Fig. 1, and for copper in Fig. 2.

The contribution due to the photoelectric effect in this energy range is vanishingly small in copper, and rather small in lead. The photoelectric values for lead, proposed by Heitler, are admittedly interpolations. They were adjusted so that the over-all effect was in agreement with what was regarded as the most reliable experimental data available, namely, that of Gray.[6]

[1] O. Klein and Y. Nishina, Zeits. f. Physik **52**, 853 (1928).
[2] I. Curie and F. Joliot, Comptes rendus **196**, 1581 (1933); J. Chadwick, P. Blackett, and G. Occhialini, Proc. Roy. Soc. **144**, 235 (1934); and S. de Benedetti, Comptes rendus **200**, 1389 (1935).
[3] P. Dirac, Proc. Camb. Phil. Soc. **30**, 150 (1934); W. Heisenberg, Zeits. f. Physik **90**, 209 (1934); W. Furry and J. R. Oppenheimer, Phys. Rev. **45**, 245 (1934); and H. Bethe and W. Heitler, Proc. Roy. Soc. **146**, 83 (1934).
[4] F. Sauter, Ann. d. Physik **11**, 454 (1931); H. Hall, Phys. Rev. **45**, 620 (1934); H. R. Hulme, J. McDougall, R. A. Buckingham, and R. H. Fowler, Proc. Roy. Soc. **149**, 131 (1935); and J. G. Jaeger and H. Hulme, Proc. Roy. Soc. **148**, 708 (1935).
[5] W. Heitler, *The Quantum Theory of Radiation* (Clarendon Press, Oxford, 1936).
[6] L. H. Gray, Proc. Camb. Phil. Soc. **27**, 103 (1931).

TABLE I. Absorption in cm^{-1} due to photoelectric effect, Compton scattering, and pair production.

Energy in Mev	1		1.5		2.5		5	
	Cu	Pb	Cu	Pb	Cu	Pb	Cu	Pb
Photoelectric effect	0.0067	0.205	0.0032	0.100	0.0015	0.047	0.0006	0.018
Compton scattering	0.503	0.555	0.412	0.455	0.308	0.340	0.199	0.220
Pair production	—	—	0.0035	0.0109	0.025	0.076	0.079	0.247
Total	0.510	0.760	0.419	0.566	0.335	0.463	0.279	0.485

The Heitler values have been subjected to experimental verification by several investigations making use of x-rays[7] and by experiments using gamma-ray sources of radium and thorium.[8] None of these sources is monochromatic and the uncertainty in the composition of the radiation introduces a possible source of error. The gamma-radiation from radium[9] is far from monochromatic, possessing several discrete energies in the range from 1.1 Mev up to 2.42 Mev. Thorium (C+C″) has often been regarded as a monochromatic source of radiation of energy 2.65 Mev, but it is now known[10] that there is also present a component of as much as 15 percent, at an energy about 1.68 Mev.

The beta-ray spectrometer has now been used to measure the energies of several gamma-rays emitted by various induced radioactive sources. This makes it possible to check absorption coefficients with greater certainty as to the energy being investigated. In this investigation the following gamma-rays are employed: 1.14 Mev from[11] zinc (65), 1.30 Mev from[12] cobalt (60), and 1.38–2.85 Mev from[13] sodium (24). The energy 2.85 Mev for the high energy component of sodium is the average of the two most recently reported values.

[7] A. Petrauskas, L. C. VanAtta, and F. E. Myers, Phys. Rev. **63**, 389 (1943).

[8] L. Meitner and H. Hupfield, Zeits. f. Physik **67**, 147 (1931); C. Y. Chao, Proc. Nat. Acad. **16**, 431 (1930); W. Gentner and J. Starkiewicz, J. de phys. et rad. **6**, 340 (1935); W. Gentner, J. de phys. et rad. **6**, 274 (1935).

[9] A. I. Alichanow and G. R. Latychev, J. Phys. U.S.S.R. **3**, 263 (1940).

[10] A. Alichanow and V. Dzelepov, Comptes rendus Acad. Sci. U.S.S.R. **20**, 163 (1938); G. C. Curran, P. I. Dee, and J. E. Strothers, Proc. Roy. Soc. **A174**, 546 (1940).

[11] C. E. Mandeville, Phys. Rev. **64**, 265 (1943).

[12] C. E. Mandeville and H. W. Fulbright, Phys. Rev. **64**, 265 (1943); M. Deutsch and L. G. Elliott, Phys. Rev. **62**, 558 (1942).

[13] C. E. Mandeville, Phys. Rev. **62**, 309 (1942); **63**, 387 (1943); L. G. Elliott, M. Deutsch, and A. Roberts, Phys. Rev. **63**, 386 (1943).

EXPERIMENTAL

The value obtained for the absorption coefficient to some extent depends upon the geometry employed. In the Klein-Nishina formula the reacting photons are considered lost. Actually they are scattered with a well-known distribution and some of these scattered photons of lower energy are received by the detector. To minimize the solid angle subtended by the detector, and hence any disturbing effect due to Compton scattering, the pressure ionization chamber is kept small in size and is placed as far from the absorber as is practicable.

The experimental arrangement used is shown in Fig. 3. The source is placed in a hole 1 cm in

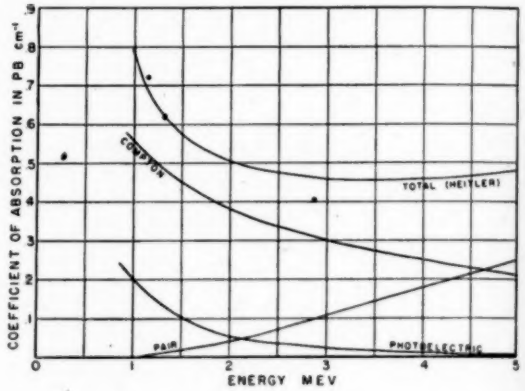

FIG. 1. The absorption of gamma-radiation in lead.

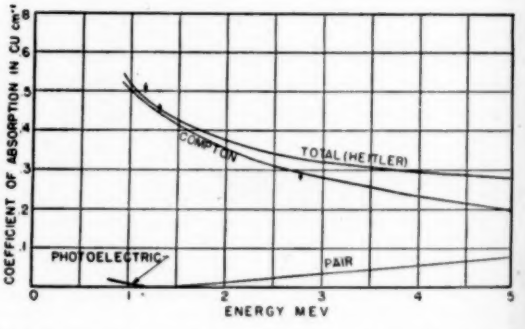

FIG. 2. The absorption of gamma-radiation in copper.

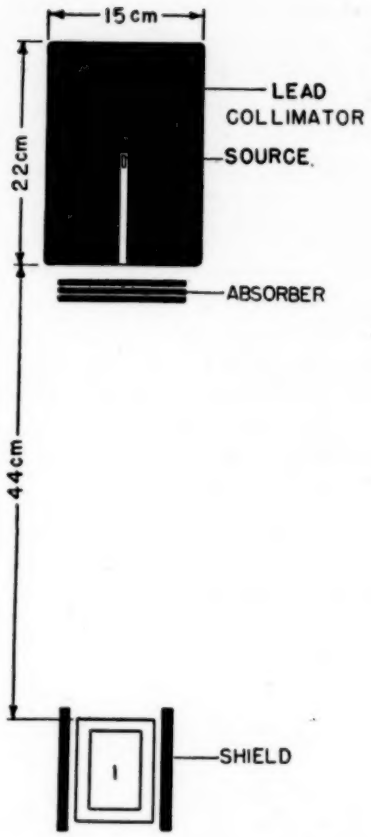

FIG. 3. Arrangement of apparatus to measure absorption coefficient.

diameter and 15 cm deep symmetrically situated in a solid cylindrical lead block. The absorbers are placed in position as shown so that adding them in turn the final plate is at a distance of 44 cm from the top of the ionization chamber.

The intensity of the sources, made in the cyclotron, was such that readings could be made in a reasonably short time although the radiation traversed several centimeters of lead. Sodium (24) could easily be made of strength equivalent to several grams of radium and the absorption was followed through 12 cm of lead. The absorption coefficient was measured by using increasingly thick absorbers and noting the activity in the pressure ionization chamber connected to a string electrometer. A background reading was obtained with an absorber of 25 cm of lead. Under this condition the background reading was practically the same whether the source was present or not, indicating a negligible scattering from the walls and neighboring bodies.

Some small part of the radiation received by the ionization chamber will be Compton scattered photons. On using successive thicknesses of lead, however, an equilibrium ratio will be reached between scattered and unscattered photons in the forward direction. This should then introduce no error in the finally observed absorption coefficient.

RESULTS

The results obtained for the absorption coefficients of zinc and cobalt radiations are within experimental error what would have been predicted by theory. These values are 0.72 cm^{-1} and 0.64 cm^{-1} in lead and 0.51 cm^{-1} and 0.46 cm^{-1} in copper, for zinc and cobalt radiations, respectively. Sodium gamma-radiation has been shown to consist of two components of energy 1.38 Mev and 2.85 Mev. Moreover, coincidence measurements indicate that for each photon of energy 1.38 Mev there is one photon of energy 2.85 Mev. The result obtained by plotting the intensity of the transmitted radiation as a function of the thickness of the lead absorber is shown in Fig. 4. The intensity is plotted logarithmically and had there been a single monoenergy gamma-ray, the values would lie along a straight line. It is ap-

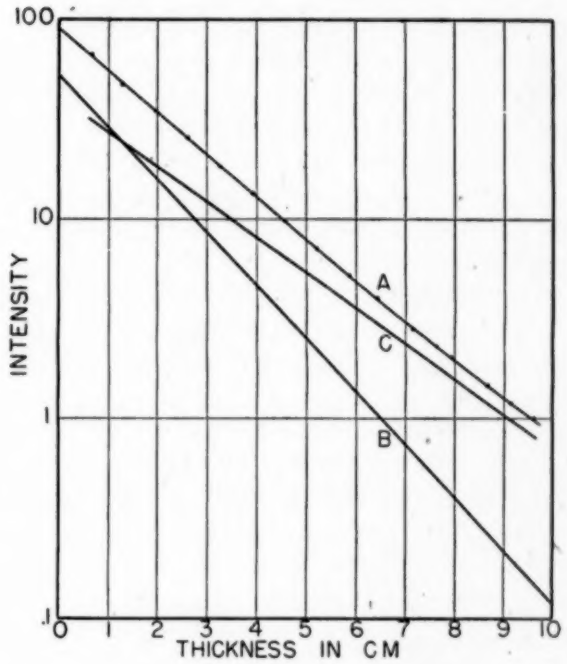

FIG. 4. Resolution of the absorption of gamma-radiation from sodium (24).

parent that the slope changes as the thickness increases. To find the absorption coefficient of the 2.85-Mev radiation it is necessary to subtract the contribution due to the 1.38-Mev radiation. If it be assumed that for zero thickness there are present equal numbers of photons of the two components, then, of the total initial activity, the contribution of each type of photon will be in the ratio of the absorption coefficients for the two radiations. Thus for the figure shown, the zero thickness intensity for the combined radiation is 92.0 in arbitrary units. This should then be resolvable into two components of initial intensities 54.0 and 38.0 expressed in the same units, for the 1.38 Mev and 2.85 Mev, respectively, since the absorption coefficients are approximately in the ratio of 60 to 40.

Since the absorption coefficient of the 1.38-Mev radiation is fairly accurately known, the decrease of this radiation with increasing thickness of lead can be predicted. This is shown in curve *B*, Fig. 4. On subtracting this activity from that actually observed shown in curve *A*, the values shown in curve *C* are obtained. This is then the true absorption curve for the 2.85-Mev radiation. The absorption coefficient obtained for lead in this way is found to be 0.405 cm^{-1}. In a similar manner the absorption coefficient, for the 2.85-Mev radiation in copper is found to be 0.285 cm^{-1}. The radiation was followed through 10 cm of copper in addition to 5 cm of lead. These values are more than 10 percent less than the Heitler summation values and are shown as points in Figs. 1 and 2. They would not be greatly changed by assuming slightly altered ratios for the intensities of the components.

The values here reported are believed to be not in disagreement with other measurements reported on the radiation from thorium (C+C″). Gray and Tarrant reported a value at 2.65 Mev of 0.465 cm^{-1} for lead. They used absorbers only up to 6 cm in thickness. Had they gone to greater thickness and corrected for the lesser energy component it is quite reasonable to expect their value might have been reduced to a value compatible with the results reported here. Chao reported a value for lead of 0.477 cm^{-1}. He also used a thickness of lead only up to 6.37 cm. The geometry of his apparatus was very favorable, having a distance of 2 meters between absorber and detector. However, a background reading was subtracted from each reading which was obtained by simply changing the direction of the primary beam so as to miss the detector. Because of the Compton scattering this would not be a true background but would be too large so that the net absorption curve would be too steep, yielding an absorption coefficient too large.

Since this difference appears clearly to be greater than the experimental error in the measurement, its explanation raises grave questions. Had it occurred only in lead then one might have attributed it to inaccuracy in the calculation of the photoelectric contribution. It would have required reducing to zero, the value attributed to lead by Heitler, for this energy. Since it also occurs in copper at an energy where the photoelectric effect is vanishingly small and where pair production is not appreciably large it is more reasonable to attribute it to some insufficiency in the Klein-Nishini formula for this energy.

This investigation was made possible by the continued support of the Horace H. Rackham Fund.

Nuclear Excitation Functions

I. $Na^{23}(d,p)Na^{24}$, $Br^{81}(d,p)Br^{82}$, and $Br(d,2n)Kr$(34 hr.)

E. T. CLARKE, *Department of Physics*

AND

JOHN W. IRVINE, JR., *Department of Chemistry*
Massachusetts Institute of Technology, Cambridge, Massachusetts

(Received September 9, 1944)

Excitation functions for production of the radioactive isotopes Na^{24} (14.8 hr.), Br^{82} (34 hr.), and Kr (34 hr.) were obtained by bombardment of a stack of NaBr films obtained by evaporation in high vacuum onto aluminum foil. Deuteron energy determinations were made by measurement of range in aluminum; the maximum deuteron energy used in these experiments was 13.5 Mev. The activities of each isotope were measured on a calibrated gamma-ray counter which yielded three excitation curves and the absolute disintegration rates for the Na^{24} and the Br^{82} whose disintegration schemes are known. The reaction $Br^{81}(d,p)Br^{82}$ exhibits an excitation function which begins at about 3 Mev, rises to a maximum absolute cross section of 3.8×10^{-25} cm² at 8.5 Mev, and decreases with further increase in energy. The excitation of the reaction $Na^{23}(d,p)Na^{24}$ shows the same shape but begins at about 1 Mev and reaches its maximum value of 4.7×10^{-25} cm² at 6 Mev. The reaction $Br(d,2n)Kr$ shows a definite threshold at 5.3 Mev and rises almost linearly with increase in deuteron energy. Comparisons of these curves with the theory of Konopinski and Bethe indicate that the angular momentum with which the compound nucleus is formed is an important factor influencing the competition for the disruption of the compound nucleus.

INTRODUCTION

AFTER Gamow[1] proposed his theory for the penetration of swiftly-moving charged ions into the atomic nucleus, its first verification was obtained in 1932 by Cockroft and Walton,[2] when they accelerated protons to energies of about a half-million electron volts and showed that energetic alpha-particles were emitted from targets of light elements such as lithium. Following these early experiments, other workers, using the newly developed cyclotron, accelerated protons, deuterons, and alpha-particles to higher and higher energies, and showed that nuclear reactions could be produced in any target struck by these particles. Evidently Gamow's fundamental ideas of the penetrability of the nucleus were correct, insofar that the yield of the reactions increased with incident energy for any particular bombarding particle, and required higher energies to produce reactions in the heavier elements. However, more careful analysis of the excitation functions of some of these reactions, where the relative reaction cross section was obtained as a function of incident energy, showed that Gamow's theory was incorrect at energies comparable to and above the height of the Coulomb barrier. As a result, Konopinski and Bethe[3] in 1938 and similarly Weisskopf and Ewing[4] in 1940 proposed refinements of the simple Gamow theory in the light of the more modern ideas of the nucleus. Their theories predicted the production, as a function of energy, of the compound nucleus composed of target nucleus plus incident particle, and took into account the varying angular momenta given to the compound nucleus in the collision.

With the achievement of a 14-Mev deuteron beam from the M.I.T. cyclotron, it was felt worth while to measure experimentally the excitation functions for a number of reactions. As a result of recent work carried out at the M.I.T. Radioactivity Center on the disintegration schemes of several radioactive isotopes[5] and

[1] G. Gamow, Zeits. f. Physik **52**, 510 (1929).
[2] J. D. Cockroft and E. T. S. Walton, Proc. Roy. Soc. **A136**, 619 (1932).
[3] E. J. Konopinski and H. A. Bethe, Phys. Rev. **54**, 130 (1938).
[4] V. F. Weisskopf and D. H. Ewing, Phys. Rev. **57**, 472 (1940).
[5] M. Deutsch and L. G. Elliott, Phys. Rev. **65**, 211 (1944).

on the development of calibrated gamma-ray counters,[6] it has become possible for the first time to set forth some of the excitation functions in terms of the absolute cross sections of the reactions. By these means, these newer theories can be checked and useful information on nuclear yields can be obtained for the efficient operation of the cyclotron as a production instrument.

THEORY

A. Excitation Functions

As is well known, the Bohr picture of the process of nuclear transmutation assumes the penetration of the target nucleus by the incoming particle, where the two merge indistinguishably into one entity called the compound nucleus. This in turn almost immediately loses energy by emission either of particles or of quantum energy, usually by both, and generally leaves the resultant nucleus in an unstable condition. Quantitative theoretical analyses have been successful in predicting the probability of formation of the compound nucleus, but since there is the possibility that the nucleus will decay by any one of a number of distinct modes, each forming a different resultant nucleus, and since the factors affecting competition among these ways of disintegration are but little known, theoretical treatments have in general been unable to predict excitation functions for complete nuclear reactions.

Theoretical excitation functions for production of the compound nucleus are obtained by calculation of the probability of penetration of the nuclear barrier by the incoming charged particle. This probability, as a function of incident energy, can then be compared with the sum of the observed cross sections of all the reactions involving that particular compound nucleus. The effects of sticking probabilities, or the chance that, once inside the nucleus, the deuteron will form with it the compound state, have been neglected since for theoretical reasons this chance should be approximately unity for energies comparable to and above the barrier energy.

The penetrability of the Coulomb barrier was first theoretically investigated by Gamow[1] and independently by Gurney and Condon.[7] Early measurements at low energies checked these conclusions.[8] However, when higher bombarding energies became available, it was found that the observed excitation functions disagreed with theory, and in 1938 Konopinski and Bethe[3] proposed a modified theory which took into account the possibility that the incoming particle could impart to the struck nucleus higher angular momenta than the zero value assumed in the original theory. Bethe's theory was expressed in terms of excitation functions for the formation of the compound nucleus at each of the various quantized angular momenta; the total probability of formation was the sum of these partial probabilities. As a result, the theory predicted that the production cross section for compound nuclei would increase continuously to a maximum, at high incident energies, equal to the geometrical cross section. This is a more reasonable behavior than that given by the simple Gamow theory, which showed a decrease at high energies inversely proportional to increasing incident energy.

An alternate mechanism, the Oppenheimer-Phillips,[9] applies to the special case of deuteron reactions in which protons are emitted. In this theory it is assumed that the deuteron dissociates in the extranuclear electric field; the neutron coasts into the nucleus while the charged proton is repelled, so that no compound nucleus of deuteron plus target nucleus is ever formed. Here the theory can predict the excitation function for the production of the resultant nucleus. Bethe's analysis,[9] however, shows that this mechanism can operate only when the deuteron energy is insufficient to carry it over the top of the Coulomb barrier surrounding the target nucleus. Since the deuteron break-up distance from the nucleus decreases with increasing incident energy, a point is reached at a critical energy slightly below that of the Coulomb barrier where the break-up distance becomes less than the nuclear radius and the deuteron as a whole penetrates to form the compound nucleus. Thus

[6] W. Peacock, Phys. Rev. **66**, 160 (1944).

[7] R. W. Gurney and E. U. Condon, Phys. Rev. **33**, 127 (1929).

[8] E. O. Lawrence, E. M. McMillan, and R. L. Thornton, Phys. Rev. **48**, 493 (1935).

[9] Oppenheimer-Phillips mechanism references will be found in G. M. Volkoff, Phys. Rev. **57**, 866 (1940).

with medium-weight target atoms and incident energies high compared with that of the barrier, the thick target (integrated) yield due to the Oppenheimer-Phillips mechanism is very small and may be neglected in comparison with that resulting from formation and disintegration of a compound nucleus. Even though the ratio of O−P to Gamow yields at very low energies may be enormous, the absolute yields here are almost negligible in comparison with those obtained at and above barrier energies.

B. Range Energy Relationships

Since high speed ions, in their passage through matter, lose energy through collision with the comparatively light extranuclear electrons of the target material, their rate of energy loss can be predicted with considerable accuracy. The energy straggling, or the energy spread of the ion beam at any given depth in the target, is small. This fact permits the use of stacks of thin foils for the determination of the effects of deuterons on matter as a function of incident energy. Simultaneous bombardment of a series of foils insures that each layer will receive an identical exposure. When the excitations produced in the foils have half-lives long enough to permit their observation after the bombardment is complete and the foils separated, the stacked-foil technique for investigation of nuclear excitation functions is by far the most satisfactory from the point of view of simplicity and accuracy.

In order to determine excitation functions by these means, it is necessary not only to know the initial energy of the incident deuterons, but also their range energy relationship in their traversal of the often heterogeneous stack of foils. Although the best-known range energy curve is that for air, it was decided to measure the initial deuteron energy by its absorption in aluminum. Livingston and Bethe[10] give a theoretical range energy curve for this absorber, and range measurements in solids are simpler and less subject to errors than those done in gases. Average deuteron energy at any point in the stack of foils was easily calculated when the range energy curve for each component in the stack was known.

[10] M. S. Livingston and H. A. Bethe, Rev. Mod. Phys. 9, 69 (1937).

The theory of loss of energy of swiftly-moving charged particles traversing matter has been set forth by Bethe.[11] His treatment shows that, for energy loss by electron ionization and for deuteron energies greater than about 1 Mev, the energy loss per unit length is equal to

$$dE/dx = kNB = k(NZ) \ln (2mv^2/I), \qquad (1)$$

where K is a function of incident energy and independent of the absorbing material, m the electronic mass, v the velocity of the incident particle, N the density of atoms in the absorber, Z their nuclear charge, I their geometric mean ionization potential, and B the stopping number. The atomic stopping power S_1 is defined at any velocity by $S_1 = B/B_{\text{air}}$. As there is no adequate theory for the value of I, this quantity must be found by experiment. This has been done for a number of absorber elements with natural alpha-particles used as projectiles.[12]

From Eq. (1) it can be seen that given a range energy relationship in a particular absorber, the relationship for any other absorber may be found if its value of I is known. This method for obtaining range energy curves is not strictly applicable to heavy elements, since here the innermost electrons are too tightly bound to be ionized by the traversing particles having velocities in the range in which we are interested. However, the departure is not great, and the accuracy obtainable is sufficient for the purposes at hand.

In order to find the value of I for a particular material, stopping power measurements were made by substitution of some of the aluminum absorber in the deuteron beam by an equivalent thickness (in mass per unit area) of the material. Then I is given by the following expression;

$$\ln I = (1-Q) \ln (2mv^2) + Q \ln (I_{\text{Al}}), \qquad (2)$$

where $Q = (Z_{\text{Al}}/Z)(M/M_{\text{Al}})(R_{\text{Al}}/R)$, and v^2 is calculated from the average energy of the interval. Here M is the atomic weight, and (R_{Al}/R) the ratio of the thicknesses of the equivalent quantities of aluminum and of the absorber. The values for aluminum used here were $Z=13$, $M=27$, and $I=158$ electron volts.

[11] H. A. Bethe, Ann. d. Physik 5, 325 (1930).

[12] R. D. Evans, *Introduction to the Atomic Nucleus* (M.I.T. notes 1938), Chap. IV–4.

Since the range relationship in terms of air-cm is given[12] by

$$L=(N_{\text{air}}/N)\int_0^R dr/S_1, \tag{3}$$

the quantity $1/S_1$ as a function of energy for the absorber in question was required. In the case of sodium bromide, the atomic stopping powers S_1 were obtained for Na and for Br by calculation with Eq. (1) of the stopping numbers B as a function of energy, and dividing these by the corresponding values of B for air. These two curves of atomic stopping power were averaged, and the result inverted to yield a curve of $1/S_1$ for NaBr. This was integrated graphically to obtain L as a function of R. The low energy end of the $1/S_1$ curve is indeterminate (below about 1 Mev for deuterons) and therefore L can be obtained only to an unknown additive constant; however, since the range energy curve is used to obtain energy differences from a known high energy, this is immaterial to the results. By use of Livingston's and Bethe's air range curves,[10] R was readily converted to Mev.

In the determination of the range curve for sodium bromide, values of I for a number of elements in the same regions of the periodic table were found, and the I values for sodium and bromine estimated by interpolation; these were 155 and 390 ev, respectively, and are approximate, as there is reason to believe that I is not a smoothly varying function of Z. The only means at present known for the accurate determination of a range energy curve is that of direct observation, by means of magnetic analysis of the energy changes produced by the absorber.

C. Determination of Cross Sections

After a stack of foils has been bombarded with a known exposure of deuterons, the foils are separated and their induced activities measured on some form of detection apparatus. If then these activities can be converted into the number of disintegrations per unit time taking place in the sample, it is possible to determine from this the total number of active atoms produced in each foil and hence the cross section for their production. Through the work of Peacock[13] at this laboratory it has become possible to determine the absolute disintegration rate of radioactive atoms of any isotope whose disintegration scheme is known and which emits gamma-rays.

Peacock prepared a platinum screen wall gamma-ray counter whose detection efficiency is calibrated as a function of gamma-ray energy. Thus, if the number and energies of the gamma-rays emitted per disintegration by a sample of a radioactive isotope are known, the counting rate of this counter can be converted directly into the disintegration rate of the sample. From this quantity, the cross section is determined by the expression

$$\sigma=\frac{(\text{activated atoms/cm}^2)/(\text{total atoms/cm}^2)}{\text{No. of deuterons/cm}^2}$$

$$=6.40\times10^{-36}\frac{TDM}{m(\mu a-\text{min.})}, \tag{4}$$

where T is the half-life, and D the disintegration rate at the end of bombardment, both in the same time units; M the atomic weight and m the milligrams/cm² thickness of the target isotope, and (μa-min.) the deuteron exposure. When the thickness of the foil is expressed in terms of the mass per unit area, the expression for the cross section is seen to be independent of both the density of the material and the area struck by the beam.

Earlier studies (see Appendix) of nuclear excitation functions have been handicapped by the inability to report accurately the absolute cross sections. The usual method was the calibration of a beta-ray counter or electroscope with a uranium compound of known strength, and then the use of this detector for observation of the induced activities on the foils. This procedure is valid only when the energy distribution and maximum energy of the electrons in the target activity are similar to those of the uranium beta-rays. The type of backing and the thickness of the sample must be carefully considered, since these have important effects upon the efficiency of detection of beta-rays.[14] Since it is seldom that the effects of the target activity and that of the standard are equivalent in the

[13] A. Roberts, L. G. Elliott, J. R. Downing, W. C. Peacock, and M. Deutsch, Phys. Rev. **64**, 268 (1943); see Fig. 6 of this paper.

[14] A general discussion by the M.I.T. Radioactivity Center of the construction, operation, and efficiency of counters is in preparation for publication.

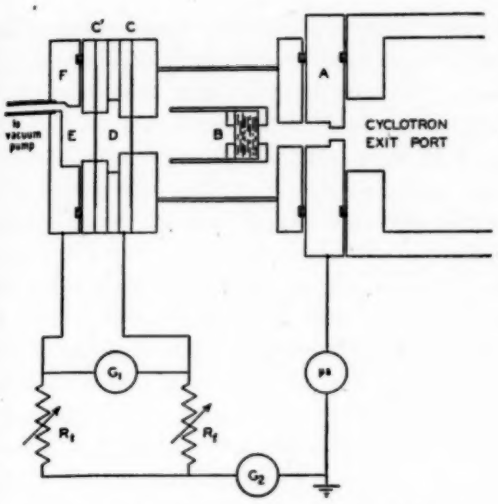

FIG. 1. Bombardment chamber assembly and wiring diagram.

detector, the cross sections obtained by these methods cannot, in general, be relied upon.

EXPERIMENTAL PROCEDURE

When sodium bromide is bombarded with 14-Mev deuterons, four radioactive isotopes are produced whose activities, a few hours after bombardment, are far greater than those of any other products resulting from the bombardment. They are the products of two types of reactions and involve all three of the stable isotopes present: Na^{23}, Br^{79}, and Br^{81}. The (d,p) type of reaction is responsible for the production of the 14.8-hr. Na^{24}, 4.4-hr. Br^{80}, and 34-hr. Br^{82}, while the radioactive krypton is produced from one of the bromine isotopes by $(d,2n)$ and has a half-life of 34 hours.

A. Production of Foils

In order that a beam of deuterons of 14-Mev initial energy traverse about twenty foils before being stopped, the films of target material must have a thickness of the order of 0.02 mm, or roughly 10 mg/cm². This figure varies considerably for different target materials, since the atomic stopping power of various substances is a function of the atomic number. In the case of sodium bromide, each foil was covered above and below by 1.7 mg/cm² aluminum foils, so that the thickness of the sodium bromide layer was made to be about 5 mg/cm².

Anhydrous sodium bromide was melted in a molybdenum boat and evaporated onto a collector in high vacuum. The resulting NaBr film can be built up to a sufficient and reasonably uniform thickness, is fine grained, cohesive, and adheres well if it is deposited on a thick plate. However, it flakes away if it is evaporated on a thin (0.25-mil) aluminum foil, and since this foil must be used as a backing for the sodium bromide film, this is a serious difficulty. Apparently the cause for this behavior lies in the difference in the expansion coefficients of the NaBr and the aluminum. The thin aluminum foil rises to much higher temperatures during the evaporation process than does the thick plate, and thus cooling produces greater strains at the interface. It was found that if a very thin layer of shellac were first coated on the aluminum foil, the heat evolved by the evaporator was sufficient to soften the shellac which would then bind the layer of NaBr to the aluminum. Fortunately, the activities induced by deuterons in aluminum and in shellac are all short-lived, and do not interfere with the measurements of activities induced in the sodium bromide.

In order to know the thicknesses of the target foils, a measured area of aluminum foil was first weighed, then coated with shellac, dried, and reweighed. Since the shellac constituted about a tenth of the weight of the aluminum, it was assumed that small departures from uniform thickness of the shellac film were negligible. After completion of the evaporation process, the composite aluminum-shellac-sodium bromide foil was punched out as a number of $\frac{3}{4}''$ disks, and each disk was weighed to obtain the mass per unit area of sodium bromide. Finally, the disks, interleaved with sheets of 0.25-mil aluminum foil, were stacked and were thus ready for bombardment.

B. Bombardment

The chamber assembly used for bombardment of the foils was also used for determining, by absorption in aluminum, the range of the deuterons used for activation of the foils. As shown in Fig. 1, part of the deuteron beam penetrated the 0.25-inch hole drilled in the cyclotron exit-port cover plate *A*, passed through the target foil holder *B* (empty if ranges were to be measured),

and emerged from the vacuum through the 0.001-inch thick duraluminum window C. In the space D graduated thicknesses of aluminum absorber, in steps of 1.5 mg/cm², could be interpolated by manipulation of a system of sliding racks. The beam then entered the evacuated space E through another duraluminum window C', and was finally stopped in the collector plate F. Rubber gaskets at all joints provided vacuum seals and electrical insulation. Control was maintained over secondary electron emission by means of overhangs at all surfaces struck by the deuterons, since the stray magnetic field present was sufficient to keep even the most energetic of the ejected electrons from traveling more than a few millimeters in a horizontal plane. Figure 1 also shows the galvanometers and microammeter used for monitoring the beam and for measuring the ratio of ion currents stopped in the foils and in the collector plate. The galvanometer-resistor network shown was employed in order to obtain this ratio independent of variations in beam intensity, and comprised a sensitive galvanometer G_1 (5×10^{-10} amp./mm) and two decade boxes of 10,000 ohms each.

In the operation of the apparatus, a resonant beam of deuterons was first obtained and its total intensity observed on the monitoring microammeter connected to the drilled plate covering the exit port. With a known thickness of aluminum in the path of the beam, the two resistors R_f and R_t were adjusted until no current flowed in the galvanometer G_1. The thickness of the absorber was then changed and a second pair of resistor values obtained; this process was repeated, varying the aluminum absorber thickness in small steps, until the range had been covered. After converting the resistance readings into the corresponding fractions of deuterons arriving at the collector plate, they were finally plotted, as in Fig. 2, as a function of thickness of aluminum. Figure 2 contains, beside this number range curve, the theoretical straggling curve[10] for the same median range, showing that the deuteron beam used for bombardment of the stack of foils was initially fairly monokinetic, with not more than twice the normal straggling appearing in the observed curve.

After completion of the range measurements, the stack of foils to be bombarded was loaded into the holder and exposed to a 0.5-microampere deuteron beam for a half-hour.

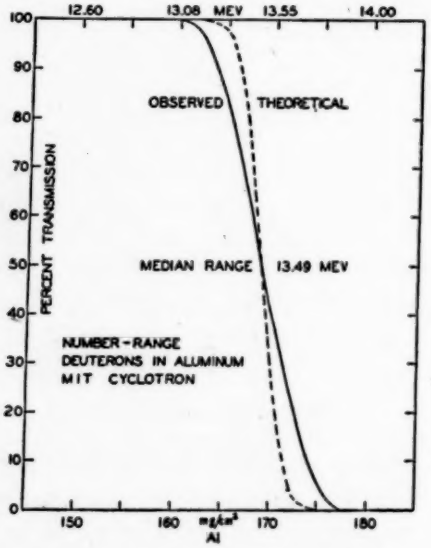

FIG. 2. Number range curve of deuterons absorbed in aluminum under operating conditions prevailing in 1943. The solid curve represents the observed distribution of energies of deuterons emerging through a ¼-inch hole, while the broken curve shows the theoretical straggling of an initially homogeneous beam of energy equal to the median energy of the observed beam.

C. Chemical Separation

When a volatile or gaseous product is formed in a solid target as a result of nuclear reactions produced by high velocity ion bombardment, it generally is retained in the structure of the solid material, even under vacuum, unless the target is altered in form by the effect of high temperatures or by solution. In the case of krypton formation from sodium bromide, Brown, Irvine, and Livingston[15] found by analysis of the gas surrounding a thick target of NaBr under heavy bombardment that practically no krypton is lost during bombardment even under vacuum, unless the target is improperly cooled and the NaBr is melted. The sodium bromide foils were therefore bombarded in vacuum with deuteron currents of about half a microampere with assurance that no krypton would be lost, since the power dissipated in the stack was only about 7 watts. In order to liberate the krypton after bombardment had been completed, it was necessary only to dissolve the foils in water. To that end a special apparatus

[15] S. C. Brown, J. W. Irvine, Jr., and M. S. Livingston, J. Chem. Phys. 12, 132 (1944).

was constructed, into which the individual foils could be introduced, the system closed, the foils immersed and dissolved in water, and the evolved krypton swept into evacuated containers. This apparatus, shown in Fig. 3, comprised a water reservoir closed by a glass stopper and fitted with stopcocks to permit air to be bubbled through the solution into a previously evacuated 100-cc flask. The reservoir was formed with two glass dimples and a sliding steel needle which together provided a support for the foil so that the latter could be dropped into the water by retracting the needle with a small magnet, thereby insuring that no krypton would be released until the system had been closed.

After the krypton fraction had been removed, the solution of each foil was poured into a small beaker and an excess of $AgNO_3$ was added. The AgBr precipitate was coagulated by boiling for a short time, and filtered out in small filtering crucibles. The filtrates were bottled since they contained the sodium activity, and the crucibles with the precipitates were dried in an oven and weighed. Since the crucibles had previously been weighed, this yielded the weight of the AgBr which was then converted to the equivalent weight of the original amount of NaBr in each foil, affording an independent check on the directly measured amounts obtained before bombardment. Finally the precipitates were redissolved in an excess of KCN solution and these solutions were bottled.

D. Measurement of Activities

Two objectives presented themselves in the problem of detection of the activities present in the sixty-odd samples resulting from the separation of the bombarded sodium bromide foils. One was to record the activities in the samples of each series with as great a relative precision as possible, in order to obtain a good excitation function; the other was to observe the disintegration rate of at least one sample in each series which could then be applied to the excitation function to determine the absolute cross section of the reaction at any energy up to the maximum bombarding voltage. If the disintegration scheme of the isotope under observation were known, the second objective could be attained. Observation of the relative excitation curves could be carried

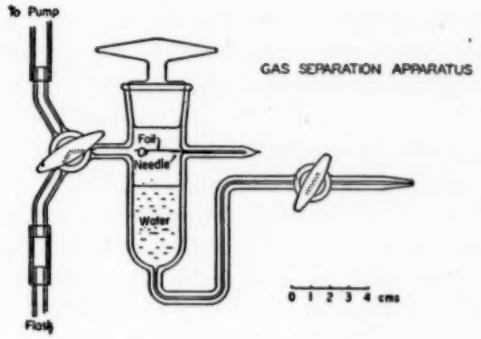

FIG. 3. Gas separation apparatus.

out by means of any of the emitted radiations of the isotope, as long as each sample was measured under identical geometrical conditions.

Detection by means of beta-ray emission was chosen as the means for obtaining the relative excitation curves of the bromine and sodium isotopes, because aliquots of the solutions containing these activities could be absorbed on small filter paper planchettes and measured on an automatically operated sample changer[16] employing mica window beta-ray counters. The sample changer was loaded with 23 active planchettes and one blank, and the counting rate owing to each sample was recorded with a recording counting-rate meter[17] over a fifteen-minute interval; thus, each sample was observed once every six hours. By operating the apparatus over a period of about 24 hours, several values for each sample were obtained, which when plotted on semilogarithmic coordinate paper gave a check, by the resulting decay curve, on the purity of the samples. It had been planned to observe in this way the composite decay curve resulting from the two bromine isotopes, 4 hour and 34 hour, but difficulty was experienced with the counters and no observations were made until practically all the 4-hour activity had decayed.

The krypton activity, because of the extended nature of the geometry of the sample, was observed on a platinum screen cathode gamma-ray counter whose efficiency as a function of gamma-ray energy had previously been calibrated. Each flask containing the krypton fractions was brought in turn to this counter, and the resulting counting rate found from the reading of the

[16] W. C. Peacock, Rev. Sci. Inst. (in preparation).
[17] A. F. Kip, A. C. Bousquet, W. N. Tuttle, and R. D. Evans, Rev. Sci. Inst. (in preparation).

associated counting rate meter. Also, one sample from each of the sodium and bromine series was compared on the counter with a standard radium source. This provided the means for determination of the absolute disintegration rates. All measurements were corrected for decay from the end of bombardment, though no correction was made for decay during bombardment since the bombardment time was short compared to the half-lives of the isotopes under investigation.

RESULTS

The data and curves resulting from the measurements of the excitation functions of the reactions $Na^{23}(d,p)Na^{24}$, $Br^{81}(d,p)Br^{82}$, and $Br^{79,81}(d,2n)Kr^{79,81}$ are shown in Fig. 4. Here

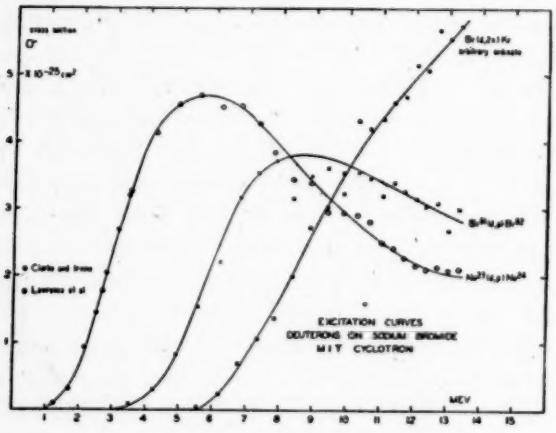

FIG. 4. Observed excitation curves.

both (d,p) reactions, since the disintegration schemes of their resultant nuclei are known, are given in terms of their absolute cross sections, while the $Br(d,2n)Kr$ ordinate is arbitrary. All that is known of the disintegration of Kr is the fact that it emits positrons[18] of approximately 0.5 Mev and probably is accompanied by soft gamma-radiation. At the low energy end of the Na curve are plotted data obtained by Lawrence *et al.*[8] by bombardment of a stack of mica sheets with deuterons of 3.5 Mev. Since their ordinate was given in arbitrary units, their vertical scale was adjusted to bring their topmost point coincident with the curve obtained here. It is seen that the two curves join smoothly, providing a check not only on the excitation curve observed here but also justifying the assumptions made in the determination of the range energy relationships assumed for the stack of foils.

By use of the methods and data given by Konopinski and Bethe[3] curves for the production of the compound nuclei $(Na+d)$ and $(Br+d)$ were constructed for several values of the unknown parameter r_0, the standard nuclear radius[10] (nuclear radius $R=r_0A^{\frac{1}{3}}\times10^{-13}$ cm). Since these curves could be calculated in terms of the absolute cross section, they provided an interesting comparison with the observed excitation curves. In Fig. 5 are shown two curves for the production of $(Br+d)$, together with the experimental $Br(d,p)$ data. If one assumes that at very low energies production of Br^{82} takes place chiefly by the Oppenheimer-Phillips process, and that at slightly higher energies, in the region of one or two Mev below the barrier, almost all reactions proceed by formation of the compound nucleus and emission of a proton is highly favored, one can reasonably select the curve given by $r_0=1.75$ as the one which best fits the observed data. Because of the O−P process, the observed (d,p) cross section should at very low energies exceed the cross section for production of the compound nucleus, and except for this, observed cross sections should always lie below those for production of the compound nucleus.

Evidence obtained from measurements of inelastic scattering cross sections of fast neutrons[19] indicates that the value of the standard nuclear radius is not a constant for all elements, but increases from about 1.60 for very light nuclei to 1.77 for zinc, and decreases for heavier nuclei so that its value is 1.50 for tin and 1.35 for lead. The standard nuclear radii obtained from our comparisons of theoretical with experimental excitation curves (1.60 for Na, 1.75 for Br) are consistent with these values.

From the theoretical curves in Fig. 5, it is evident that at higher energies the compound nucleus decays by some means other than the emission of a proton and the consequent formation of Br^{82}, and that the total probability of this competitive decay will be given by curve *C*, the difference between the two curves *A* and *B*.

[18] W. H. Barkas, E. C. Creutz, L. A. Delsasso, and R. A. Sutton, Phys. Rev. **57**, 1087 (1940).

[19] D. C. Grahame and G. T. Seaborg, Phys. Rev. **53**, 795 (1938).

Since the observed Br(d,2n)Kr is such a competitor, its data were plotted on Fig. 5. The ordinates were adjusted so that the highest energy point coincided with curve C. It will be seen that the agreement is very close, suggesting the possibility that the compound nucleus, in the range of incident energies investigated, decays predominantly by emission either of a proton or of two neutrons. Since the theoretical probability of energy loss by neutron emission, when at all possible, is far greater than that by gamma-radiation,[10] it would be expected that for incident energies above the (d,2n) threshold the compound nucleus would be much more likely to emit two neutrons than one neutron and a gamma-ray. In the energy range below the (d,2n) threshold, however, unless the cross section for production of the compound nucleus is increased by assuming an appreciably greater nuclear radius, there seems to be little evidence for any large proportion of (d,n) reaction. This is rather surprising since the (d,n) reaction, though it leads here to a stable isotope and thus cannot be observed by these methods, should be very probable at lower energies and should compete successfully with the (d,p).

When the krypton data are fitted in this way, the resulting cross section can be used to estimate a detection efficiency for Kr radiations. With a platinum screen cathode gamma-ray counter and a lead absorber 0.16 cm thick, the counting efficiency turns out to be 0.10 that for radium. This figure is not unreasonable, since an isotope disintegrating only by positron emission would give a counting efficiency on this counter, comparing its annihilation radiation to the gamma-rays of radium, of 0.5, and it is to be expected that the krypton will disintegrate to an appreciable extent by K capture, reducing this efficiency by a factor of from 2 to 5. The determination of the disintegration scheme of Kr would provide the needed information to check the above conclusions.

The knowledge of the disintegration scheme of Kr would also permit the calculation of the threshold energy for the Br(d,2n)Kr reaction, since the decay of Kr by positron emission returns the nucleus to the original Br isotope. Its threshold energy should be 1.025 (3.95+E) Mev where E is the disintegration energy, including the positron kinetic energy and gamma-rays in cascade to the ground state. The observed threshold is about 5.3 Mev, yielding $E=1.2$ Mev; since the positron energy is reported to be 0.5 Mev,[18] it is expected that the remaining energy loss by gamma-radiation will be about 0.7 Mev.

The calculation of theoretical production curves for compound nuclei can be performed in a different way. The contribution of each value of angular momentum is derived as a function of incident energy, and a series of curves plotted, each the sum of contributions to the cross section of angular momenta from zero to successively higher values. The lowest curve then represents the probability of formation of the compound nucleus with zero angular momentum, the simple Gamow-Condon-Gurney theory, and the curve for the sum of all values of angular momenta is the same as that obtained by the integral method of calculation given by Konopinski and Bethe. For incident energies up to 14 Mev on sodium and bromine, the total production curve is closely approximated when only the first few values of angular momentum are used, and so these curves were calculated for values of l up to 4. For very

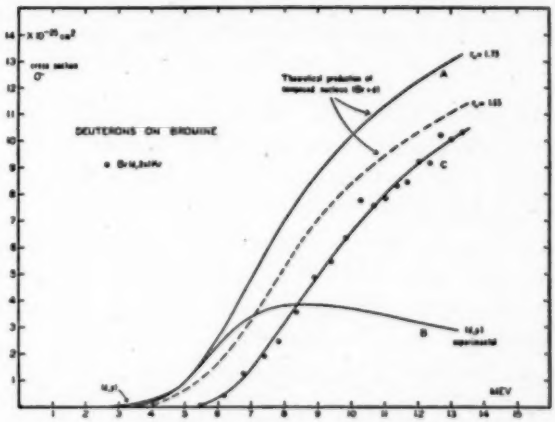

FIG. 5. Comparison of observed excitation curves with the compound nucleus production theory of Konopinski and Bethe (reference 3). The theoretical compound nucleus production for all values of l (same as the uppermost curve in Fig. 7) is shown for two values of the standard nuclear radius r_0; curve A, with $r_0=1.75$, is assumed to give the best fit with curve B (corresponding to the experimental values shown in Fig. 4) at low energies where the (d,p) reaction has little competition. The difference between curves A and B is given by curve C. The experimental data (circles) of the Br(d,2n)Kr reaction, when they are fitted at the high energy end, are seen to coincide with curve C.

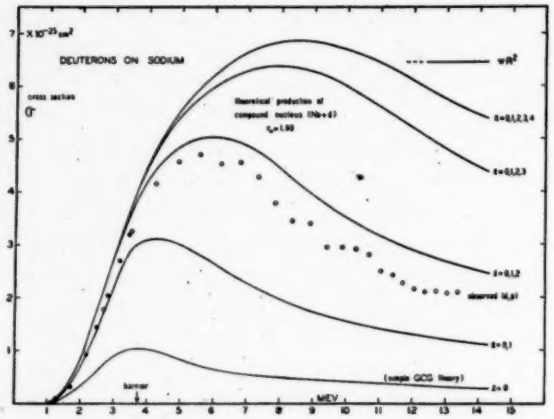

FIG. 6. Comparison between the observed excitation function of the $Na^{23}(d,p)Na^{24}$ reaction and theoretical curves for the production of the compound nucleus $(Na^{23}+d)$ with different values of angular momentum.

large incident energies, the total production curve approaches a cross section equal to πR^2.

These curves were calculated for sodium and bromine and are shown, together with the observed excitation functions for the (d,p) reactions, in Figs. 6 and 7. In each case, the similarity between the observed curve and that of the production of the compound nuclei with angular momenta from zero to two is quite striking. It is also evident that the original Gamow theory is inadequate in predicting excitation functions, and that the effects of angular momentum upon the formation of the compound nucleus must be considered. The comparisons indicate that almost all of the compound nuclei which have been formed with angular momenta of 0, 1, and 2 decay by proton emission and that compound nuclei with higher angular momenta decay by some means other than proton loss. In the case of sodium, the (d,n) and (d,α) reactions lead to stable isotopes, while the $(d,2n)$ results in an isotope having the unmanageably short half-life of 11 seconds; the two (d,n) reactions on bromine result in stable isotopes, the (d,α)'s are very improbable because of the high Z of bromine, and the cross section for the observed $(d,2n)$ is unknown; thus competition for decay of these compund nuclei could not be determined quantitatively by experiment.

Finally, thick target yield curves, giving activities per microampere hour of bombardment, were calculated from the absolute excitation curves in conjunction with the range energy curve of deuterons in sodium bromide. Equation (4), combined with the definition[12] of the curie unit, 1 curie $=3.7\times10^{10}$ disintegrations per second, can be rewritten

$$\frac{\text{millicuries}}{(\text{mg/cm}^2)\ \text{microampere-hour}}=4.23\times10^{27}\frac{\sigma}{TM}. \quad (5)$$

The number of mg/cm² of sodium bromide in each 0.5-Mev energy interval was multiplied by the average cross section in the interval, and the number of millicuries per microampere-hour in the interval obtained. These activities were then summed over the energy range to give the thick target yield at any energy, and are shown in Fig. 8. The yield of krypton is given in terms of micrograms radium equivalent, comparing activities on a platinum cathode gamma-ray counter shielded by 0.16-cm lead.

By using the range energy curve for metallic sodium, the thick target yield of Na^{24} for the elementary target was also derived. It was found to be almost identical in shape with the curve in Fig. 8; thus the yield for metallic sodium can be obtained from Fig. 8 by multiplying the Na^{24} ordinate by 3.48.

The authors wish to acknowledge the friendly interest of Professors R. D. Evans and M. S. Livingston, and the close cooperation of their colleagues, particularly Dr. Wendell C. Peacock, at the Radioactivity Center. Thanks are also due the members of the M.I.T. cyclotron crew for their assistance in the bombardment.

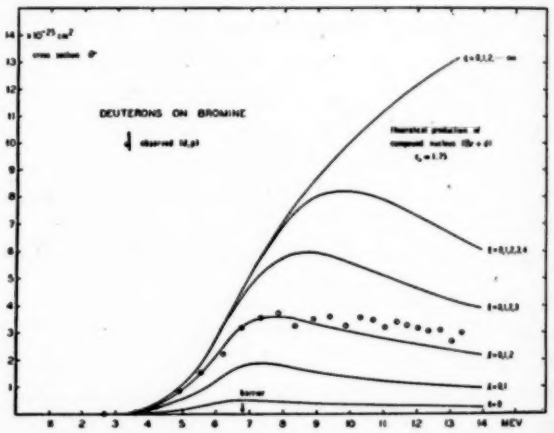

FIG. 7. Comparison between the observed excitation function of the $Br^{81}(d,p)Br^{82}$ reaction and theoretical curves for the production of the compound nucleus $(Br^{81}+d)$ with different values of angular momentum.

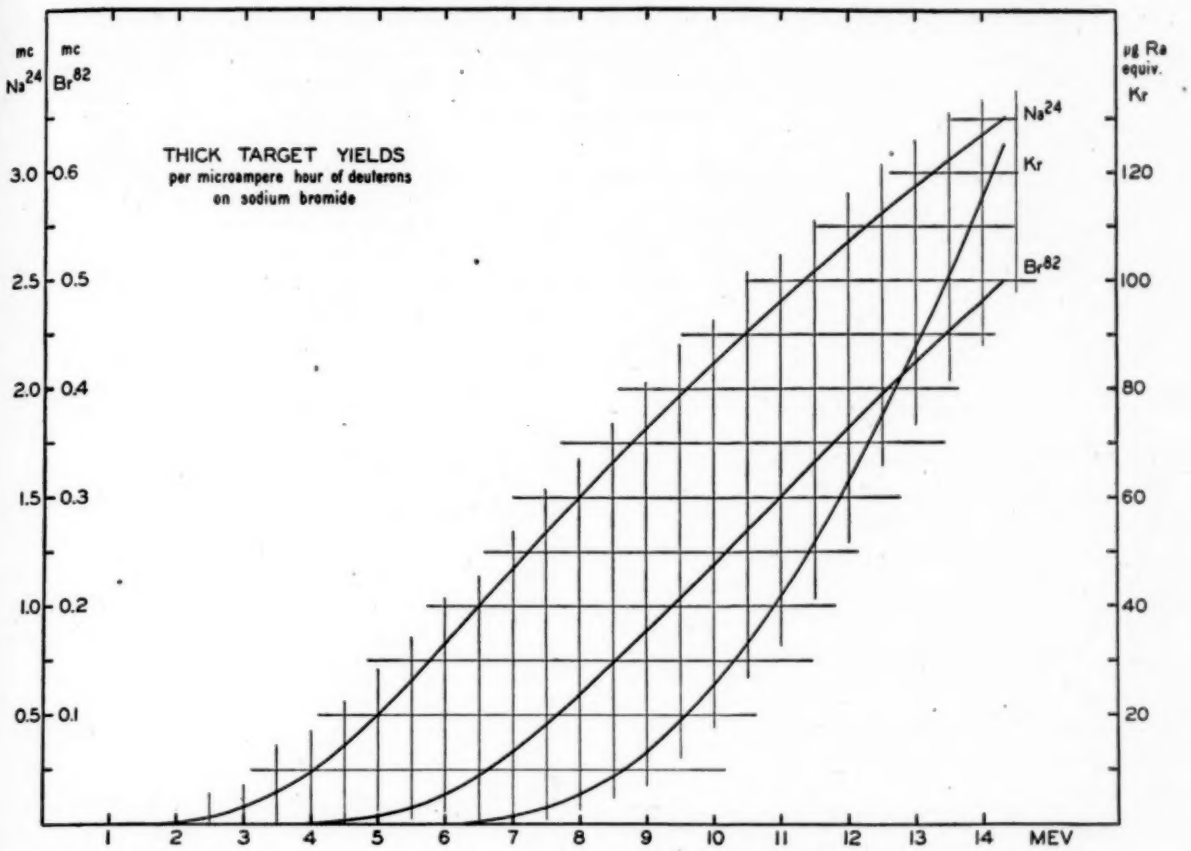

FIG. 8. Thick target yield curves for deuterons in NaBr, obtained by integration over the deuteron range of the curves in Fig. 4. To obtain the yield curve of Na^{24} in a metallic sodium target, multiply the Na^{24} ordinate by 3.48.

APPENDIX

Bibliography of experimental excitation functions of reactions produced by cyclotron-accelerated deuterons:

3.5 Mev:

$Al^{27}(d,p)Al^{28}$; $Na^{23}(d,p)Na^{24}$; $Si^{30}(d,p)Si^{31}$; $Cu^{63}(d,p)Cu^{64}$—E. O. Lawrence, E. McMillan, and R. L. Thornton, Phys. Rev. **48**, 493 (1935).

$Mg^{26}(d,p)Mg^{27}$; $Mg^{26}(d,\alpha)Na^{24}$—M. C. Henderson, Phys. Rev. **48**, 855 (1935).

5 Mev:

$Cu^{63}(d,p)Cu^{64}$—S. N. Van Voorhis, Phys. Rev. **50**, 895 (1936).

$Ni^{60}(d,n)Cu^{61}$—R. L. Thornton, Phys. Rev. **51**, 893 (1937).

$N^{14}(d,n)O^{15}$; $O^{16}(d,n)F^{17}$; $C^{12}(d,n)N^{13}$—H. W. Newson, Phys. Rev. **51**, 620 (1937).

6 Mev:

$Pd(d,p)Pd$ (13 hr.); $[Pd^{105}(d,n)+Pd^{106}(d,2n)]Ag^{106}$—J. D. Kraus and J. M. Cork, Phys. Rev. **52**, 763 (1937).

9 Mev:

$Bi^{209}(d,p)Bi^{210}$(RaE); $Bi^{209}(d,n)Po^{210}$—D. G. Hurst, R. Latham, and W. B. Lewis, Proc. Roy. Soc. **A174**, 126 (1940).

$Ag(d,2n)Cd^{107,109}$ (90 days); $Ag(d,2n)Cd^{107,109}$ (6.7 hr.); $Ag^{109}(d,H^3)Ag^{108}$; $Ag^{109}(d,p)Ag^{110}$—R. S. Krishnan, Proc. Camb. Phil. Soc. **36**, 500 (1940).

$Au^{197}(d,p)Au^{198}$; $Au^{197}(d,2n)Hg^{197}$—R. S. Krishnan, Proc. Camb. Phil. Soc. **37**, 186 (1941).

$Cu^{63}(d,p)Cu^{64}$; $Cu^{63}(d,H^3)Cu^{62}$; $Sb^{121}(d,p)Sb^{122}$; $Sb^{121}(d,H^3)$-Sb^{120}—R. S. Krishnan, T. E. Banks, Proc. Camb. Phil. Soc. **37**, 317 (1941).

$Pt^{196}(d,p)Pt^{197}$; $Pt^{198}(d,p)Pt^{199}$—R. S. Krishnan and E. A. Nahum, Proc. Camb. Phil. Soc. **37**, 422 (1941).

$Pb^{208}(d,p)Pb^{209}$; $Pb^{206}(d,n)Bi^{207}$—K. Fajans and A. F. Voigt, Phys. Rev. **60**, 619 (1941).

$Tl^{205}(d,p)Tl^{206}$; $Pb^{208}(d,p)Pb^{209}$; $Bi^{209}(d,p)Bi^{210}$(RaE); $Tl^{205}(d,n)Pb^{206}$; $Bi^{209}(d,n)Po^{210}$—R. S. Krishnan and E. A. Nahun, Proc. Roy. Soc. **A180**, 333 (1942).

10 Mev:

$Fe^{54}(d,n)Co^{55}$; $Fe^{54}(d,\alpha)Mn^{52}$—J. M. Cork and J. Halpern, Phys. Rev. **57**, 667 (1940).

$Bi^{209}(d,p)Bi^{210}$(RaE); $Bi^{209}(d,n)Po^{210}$—J. M. Cork, J. Halpern and H. Tatel, Phys. Rev. **57**, 371 (1940).

15 Mev:

$Cu^{63}(d,p)Cu^{64}$; $Cu^{63}(d,2n)Zn^{62}$—R. S. Livingston and B. T. Wright, Phys. Rev. **58**, 656 (1940).

PHYSICAL REVIEW VOLUME 66, NUMBERS 9 AND 10 NOVEMBER 1 AND 15, 1944

Exchange Forces Between Li^+ and He, and the Mobility of Li^+ in He*

ROLAND MEYEROTT
Sloane Physics Laboratory, Yale University, New Haven, Connecticut
(Received August 7, 1944)

A calculation of the exchange force between Li^+ and He has been made with the use of simple hydrogenic state functions to represent the charge distributions of the ion and atom. The force so obtained was added to that arising from the polarizability and the van der Waals interaction between Li^+ and He. The result was then used to calculate the mobility of Li^+ in He gas. The theoretical value thus found, 19.4 cm^2/sec. volt at a temperature of 18°C, is somewhat lower than the experimental one of 25.8 cm^2/sec. volt, reported by Hoselitz.

INTRODUCTION

THE theory of the mobility of positive ions in gases has been developed first by Langevin[1] and later, with more rigor, by Chapman[2] and Enskog[3] independently. It has been applied by Hassé and Cook,[4] and, considering the fact that they used hard sphere models with long range polarizability forces and took little or no account of charge exchange, the results were highly satisfactory. With the development of quantum mechanics, it became possible both to calculate the correct force law and to take proper account of charge exchange. This was done by Massey and Mohr[5] but with very unsatisfactory results. Their value of 12 cm^2/sec. volt for the theoretical value of the mobility of He^+ in He is in greater disagreement with the experimental value of 21.4 cm^2/sec. volt quoted by Tyndall and Powell[6] than were earlier calculations. Massey and Mohr recalculated the force law by the method of Hylleraas[7] and found little difference from their original one calculated by the method of Majorana[8] and Pauling.[9] The present author has checked their interaction with that more recently suggested by Weinbaum[10] and found satisfactory agreement, so that the discrepancy cannot be ascribed to the force law.

The reason for this difference between theory and experiment is still unknown. Mott[11] has suggested that Massey and Mohr may have overestimated the effect of the exchange forces by their assumption that the mean period of electron exchange is small compared to the time of passage of the ion past the atom. This is equivalent to an overestimate of the range of the interaction and would lead to a value too low for the mobility. If this is the cause of the discrepancy, the calculation of the mobility for a similar structure in which the exchange effect is small should give better results. The most suitable molecular-ion combination is that of Li^+ in helium gas. Here the exchange forces are small except at very short distances. Electron exchange is impossible because of the large difference in the ionization energies of Li and He. Hence, we have chosen the above ion molecule combination for investigation.

Before calculating the mobility of Li^+ in He we must know the exchange forces between the ion and the atom. Since this is a problem of some importance in itself, this work will be considered first.

THE EXCHANGE FORCES BETWEEN Li^+ AND He

We have selected for this calculation simple hydrogenic state functions to represent the charge distribution of the ion and atom. Since the Hartree functions were not available for Li^+, we chose those screening constants for the atom and ion that minimized the atomic energy. The procedure followed for the greater part of this section

* Part of a dissertation presented to the faculty of the Graduate School of Yale University in candidacy for the degree of Doctor of Philosophy.

[1] P. Langevin, Ann. Chim. Phys. **5**, 245 (1905).
[2] S. Chapman, Phil. Trans. **A216**, 279 (1916); **A217**, 115 (1917).
[3] D. Enskog, Inaug. Diss. (Uppsala, 1917).
[4] H. R. Hassé and W. R. Cook, Phil. Mag. **12**, 554 (1931).
[5] Massey and Mohr, Proc. Roy. Soc. **A144**, 188 (1934).
[6] A. M. Tyndall and C. F. Powell, Proc. Roy. Soc. **A134**, 125 (1931).
[7] E. A. Hylleraas, Zeits. f. Physik **71**, 739 (1931).
[8] E. Majorana, Nuovo Cimento **8**, 22 (1931).
[9] L. Pauling, J. Chem. Phys. **1**, 56 (1933).
[10] S. Weinbaum, J. Chem. Phys. **3**, 547 (1935).
[11] See A. M. Tyndall, *The Mobility of Positive Ions in Gases* (Cambridge University Press, 1938), p. 36.

was one outlined by Rosen.[12] The one-electron function used for Li^+ was

$$a=\left[\left(\frac{43}{16a_0}\right)^3\frac{1}{\pi}\right]^{\frac{1}{2}}\exp\left(-\frac{43}{16}r_a\right),$$

that for He

$$b=\left[\left(\frac{27}{16a_0}\right)^3\frac{1}{\pi}\right]^{\frac{1}{2}}\exp\left(-\frac{27}{16}r_b\right),$$

where a_0 is the radius of the first Bohr orbit, r is measured in a_0. The theory and some of the functions necessary for the evaluation of the integrals occurring in the expression for the energy are given by Rosen, whose notation will be followed here. For the long range repulsive forces, several approximations are valid. We may take

$$I^2K_2\sim I^2/R,$$
$$IJ_3(a)\sim IJ_1(a),$$
$$IJ_3(b)\sim IJ_1(b).$$

The appearance of two screening constants in the integrals causes slightly more labor in evaluation of the integrals than in the case of one, but, with the exception of J_2, the exchange integral, little difficulty was encountered. J_2, on the other hand, turns out to be an infinite series and, when the difference in screening constants is unity as it is in this case, a large number of terms would be needed. To avoid this, the following approximation used previously by Gentile[13] was employed.

$$J_2=\int\int\frac{a_1b_1a_2b_2dv_1dv_2}{r_{12}}$$
$$\sim\int\int a_1b_1a_2b_2dv_1dv_2\frac{\int\int\frac{a_1^*b_1^*a_2^*b_2^*dv_1dv_2}{r_{12}}}{\int\int a_1^*b_1^*a_2^*b_2^*dv_1dv_2}$$

TABLE I. Repulsion energy between Li^+ and He.

R in A	Δw in ergs
1.05	3.442×10^{-12}
1.58	1.508×10^{-13}
2.11	6.846×10^{-15}
2.64	3.109×10^{-16}
3.16	1.412×10^{-17}

[12] N. Rosen, Phys. Rev. **38**, 255 (1931).
[13] G. Gentile, Zeits. f. Physik **63**, 795 (1930).

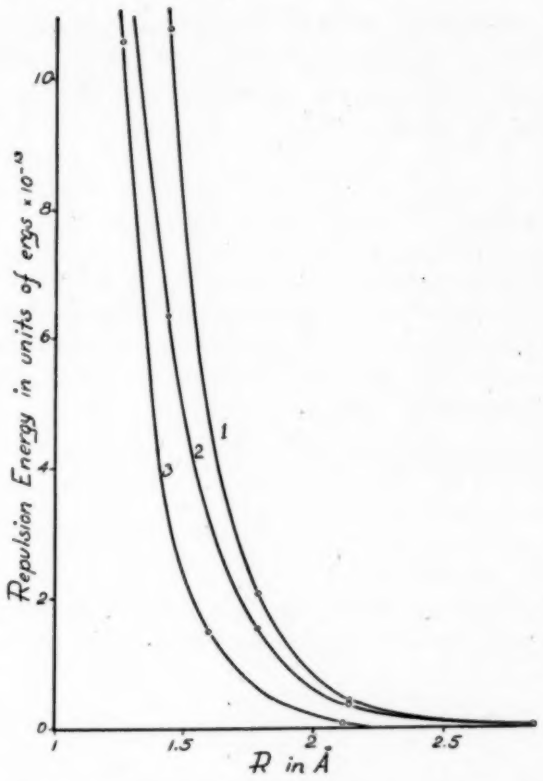

FIG. 1. (1) Repulsion energy between two He atoms as calculated by Slater. (2) Repulsion energy between two He atoms as calculated by Rosen. (3) Repulsion energy between Li^+—He.

where

$$a_1^*=b_1^*=\left[\left(\frac{43+27}{2\times16a_0}\right)^3\frac{1}{\pi}\right]^{\frac{1}{2}}\exp\left(-\frac{43+27}{2\times16}r_1\right).$$

Carrying out the above calculations, one obtains the values shown in Table I for Δw, the repulsion energy between Li^+—He. To the degree of accuracy of the calculations, Δw can be represented by

$$\Delta w=1.61\times10^{-9}\,e^{-5.89R}\text{ ergs},\quad R\text{ in A}.$$

Figure 1 is a graph of this interaction compared with the repulsion energy between two helium atoms as calculated by both Rosen[12] and Slater.[14]

THE MOBILITY OF Li^+ IN He

The mobility K of ions in a given gas is proportional to the diffusion coefficient D_{12} of the ions in that gas. The expression for this is

$$K=D_{12}e/RT,\qquad(1)$$

[14] J. C. Slater, Phys. Rev. **34**, 1293 (1929).

e being the charge on the ion, R the gas constant, and T the absolute temperature of the gas. The theory necessary for the calculation of D_{12} is given by Chapman.[2]

$$D_{12}=\frac{1}{1-\epsilon_0}\frac{3}{4\pi\nu_0 JM}\frac{1}{\mathrm{K}'_{12}(0)}, \tag{2}$$

where $M=M_aM_b/(M_a+M_b)$ and M_a and M_b are the masses of the ion and gas molecule, respectively, $J\equiv 1/2RT$, ν_0 is the number of molecules per unit volume, ϵ_0 is a correction term that is usually small, and

$$\mathrm{K}'_{12}(0)=8\pi^{-\frac{1}{2}}\{JM\}^{5/2}\times\int_0^\infty \exp(-JMV^2)Q_D V^5 dV. \tag{3}$$

V is the velocity of the ion relative to the atom, and Q_D, the cross section for diffusion, is given by

$$Q_D=2\pi k^{-2}\sum_{n=0}^{\infty}\left\{(2n+1)\sin^2\eta_n -2(n+1)\left(\frac{\sin 2\eta_n \sin 2\eta_{n+1}}{4}+\sin^2\eta_n\sin^2\eta_{n+1}\right)\right\}, \tag{4}$$

where $k=2\pi MV/h$, and the η_n are the phase shifts introduced by the potential $\delta(r)$. The phases are defined in the following way. Let $G_n(r)$ be the bounded solution of

$$G_n''(r)+\left[k^2-U(r)-\frac{n(n+1)}{r^2}\right]G_n(r)=0, \tag{5}$$

with $U(r)=(8\pi^2M/h^2)\delta(r)$, then, for large r, $G_n(r)$ will have the asymptotic form

$$G_n(r)\sim\sin(kr-\tfrac{1}{2}n\pi+\eta_n). \tag{6}$$

η_n is thus defined. Approximate expressions for η_n have been derived for special cases. When the phases are small, i.e., less than $\pi/2$, and n large, the Born[15] approximation

$$\eta_n=-\frac{4\pi M}{h^2}\int_0^\infty \delta(r)[J_{n+\frac{1}{2}}(kr)]^2 r dr, \tag{7}$$

in which $J_{n+\frac{1}{2}}(kr)$ is the Bessel function of order $n+\frac{1}{2}$, is particularly useful. When the phases are large and n small, the approximation due to Jeffreys,[16]

$$\eta_n=\int_{r_0}^{r}\left[k^2-U(r)-\frac{n(n+1)}{r^2}\right]^{\frac{1}{2}}dr+\frac{(2n+1)\pi}{4}-kr, \tag{8}$$

r_0 being the largest zero of $[k^2-U(r)-(n(n+1)/r^2)]$, is valid. In the intermediate region where both approximations fail, the phases are usually obtained by plotting the phases as calculated by both methods against the order n and interpolating.

A difficulty arises when the above procedure is applied to the present problem. The phases are not continuous functions of the order n; several discontinuities may occur. In our case a discontinuity occurs in about the region where both the above approximations fail. This makes interpolation difficult and inexact. To avoid this difficulty a modification of the Jeffreys approximation has here been developed which enables one to pass, without interpolation, from the region where the phases are large into that where the Born approximation is valid.

Most of the error in the Jeffreys approximation arises in the neighborhood of the point $r=r_0$. Here the terms, assumed to be small, become infinite and, the phase not being known exactly, is taken to be $\pi/4$. A much better point to start the integration is at the first zero of G_n after r_0, which we will call r_1, i.e., $G_n(r_1)=0$. Here the phase is π and we have passed over the region where the neglected terms contribute anything appreciable. If this is done, the phase becomes

$$\eta_n=\int_{r_1}^{r}\left[k^2-U(r)-\frac{n(n+1)}{r^2}\right]^{\frac{1}{2}}dr+\frac{(n+2)\pi}{2}-kr. \tag{9}$$

r_1 is obtained by expressing $U(r)$ at r_0 in the form

$$U(r)=A+B/r^2.$$

[15] See N. F. Mott and H. S. W. Massey, *The Theory of Atomic Collisions* (Oxford University Press, 1933), p. 28.

[16] H. Jeffreys, Proc. Lond. Math. Soc. [II] **23**, Part 6; Phil. Mag. **33**, 451 (1942).

TABLE II. Comparison of the phases for $k=6\times10^8$ as calculated by different methods.

n	η_n (Jeffreys)	η_n (Modified Jeffreys)	η_n (Born)
23	0.86π	0.76π	0.62π
24	0.71π	0.64π	0.55π
25	0.60π	0.55π	0.49π
26	0.50π	0.48π	0.45π
27	0.44π	0.42π	0.39π
28	0.40π	0.37π	0.35π
29	0.36π	0.33π	0.32π
30	0.33π	0.30π	0.29π
31	0.29π	0.27π	0.26π
32	0.26π	0.23π	0.24π
33	0.24π	0.22π	0.22π

Then Eq. (5) takes the form

$$G_n''(r)+\left[k^2-A-\frac{n(n+1)+B}{r^2}\right]G_n(r)=0. \quad (10)$$

This is Bessel's equation of order $p=[n(n+1)+B+\frac{1}{4}]^{\frac{1}{2}}$ in the variable $cr=r(k^2-A)^{\frac{1}{2}}$. The value of r_1 can be obtained from a table of first roots of Bessel's functions of order p. Table II shows the phases for $k=6\times10^8$ in the critical region. Here the Jeffreys approximation is usually too high while the Born approximation is too low. Our modified Jeffreys approximation seems both to divide the region and converge rapidly to the Born result which is known to be valid for large r.

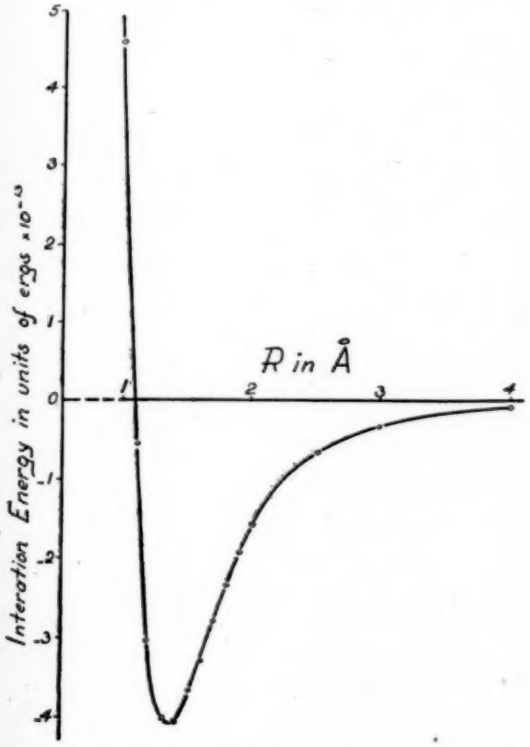

FIG. 2. Calculated interaction energies $\delta(r)$ of Li^+-He.

The calculation of the phases for collisions between Li^+ and He requires a knowledge of the potential $\delta(r)$ (or $U(r)$) in Eq. (5). This potential is an attraction at large distances of separation and turns to a repulsion only at small distances due to the effect of the exchange forces calculated in the previous section. Margenau[17] has shown that the attraction may be approximated by two terms; one varying as r^{-4}, the other as r^{-6}. These terms arise from the polarizability of both the ion and the atom. When the atom moves into the field of the ion, it acquires not only an induced dipole moment but also quadrupole moment and higher moments. The dipole moment gives rise to the term in r^{-4} while the quadrupole moment contributes to the term in r^{-6}. The remaining contribution to this term arises from the polarizability of the ion itself. This is analogous to the van der Waals interaction between neutral atoms and also varies as r^{-6}. The total interaction is given by

$$\delta(r)=v(r)-(\alpha/r^4)-(\beta/r^6), \quad (11)$$

where $v(r)$ is the repulsion energy. From Margenau's paper we obtain the following values for these constants $\alpha=2.36\times10^{-44}$ erg cm^4; $\beta=1.84\times10^{-60}$ erg cm^6. The graph of this interaction is shown in Fig. 2.

To simplify the calculation, we have employed an approximation used by Massey and Mohr[5] and others. The phases start out large for small values of n and suddenly become small (at the discontinuity mentioned before), then diminish asymptotically to zero. In the region of large phase, $\sin\eta_n$ oscillates rapidly. Hence we permit ourselves to replace $\sin^2\eta_n$ and $\sin\eta_n$ by their average values $\frac{1}{2}$ and 0 in this region. Thus, if the first small phase occurs for $n=m$, the contribution to the collision cross section, $Q_D^{(1)}$, say, is

$$Q_D^{(1)}=\tfrac{1}{2}\pi k^{-2}m(m+1). \quad (12)$$

The contribution for $n>m$, $Q_D^{(2)}$, is calculated and added to $Q_D^{(1)}$, to give the total collision cross section for diffusion. Thus

$$Q_D=Q_D^{(1)}+Q_D^{(2)}. \quad (13)$$

[17] H. Margenau, J. Phil. Sci. 8, 603 (1941).

For $n \geqq m$, η_n was calculated by the improved Jeffreys approximation up to that value of n for which this approximation agreed numerically with the Born approximation. For higher n, the Born expression was used. The cross section Q_D was calculated for $k \times 10^{-8} = 2, 4, 6, 8, 10$, and 20. The results plotted against $1/k$ are shown in Fig. 3 to a good approximation; Q_D can be expressed as

$$Q_D = 2\pi \times 10^{-16}\left(\frac{28.95}{k} - 0.68\right). \quad (14)$$

When this is put into expressions (3), (2), and (1), we obtain the following result for K in cm²/volt sec.

$$K = \frac{19.7}{1.265 - 0.0146T^{\frac{1}{2}}}. \quad (15)$$

Table III shows the value of K for various temperatures as calculated by this formula and the experimental ones as given by Hoselitz.[18]

DISCUSSION OF RESULTS

It is seen that the calculated values of the mobility are lower than the experimental ones. At 18°C the error is about 30 percent. This discrepancy is greater than the errors introduced into the calculations. One source of error might be the approximation involved in setting $\sin^2 \eta_n = \frac{1}{2}$ for large phases, hence, this was checked for several values of k. For $k = 4 \times 10^8$, the approximation was found to yield too low a value, while for $k = 6 \times 10^8$ it was exact. Since this error is likely to be greater at lower k values where there are fewer terms to average out the deviations in $\sin^2 \eta_n$, the points for determining Q_D were taken in the region $k \times 10^{-8} = 6, 8, 10, 20$, as shown in Fig. 3. This is also the important region in determining the mobility for the temperature range considered. It seems unlikely that the error in Q_D as derived from our potential function is greater than 10 percent. It was also thought that the neglect of ϵ_0 in Eq. (2) might give rise to an appreciable error. This was checked and preliminary calculations indicate that it can be neglected. This is to be expected as the mobility is determined largely by the r^{-4} term in $\delta(r)$ and, classically, ϵ_0 is zero for this force law.

TABLE III. Experimental and theoretical values of K at various temperatures.

T	K_{exp}	K_{th}
20	20	16.4
78	21.8	17.4
90	22.2	17.5
195	23.9	18.6
291	25.8	19.4
389	27.8	20.1
483	29.2	20.9

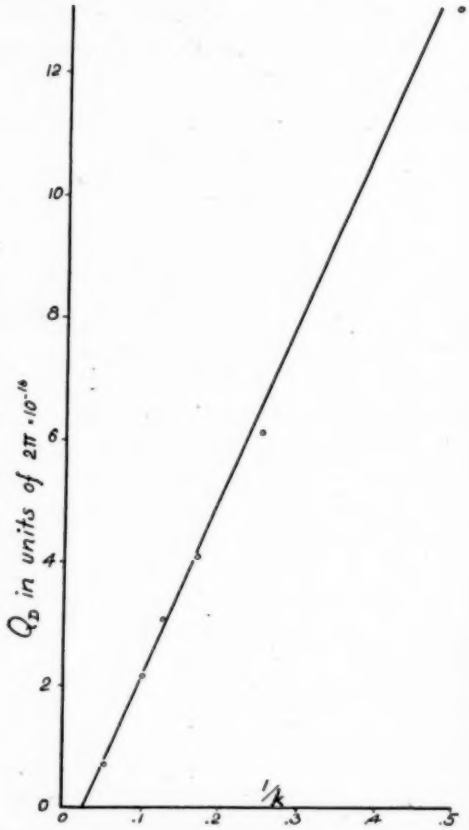

FIG. 3. Q_D plotted as a function of $1/k$.

It should also be pointed out that theoretically we are not justified in using the zero velocity approximation for the force law, whereas the correct expression contains velocity-dependent terms.[19] This approximation should cause little trouble in the present calculation, as the mobility is determined primarily by the polarizability term, and there is very little difference between the polarizability of He for radiofrequencies and for optical frequencies.

[18] K. Hoselitz, Proc. Roy. Soc. **A177**, 200 (1940).

[19] See H. S. W. Massey and R. A. Smith, Proc. Roy. Soc. **A142**, 142 (1933).

It is very probable that the greatest error arises in the addition of the first-order exchange energy as calculated from wave functions satisfying the Pauli principle to that arising from the polarizability calculated by an entirely different method. In the region of the minimum in $\delta(r)$ both calculations break down, so that its depth can never be accurate. Calculations of this potential minimum from clustering data of Li^+ and He at low temperatures indicate indeed that our minimum may be several times too deep.[20] Should the exact calculation give rise to a saturation in the polarizability of He at a distance of separation of about 2.5A, good agreement between the theoretical and experimental mobility of Li^+ in He would result. It would seem very desirable, therefore, to check the addition of the polarizability term in a way similar to the check made on the van der Waals term by Margenau.[21]

While the present calculations are not in complete agreement with experimental determinations of Li^+ in He gas, the agreement is better than between the calculations of the mobility of He^+ in He and the accepted experimental value. This improvement might be taken to support Mott's suggestion that Massey and Mohr may have overestimated the effect of the exchange forces in their assumption concerning the mean period of electron exchange, which they took to be small compared to the time of passage of the ion past the atom.

Unfortunately the He^+-He problem is not so clear-cut. It is also possible that the experimental results may be confused by "clustering" of the ion. An examination of the exchange forces between He^+ and He shows that they have a considerable range; they become important at about 3A separation between the atom and the ion. The exchange energy between two He atoms becomes important at a shorter range, about 2A. Considering the fact that the internuclear separation between the two atoms in He_2^+ is only 1A, it is quite possible that the repulsion energy between the clustered ion and He, i.e., between He_2^+-He, would not be much greater than at 3A. In this case, the interaction between this "clustered" ion, He_2^+, and He would differ very little from the antisymmetrical case V_a, calculated by Massey and Mohr.[22] They calculated, using V_a alone, that the mobility of He^+-He should be 25 cm^2/volt sec. If this were corrected for an ion of mass 8 instead of 4, the value comes out around 22 cm^2/sec. volt. This agrees very well with the value 21.4 cm^2/sec. volt measured by Tyndall and Powell. If this conjecture proves correct, we have the anomalous situation of the "clustered" ion, He_2^+, having a higher mobility than the unclustered one, He^+.

An examination of the work of Tyndall and Powell[23] lends support to this hypothesis. These workers have made two different determinations of the mobility of He ions in He gas. The gas, in both cases, was of equal purity, but a different ion source was used in each case. From their first measurements using an α-particle source they obtained ions having the mobility of 13 cm^2/sec. volt. They express their disappointment in obtaining a value so much lower than the theoretical values existing at that time. They made another determination using another ion source, this time ions formed from a glow discharge in He, and were gratified in obtaining a mobility, which they attribute to He^+ in He gas, of 21.4 cm^2/sec. volt, which agreed favorably with the theoretical values at that time. Three years later, Massey and Mohr made their calculation of the mobility of He^+ in He and found that their value of 12 cm^2/sec. volt was in sharp disagreement with the accepted value.

The question as to whether the above disagreement is due to an anomalous behavior of the clustered He_2^+ ion or to an error in the calculations can be settled unambiguously only by an identification of the ions whose mobility is measured. However, some information can be gained from an examination of the type of ion sources used. From a consideration of these ion sources it would seem that an incorrect assignment of mobilities may have been made. Arnot and M'Ewen[24] have investigated the production of He_2^+ in He and find that the relative number

[20] R. S. Munson and K. Hoselitz, Proc. Roy. Soc. **172**, 43 (1939).
[21] H. Margenau, Phys. Rev. **56**, 1000 (1939).
[22] See reference 5. Massey and Mohr calculated the mobility using the symmetrical V_s and antisymmetrical potential V_a alone to investigate the effect of charge exchange. This case corresponds to the latter.
[23] A. M. Tyndall and C. F. Powell, Proc. Roy. Soc. **A129**, 162 (1930).
[24] F. L. Arnot and M. B. M'Ewen, Proc. Roy. Soc. **A171**, 106 (1939).

of He_2^+ ions increases with pressure. At discharge pressures one would expect that many, if not all, the ions would be He_2^+. For their gas discharge source, Tyndall and Powell find only *one* ion present; one would expect, then, that this ion be He_2^+. They find this ion to have the high mobility of 21.4 cm²/sec. volt. While this is not a proof of the incorrectness of the identification of the mobility ions in He, this point should certainly be cleared up before any more theoretical work is done to attempt removal of the discrepancy.

ACKNOWLEDGMENT

The author wishes to express his thanks to Professor H. Margenau of Yale University for suggesting this problem and for valuable suggestions and criticisms during the progress of the work and also to Professor Lars Onsager for valuable discussions and criticisms.

PHYSICAL REVIEW VOLUME 66, NUMBERS 9 AND 10 NOVEMBER 1 AND 15, 1944

The Photo-Conductance of Evaporated Bismuth Films

ALFRED H. WEBER AND LAWRENCE W. FRIEDRICH, S. J.
Department of Physics, Saint Louis University, St. Louis, Missouri
(Received August 10, 1944)

The electrical conductance of Bi films evaporated on Pyrex in high vacuum was measured when the films were "dark" and when illuminated with 2537A radiation. A photo-conductance effect was observed for all films less than about 292 atom layers thick whether the Bi was deposited at room temperature or at liquid-air temperature. The photo-conductance effect disappears with increasing film thickness much more rapidly for films kept at liquid-air temperature than for those at room temperature. For films deposited discontinuously (that is, successive layers are allowed to age), the effect disappears at about 11 atom layers thickness for liquid air-temperature-deposited films and at about 172 atom layers thickness for room-temperature-deposited films. The experiments definitely point to the conclusion that *true* photo-conductance is not present in these films, that the films which exhibit photo-conductance are patch-like in structure; therefore, the observed photo-conductance is assigned to photo-electric emission between film patches.

IN reported[1] investigations of the effect of light on thin metallic films there is evident uncertainty about the existence of *true* photo-conductance in these films. *True* photo-conductance may be defined as the increased electrical conductance of a metallic substance caused by additional electrons (which have absorbed incident quanta) in the conduction band. True photo-conductance has been shown to be a property of the semimetallic element selenium and of compounds like zincblende, but its existence, or non-existence, in pure metals has not been established. Photo-conductance in general is here defined as the electrical conductance of an illuminated substance; it has a wider meaning than *true* photo-conductance and is contrasted with dark conductance.

The present paper reports an investigation of the photo-conductance of Bi films, deposited on Pyrex by evaporation in high vacuum, aimed at determining whether true photo-conductance exists. The influence of temperature (both of deposition temperature and varying film temperature), of film thickness, and of film aging were systematically studied.

EXPERIMENTAL

All experiments were with Bi deposited on Pyrex by evaporation (at 1.11 atom layers min.$^{-1}$) in high vacuum. The experimental tube, outgassing procedure, and measurement of film thickness have been described.[2] Figure 1 with its legend describes the circuit used for measuring

[1] B. Gudden and R. Pohl, Physik. Zeits. **23**, 417 (1922); R. S. Bartlett, Phys. Rev. **26**, 247 (1925); A. Etzrodt, Physik. Zeits. **35**, 433 (1935); R. Suhrmann and G. Barth, Zeits. f. Physik **103**, 133 (1936); T. Fukuroi, Sci. Pap. Inst. Phys. Chem. Research **32**, 187 (1937); Q. Majorana, Physik. Zeits. **38**, 663 (1937); T. C. Wilson, Phys. Rev. **55**, 316 (1939); A. H. Weber and D. F. O'Brien, Phys. Rev. **60**, 574 (1941).

[2] A. H. Weber and L. J. Eisele, Phys. Rev. **60**, 570 (1941).

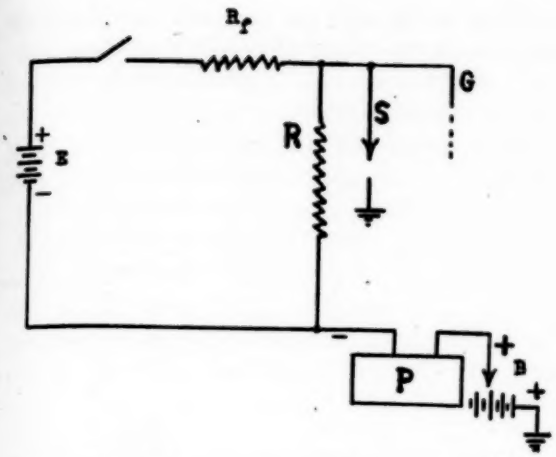

FIG. 1. Circuit for measuring conductances. E, 22.5 v B battery; R_f resistance of Bi film; R, 9.6×10^{11} ohm fixed resistor; P, L and N potentiometer; B, bank of 16 1.5-v cells with tap switch; S, earthing switch; G, grid of d.c. amplifier tube (D-96475) in Barth-Penick circuit.

electrical conductances. The null method as follows was employed. (1) The dark conductance current is balanced out (by adjustment of B and potentiometer) and measured; (2) the film is illuminated with the 2537A line of mercury[3] and any additional conductance current is balanced out and measured. This arrangement is sensitive to conductances as small as 8.62×10^{-17} ohm^{-1}.

Dark conductances and photo-conductances were measured as a function of Bi film thickness in four types of runs: (1) deposition at room temperature, conductances measured during periods when deposition of Bi was interrupted; (2) deposition at liquid-air temperature (measured as about −179°C), deposition interrupted for conductance measurements; (3) deposition at room temperature, conductances measured without interrupting deposition; (4) deposition at liquid-air temperature, conductances measured without interruption of deposition.

Also, dark conductances and photo-conductances were measured as a function of film temperature for a given film thickness by allowing films for which a type 2 run had been completed to warm up to room temperature during the conductance measurements (type 5 run).

[3] Radiation of 2537A wave-length caused photoelectric emission in the thinnest films obtained in these experiments. See reference 2.

RESULTS AND DISCUSSION

Figures 2–6 show the results of the five types of runs just described. The experiments show definitely that the observed photo-conductance is limited to *thin* Bi films. In no case was the

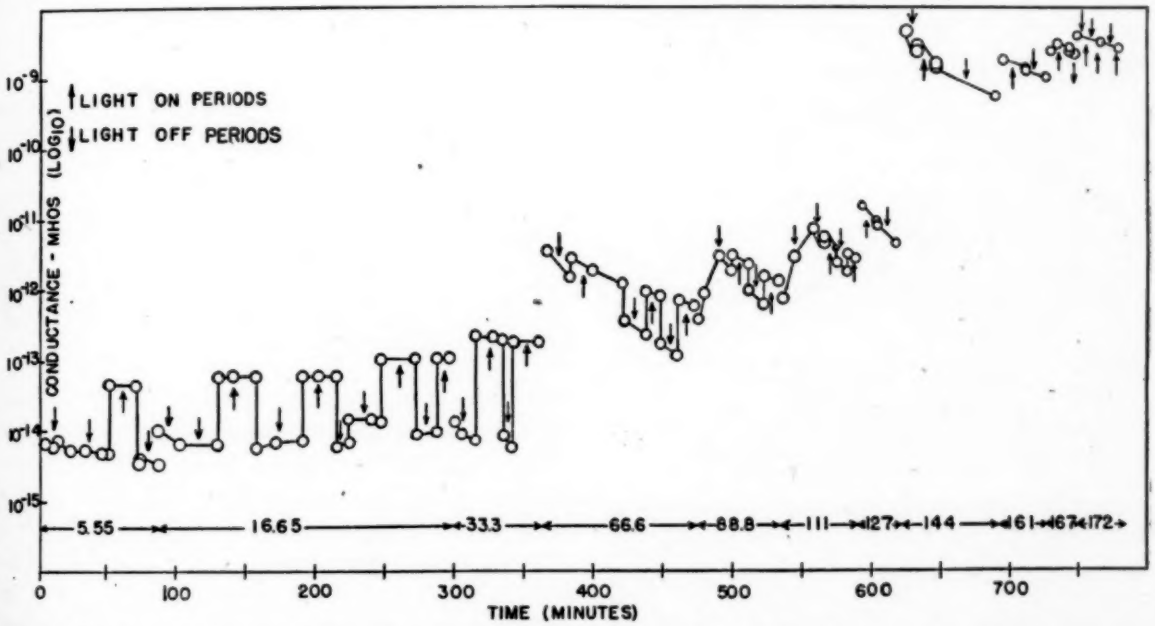

FIG. 2. Dark conductance ("light off") and photo-conductance ("light on") for interrupted deposition of Bi at room temperature (type 1 run). 235 points are included, all of which cannot be shown. Numbers between horizontal arrows indicate film thickness in atom layers. Intervals during which the film was deposited or during which the film aged without observations being made (varying between 19 min. and 91.5 hr.) are omitted. Conductance measurements at each thickness were begun immediately after interrupting deposition. Total time to obtain data—10 days approximately.

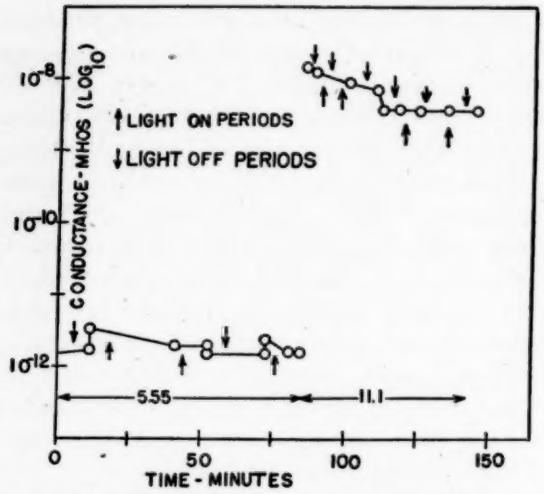

FIG. 3. Conductances for interrupted deposition of Bi at liquid-air temperature (type 2 run). Numbers between horizontal arrows indicate film thickness in atom layers. The positions of the vertical arrows indicating "light on" and "light off" are not precise as to time for the 11.1 atom layers thickness since the light was turned on and off many times without noticeable effect on the conductance. Intervals during which the film was deposited or during which the film was aged without observations being made (but maintained always at liquid-air temperature) are omitted.

electrical conductance of a film influenced by the 2537A radiation beyond a thickness of 292 atom layers (for the room-temperature-deposited, unaged film of Fig. 4); for films kept at liquid-air temperature the effect of light (2537A) on electrical conductance was not observable beyond some 11–33 atom layers (Figs. 3, 5). Even for the room-temperature-deposited (but aged) film of Fig. 2, the maximum effect of the light is in the region of 33 atom layers as is shown by Fig. 7.

The observed large influence of the temperature of deposition on the photo-conductance is strongly suggestive of a patch structure of the thin films. All results of this investigation are consistent with the hypothesis that the Bi on

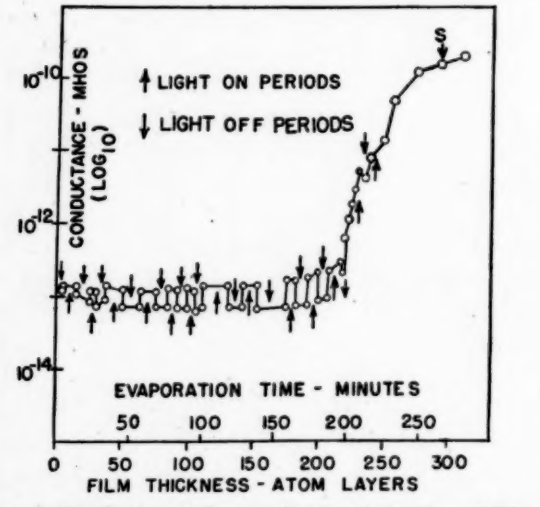

FIG. 4. Conductances for continuous deposition of Bi at room temperature (type 3 run). 116 points are included, all of which cannot be shown. *S* at the upper right indicates the thickness, 292 atom layers, for which the photo-conductance effect disappeared. Because of the rapid increase in conductance during deposition and the rapidly decreasing magnitude of the photo-conductance effect beyond film thicknesses of about 225 atom layers, the increase in conductance when the film was illuminated (definitely present to 292 atom layers thickness) could not be measured with sufficient accuracy to permit plotting.

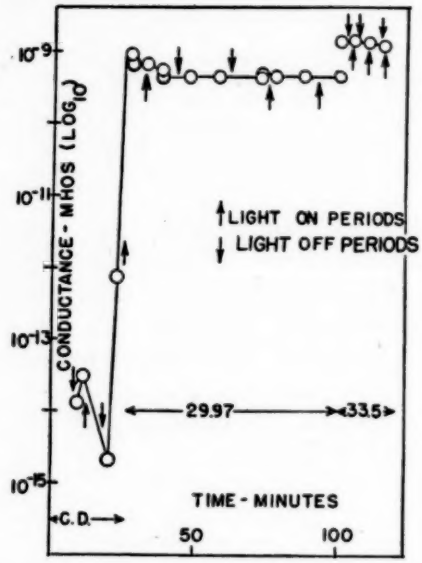

FIG. 5. Conductances for attempted continuous deposition of Bi at liquid-air temperature (type 4 run). C. D. between the horizontal arrows indicates the period of continuous deposition. After attaining a film thickness of 29.97 atom layers continuous deposition was stopped since the conductance (both dark conductance and photo-conductance) was changing too rapidly to permit any observations of the effect of the radiation. For the 29.97 atom layers thickness a slight photo-conductance effect was observed; at the next thickness, 33.5 atom layers, there was no observable difference between dark conductance and photo-conductance.

deposition has a marked tendency to form discrete aggregations. At room temperature increased thermal mobility of the deposited atoms initiates or at least accelerates this aggregation process. Hence film cracks develop readily in thin films at room temperature. At the lower (liquid-air) temperature the aggregation process is inhibited since thermal mobility of the condensed atoms is correspondingly small.

As a result of this assumed patch structure the observed increase in electrical conductance of the

illuminated Bi films is assigned to photoelectric emission between patches, for the large temperature sensitivity of the effect would be difficult to explain as true photo-conductance. Evidently at some thickness (not over 292 atom layers in the present experiments) the film cracks will disappear and the metal will deposit continuously over the deposition surface. The rapid disappearance with increasing film thickness of the photo-conductance effect for the liquid-air-temperature-deposited films (in Figs. 3 and 5 the effect of light disappears at about 11–33 atom layers thickness) where movement toward aggregation is small, is in obvious agreement with the patch photoelectric emission explanation. The reappearance of the phenomena, in a film which no longer exhibited the photo-conductance effect at liquid-air temperature, by simply warming the film to room temperature (Fig. 6) is considered the clinching evidence here for it is expected that the film will begin to "crack" with the onset of the aggregation process as thermal mobility of the deposited atoms increases.

Aging of a thin film at room temperature should increase the degree of aggregation of the film material and should normally result in further widening of film cracks so that photo-conductance (and dark conductance also) is expected to decay with time. This result is clearly present in these experiments as from Fig. 2 it is seen that as a general rule both dark conductance and photo-conductance decrease with time at all film thicknesses.[4,5]

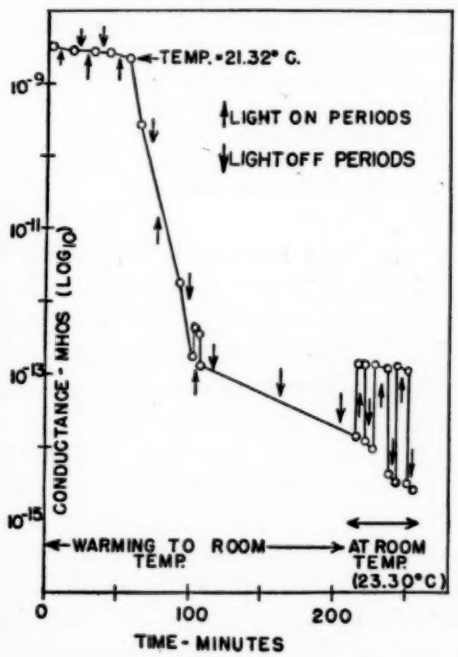

FIG. 6. Reappearance of photo-conductance effect of a Bi film deposited at liquid-air temperature upon warming to room temperature (type 5 run). Same film as Fig. 3 (film deposited and maintained at liquid-air temperature; photo-conductance effect had disappeared at 11.1 atom layers thickness).

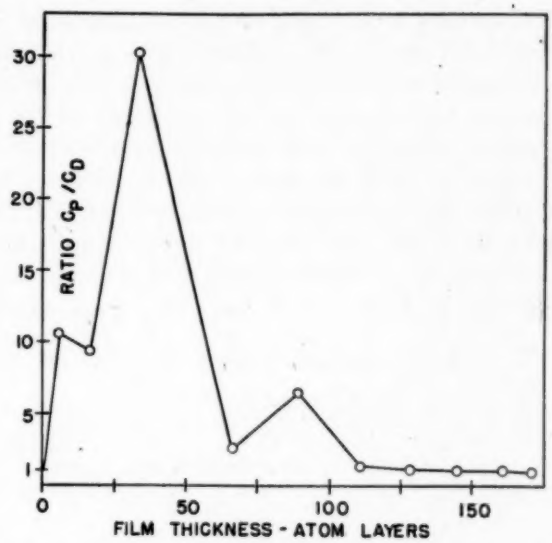

FIG. 7. Ratio of photo-conductance to dark conductance with increasing film thickness for the film of Fig. 2 (interrupted-room-temperature-deposit).

It is clear, furthermore, that as the thickness of the film approaches that at which photo-conductance disappears, aging, which would permit more time for film patches to coalesce, might reasonably act to cause the photo-conductance effect to disappear at smaller film thicknesses than would be so if aging were avoided. Comparison of Fig. 4 for an unaged film with Fig. 2 for a film of successively aged layers indicates that this is apparently what takes place since the effect disappears at 172 atom layers thickness for the aged film and persists until 292 atom layers thickness is reached for the unaged film.

Evidence in the literature supporting the con-

[4] Slight increases or lack of decreases with time in the conductances of the thinner films of Fig. 2 is ascribed to film instability or to some unknown action of the light on these very thin films as perhaps a charging and discharging of the film patches.

[5] It should be stated explicitly that light (2537A) does not affect permanently the film conductance for Fig. 2 shows that after interrupting the incident light the film conductance drops directly to a value which appears to be the same as that which would have been recorded had the film not been illuminated.

clusions and hypotheses of this investigation is found: (1) in the experiments on photoelectric emission and electrical conductance of Bi films[6] reported by one of the present authors (A.H.W.) which in turn are confirmed by Armi's experiments with thin Pb films,[7] (2) in Kirchner's[8] electron diffraction study of Bi films less than 100A thick which led him to conclude that the films were of a fibrous nature;[9] (3) in electron microscope pictures of various thin films which show that patches some 500A long separated by gaps of about half this length are present.

The results of the present investigation are considered very definite evidence that true photo-conductance is not a property of thin metallic films. This is the majority opinion of other investigators.[1] The experiments of Fukuroi[1] and Bartlett[1] most nearly resemble the present ones. Fukuroi's experiments with thin films of mercury, cadmium, and zinc condensed on glass or quartz are in agreement with this investigation. Bartlett measured the photo-resistance of bismuth films deposited by cathode sputtering and found a small photo-conductance effect but comparison with the present results is difficult because he reports no film thicknesses.

[6] A. H. Weber and D. F. O'Brien, Phys. Rev. **60**, 574 (1941).
[7] E. L. Armi, Phys. Rev. **63**, 451 (1943).
[8] F. Kirchner, Zeits. f. Physik **76**, 576 (1932).
[9] A "cracked" crystalline film is as useful to "explain" the present results as is a fibrous film which necessarily contains cracks. An electron diffraction study of thin Bi films is in progress at Saint Louis University.

PHYSICAL REVIEW VOLUME 66, NUMBERS 9 AND 10 NOVEMBER 1 AND 15, 1944

Atom-Annihilation Cosmic Rays at Mexico City

DANA T. WARREN
The Municipal University of Omaha, Omaha, Nebraska

(Received August 14, 1944)

The directional intensity studies at Mexico City made by Schremp and Baños indicate the value of this method of studying the bright lines predicted by the atom-annihilation hypothesis of Millikan, Neher, and Pickering. The observed peak seems clearly to be such a bright line, as shown by the shape and slope of the curves at the zenith, and the effect of atmospheric absorption at large zenith angles. However, the agreement with the observations of Millikan, Neher, and Pickering is much more doubtful, as shown by the following discrepancies: The peak comes at too small a zenith angle, and would be observed over too wide a range of latitude. These difficulties are of such a sort as to be readily cleared up by further directional studies.

IN two papers,[1] Millikan, Neher, and Pickering present the atom-annihilation hypothesis of the origin of cosmic rays, which supposes the primaries to arise from the change of the mass of atoms into energy of two particles in interstellar space. This results in what in optics is called a "bright line" spectrum with all the particles occurring at definite energy values. Besides the balloon measurements, they present a few data on vertical intensity variations at ground level in Mexico. The possible error assumed is 2 percent while the changes measured are some 4.8 percent. They interpret their values in terms of a two-step increase in intensity which is possible. But it is equally true that a straight line can be drawn through all their values hitting within the 2 percent error every point except Junction, Texas (magnetic latitude $\lambda = 39.5°$, incorrectly given in II as 38.5°), and this point falls even farther off the broken curve assumed in II.

Particular interest therefore attaches to the ground level measurements of Schremp and Baños[2] on the directional intensities at Mexico City. Despite certain inconsistencies,[3] some of which are pointed out below, some important facts can be deduced from a direct consideration of the curves they give. They themselves point

[1] R. A. Millikan, H. V. Neher, and W. H. Pickering, Phys. Rev. **61**, 397 (1942) (hereafter called I); Phys. Rev. **63**, 234 (1943) (called II).

[2] E. J. Schremp and A. Baños, Phys. Rev. **58**, 662 (1940) (called III); Phys. Rev. **59**, 614 (1941) (called IV).
[3] The N–S and E–W asymmetries near the zenith are in very poor agreement with those found by T. H. Johnson [Phys. Rev. **47**, 91 (1935); **48**, 287 (1935)] at Mexico City.

out the existence of a prominent maximum of positive primaries in the exact direction (20° S of west) in which the theory of Lemaitre and Vallarta[4] predicts the maximum admission. Though the uncorrected theory assigns to these primaries an energy 10 or 11 Bev, the correction for the weakness of the earth's field on this side of the world will bring the value of the energy much closer to that of the oxygen-annihilation band found in II at a latitude not very different from this. Such a peak might represent either a banded or continuous spectrum; this appears to be the former. Since the observations give directly the total intensity from all primaries of energy greater than the critical energy[5] corresponding to the given latitude and direction, the energy distribution $I(E)$ of the primaries must be obtained as the negative derivative of the observed intensity distribution. Now the peak represents an increase of some 2.5 percent per degree from the zenith, or more if an allowance is made for the absorption at the peak. It is clear from the curves that if the same rate of increase continues during the next 12° interval, the absorption of the atmosphere must reduce the intensity by a factor about 100/160 which seems impossibly large. A calculation based on the usual formula [Eq. (85) of reference 5] with the exponent 2.5 gives a weakening of about 15 percent, which is much more easily compatible with a decrease from 130 percent to 100 percent of the zenith intensity, as would be required if the increase ceased with the passage of the peak. A drop of some 30 percent is indeed observed in the NE azimuth.

Such difficulties due to atmospheric absorption are a minimum at the zenith, where the absorption is least and varies most slowly. Hence the clearest indication that the peak does indeed correspond to a bright line of a discrete spectrum are found here. The first of these is the immediate observation that the curves are concave upward at the zenith. Now, of the three factors that determine the intensity variation at the zenith, the absorption of the atmosphere and the directional dependence of the critical energy[4] can only give a curve convex upward. Hence the curve of total intensity must be concave upward at this point, which is just past the high energy edge of the peak. In other words, the peak must represent a sharp step in the total intensity, or a bright line in $I(E)$.

A similar conclusion may be reached by the comparison of the east–west and north–south asymmetries at the zenith. Since the E–W asymmetry is due to the difference of the positive and negative primaries, while the N–S is due to their sum, it is first necessary to consider whether there exist negative primaries, and in what amount. Reference III shows an actual peak at 18° in the east,[6] but this disappears in IV. However, the authors conclude, from a comparison with the NE azimuth, that such a hump, due to negative particles, exists. On the basis of a continuous spectrum, the NE and E curves should fall off most steeply, the N and SE curves next.* The E curve lies above the NE, but the SE does not lie above the N. Hence the indication cannot be considered clear unless there is some influence that would invalidate the north curve. Such an influence might be the presence of the penumbra[7] of the positive particles in the N and NW azimuths. If this invalidates the N curve as a basis for comparison, then the negative peak is present to the extent of about 39 percent of the positive. This will reduce the expected E–W asymmetry by a factor 0.61, and increase the N–S by a factor 1.39, so that the ratio of asymmetries, E–W/N–S, will be decreased to 0.44 of what it would be with positives alone.

The theoretical value for positives alone may best be scaled off from Fig. 7 of reference 4, which gives a value of 2.08 for the ratio E–W/N–S. If there is a penumbra in the north, and hence a negative peak, the ratio would be 0.91. The experimental value of this ratio is somewhat uncertain.[8] As measured from III, it comes out

[4] G. Lemaitre and M. S. Vallarta, Phys. Rev. **50**, 493 (1936).

[5] Cf. T. H. Johnson, Rev. Mod. Phys. **10**, 193 (1938).

[6] The position is precisely symmetrical to the 12° west, with respect to the magnetic meridian, here tilted some 3° east.

* Cf. reference 4, Fig. 7.

[7] The effect of the penumbra may be roughly inferred from the work of R. A. Hutner, Phys. Rev. **55**, 15 (1939); *ibid.* **55**, 614 (1939).

[8] A similar determination of the asymmetries at high latitudes [D. Cooper, Phys. Rev. **58**, 288 (1940), H. S. Ribner, Phys. Rev. **56**, 1069 (1939)] gives, as might be expected, a null result. The agreement between the two high latitude papers is very poor. I am indebted to Dr. L. N. Garlough for the calculation of the correlation coefficient as −0.82, a value which has a probability of 1/30 of being accidental in the small sample available.

2.28; from IV it is 3.57. This difference is largely due to a marked decrease in the slope of the N–S curve, which, however, leaves its shape unchanged. If we consider the later curves more reliable, the discrepancy between 3.57 and 2.08 would make the continuous spectrum theory untenable. If the difference is to be attributed to the penumbra, which would raise the northward intensity and lower the asymmetry ratio, then the negative primaries must be included, and the comparison becomes 3.57 to 0.91. It seems very doubtful that the presence of the penumbra could lower the experimental value of the N–S asymmetry by a factor of four. Hence in either case it is difficult to accept the continuous spectrum as determining the conditions at the zenith.

Having thus determined the existence of a bright line in the primary energy spectrum at Mexico City, the next step is the attempt to identify it with one of those found by Millikan, Neher, and Pickering in II. The nearest line found by them is what they call the oxygen-annihilation band, which sets in sharply at Victoria, $4\frac{1}{4}°$ north of Mexico City, but is not observed at all at Valles, only $2\frac{1}{2}°$ north. The intensities seem to depend greatly on method of measurement and depth (considerably greater in II), and afford little basis for comparison. But the theory[4,9] gives clear indications of the relation between the latitude and zenith angle effects in these latitudes. The vertical direction would correspond to a rigidity difference of 0.040 stoermer between Victoria and Mexico City, and this would correspond to a zenith angle of some 40° at Mexico City. This is not very close to the observed value of 12°.

Another difficulty is with the sharpness of the edge observed. If the solid angle covered by the balloon telescopes is 25°×45° ($\frac{1}{2}$ effective), as in I, then at Valles, well north of Mexico City, and where the present peaks must occur at smaller zenith angle, considerable intensity should be observed. This is not found. It will be noted that these discrepancies are of the sort that can largely be straightened out by further studies of the directional effects at different latitudes and atmospheric depths. Such studies clearly would reveal a great deal about the details of the different atom-annihilation bands.

[9] G. Lemaitre and M. S. Vallarta, Phys. Rev. 49, 719 (1936).

PHYSICAL REVIEW VOLUME 66, NUMBERS 9 AND 10 NOVEMBER 1 AND 15, 1944

Cascade Showers in Lead

WAYNE E. HAZEN
Department of Physics, University of California, Berkeley, California

(Received September 9, 1944)

Cascade showers of energies up to 500–1000 Mev have been photographed in a cloud chamber that contained eight lead plates. A comparison with theory is made in terms of the size of a shower at its maximum as a function of the total number of particles in the shower. The conclusion reached is that the theoretical cross sections for radiation and pair production are essentially correct for energies up to 500–1000 Mev.

VERY few experiments have been performed that allow an experimental verification of shower theory for monoenergetic electrons. Anderson[1] and others have measured the energy loss of electrons in solid plates as a function of incident energy. Recent developments[2] indicate that an interpretation of atmospheric absorption curves in terms of shower theory is considerably obscured by the additional difficulties of separating shower phenomena from mesotron production, etc. Other experiments[3] have involved the average effects of electrons (and mesotrons) of all energies. On the other hand, detailed theo-

[1] S. H. Neddermeyer and C. D. Anderson, Phys. Rev. 51, 884 (1937); P. M. S. Blackett, Proc. Roy. Soc. A164, 257 (1938); C. D. Anderson, Phys. Rev. 57, 357 (1940).
[2] M. Schein, W. P. Jesse, and E. O. Wollan, Phys. Rev. 57, 847 (1940).
[3] M. A. Starr, Phys. Rev. 53, 960 (1938); see, e.g., D. K. Froman and J. C. Stearns, Rev. Mod. Phys. 10, 133 (1938).

retical results accurate to perhaps 10 or 20 percent are now available.[4–6]

It is possible to observe the histories, at as many as eight stages, of showers initiated by electrons of energies less than 500 Mev, by placing eight 0.7-cm lead plates in a Wilson cloud chamber.[7] Random photographs with such a cloud chamber have been examined for showers whose entire histories appear to have been recorded. Fifty such showers were found, and the detailed history of one of the best is shown in Fig. 1. Since the total number of showers was rather small, there were no reasonably narrow energy groups containing more than four or five showers. Statistical fluctuations, as predicted,[4] are so large that it is not especially instructive

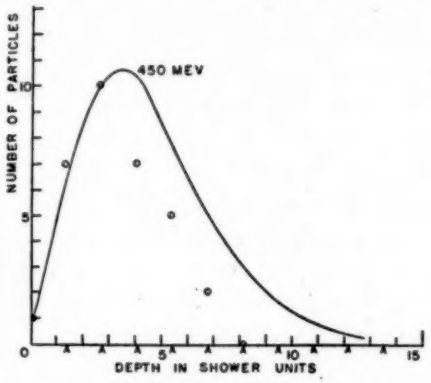

FIG. 1. The complete history of a cascade shower initiated by an electron of energy ~500 Mev. The curve is from the calculations of Bhabha and Chakrabarty (reference 5). The experimental points should be shifted slightly to the right since the electron had passed through several millimeters of wood and glass before reaching the lead plates. The arrows on the abscissa scale indicate depth in terms of lead plates.

to compare individual histories with theoretical curves. This conclusion is particularly true in the present experiment where the original energy can be estimated only from the total number of particles in a shower. When more data are available, it will be possible to compare the average histories of showers in selected energy groups with the theoretical curves.

The best procedure that the author has devised for comparing the experimental results with

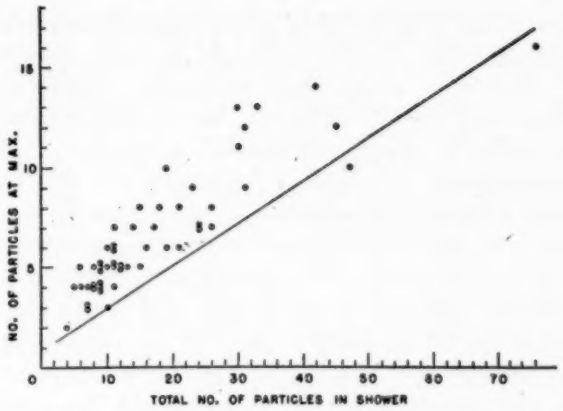

FIG. 2. Experimental points and theoretical curve for the number of particles at the maximum of a cascade shower in lead *versus* total number of particles in the shower.

theory is to plot the number of particles at the shower maximum against total number of particles in the shower. By total number of particles in the shower we here mean the sum total of all the tracks belonging to a particular shower under all of the lead plates. The observed showers are plotted in this manner on the graph of Fig. 2. The theoretical curve of Fig. 2 was obtained from the shower curves of Fig. 3 by plotting the height of a curve at its maximum as a function of the

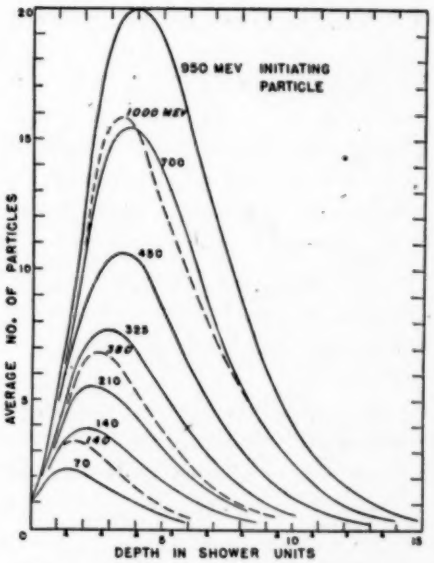

FIG. 3. Theoretical curves for cascade showers in lead. The arrows on the abscissa scale indicate depths in terms of the lead plates used in the experiment. The solid curves were obtained from Rossi and Greisen (reference 4) and the dotted curves from Bhabha and Chakrabarty (reference 5).

[4] B. Rossi and K. Greisen, Rev. Mod. Phys. **13**, 240 (1941).
[5] H. J. Bhabha and S. K. Chakrabarty, Proc. Ind. Acad. Sci. **A15**, 464 (1942).
[6] H. J. Bhabha and S. K. Chakrabarty, Proc. Roy. Soc. **A181**, 267 (1943).
[7] W. E. Hazen, Phys. Rev. **65**, 67 (1944).

sum of the numbers of particles at depth intervals corresponding to the lead plates. The solid curves of Fig. 3 were obtained from Eq. (2.104) of Rossi and Greisen[4] and the dotted curves from the more accurate calculations of Bhabha and Chakrabarty.[5] A comparison of the two sets of curves shows that the more accurate calculations give essentially the same curves as the earlier results, except for the energies of the initiating particles. Since a point on Fig. 2 is determined solely by the shape of a curve in Fig. 3 and not by the initiating energy as such, there is no way in the present analysis to distinguish between the two sets of curves in Fig. 3.

It is seen that almost all of the experimental points lie above the theoretical curve. This result is not entirely unexpected since most of the uncertainties give rise to errors in this direction. In applying the criterion that the entire history of a shower must be observed, it is difficult to eliminate cases in which a few of the divergent particles might have passed out of the illuminated region. Since the lateral spread and hence the likelihood of missing a few particles increases with depth, the total number of observed particles is more likely to be affected than the number of particles observed at the maximum. It is believed that this error is not serious inasmuch as the illuminated volume was large and the change in illumination at the edge of the beam was not abrupt. Furthermore, the lead sheets were covered with steel reflectors of one mm thickness. Iron has a lower atomic number than lead, consequently the transition to iron, which precedes the transition to air, reduces the number of particles. However, the transition thickness is roughly one shower unit[6] whereas one mm of iron is equal to only 1/18 shower unit, and consequently the lead-air transition is not seriously modified.

Let us next consider the approximations in the theoretical calculations. It was assumed that the ionization loss is a constant, independent of energy. This assumption has little effect in the region of high energies since the ionization increases only logarithmically, but it gives a significantly greater range for the low energy particles. The error can be roughly estimated as follows: Assume that multiplication continues until all of the electrons are slowed to the critical energy and then ionization loss predominates. Since the critical energy in lead is seven Mev and the last one Mev of energy is dissipated in a very short distance, the average path of an electron should be shortened by perhaps 14 percent, i.e., the predicted total number of particles in a shower might be too large by 14 percent, whereas the number at the maximum would not be appreciably affected since the average energy is still high at the shower maximum. Scattering also results in a marked reduction of the longitudinal component of the range of the low energy electrons. The calculations of Bhabha and Chakrabarty make use of approximate multiplication cross sections[6] that are too large for all except extremely high energies. This approximation, for the most part, would simply change the scale of a shower curve without marked alteration of the shape of the curve if it were not that the approximation becomes progressively worse for lower energies; this fact leads to a relative increase in height of the tail of a shower curve, where the average particle and photon energies become smaller.

All of the predicted errors, both experimental and theoretical, are in a direction such as to account for the fact that the experimental shower curves are narrower (i.e., fall off more rapidly) than the theoretical curves, and the estimated magnitudes of the errors are sufficient to account for the discrepancy. Therefore it can be concluded that the present experiments, in which detailed observations of the histories of small showers were made, indicate the essential correctness of the radiation and pair production cross sections for energies up to 500–1000 Mev.

Inertia of the Carrier of Electricity in Copper and Aluminum

C. F. KETTERING AND G. G. SCOTT
Research Laboratories Division, General Motors Corporation, Detroit, Michigan
(Received April 20, 1944)

In this experiment the mass-charge ratio of the carrier of an electric current in a metallic conductor was precisely determined. This was done by measuring the change in amplitude resulting from reversing the current in a cylindrical coil supported as a torsional pendulum. Determinations of m/e of the carrier were made for coils of both copper and aluminum and various current values were used in each coil. The average value obtained for m/e of the carrier is 5.69×10^{-9} gram per coulomb. The accepted value of this ratio for the electron is 5.68×10^{-9} gram per coulomb.

INTRODUCTION

IN this work, the mass-charge ratio of the electric carrier in a metallic conductor was determined by means of a very direct measurement on a coil supported as a torsional pendulum. The set-up to determine this ratio was made during the latter part of 1940 by use of a technique which had been previously developed for other work.

The acceleration of a metallic conductor owing to the inertia of an electric current was predicted by Maxwell. It was first experimentally investigated by Barnett,[1] in 1930, who obtained an approximate value for the mass-charge ratio of the electric carrier. The production of an e.m.f. by acceleration, which is the converse of this experiment, has also been investigated.[2] The present experiment, however, is much more precise and the results show conclusively that the carrier of the electric current has the same mass-to-charge ratio as that of the electron.

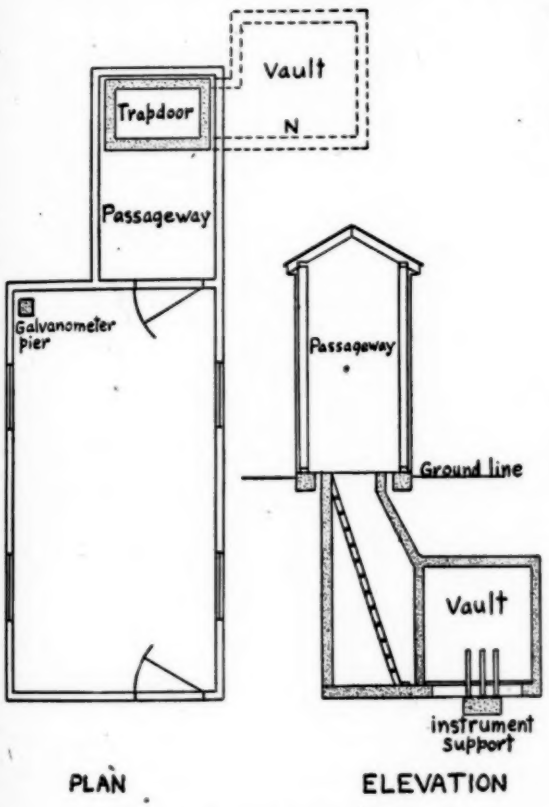

FIG. 1. Magnetic test station.

The theory involved in this experiment is exceedingly simple. However, because of the extremely small changes in angular momentum involved, the experimental difficulties are considerable. Therefore, the greater part of this paper gives a description of the apparatus and the technique necessary to obtain with accuracy these very small measurements.

Three copper coils of various shapes and one aluminum coil were used in this experiment. Also the ratio m/e for two or three different current values was measured for each coil. The m/e values for the various coils check each other very closely and the average of the four coils checks the generally accepted value for m/e of the electron within 0.2 percent.

MAGNETIC TEST STATION AND FIELD NEUTRALIZING COILS

The apparatus necessary for this experiment was set up in a test station located at the General Motors Proving Grounds. This station had been

[1] S. J. Barnett, Phil. Mag. **12**, 349 (1931).
[2] R. C. Tolman and T. D. Stewart, Phys. Rev. **8**, 97 (1916); R. C. Tolman, S. Karrer, and E. W. Guernsey, Phys. Rev. **21**, 525 (1923); R. C. Tolman and L. M. Mott-Smith, Phys. Rev. **28**, 794 (1926).

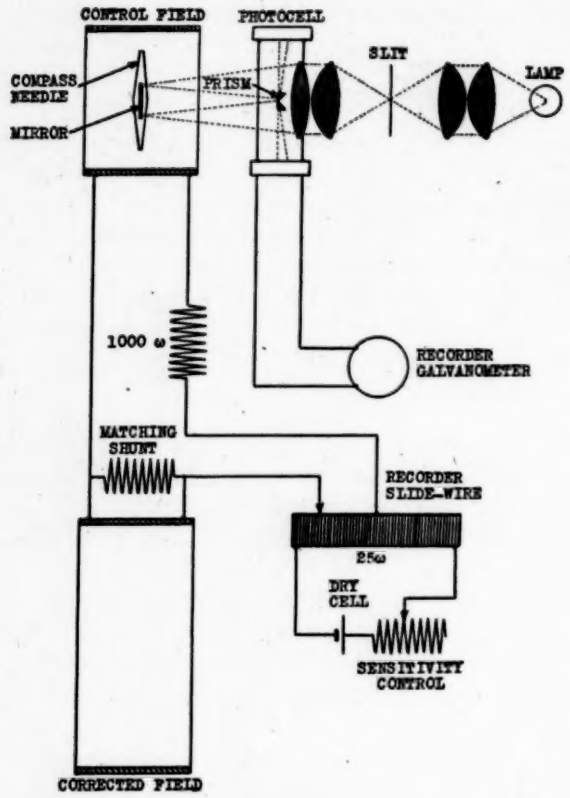

FIG. 2. Magnetic potentiometer system for automatically compensating changes in E–W component of earth's magnetic field.

previously established by the Research Laboratories for making measurements which required the elimination, as far as possible, of vibration and magnetic disturbance. The station is approximately 1000 feet from the nearest road and is almost completely free from all artificial vibration and magnetic disturbance. It consists of a small building, an underground instrument vault, and a connecting passageway. The sensitive instrument was located in the underground vault. The operator took readings in the building above by means of a remote operating amplifying system. The general plan of the test station is shown in Fig. 1.

The instrument vault is approximately a six-foot cube. The top of it is about seven feet below the ground. It is built of concrete and is entirely non-magnetic.

A vault of this kind is ideal for taking precision measurements. There are no disturbing air currents, it is absolutely dark, exceedingly quiet, and the temperature change during a 24-hour period rarely exceeds $\frac{1}{4}$°F.

In the vault are located three mutually perpendicular coil systems having a common center. These coils are used for neutralizing and controlling the various components of the earth's field. The N-S component is neutralized by a Helmholtz coil system[3] 44 inches in diameter. The vertical component is neutralized by another Helmholtz system 37 inches in diameter. In the E-W direction are two cylindrical coils wound on the same form. One is used to give a small E-W bias and the other is used to correct for the natural variations which occur in the E-W component.

DEVICE FOR COMPENSATING CHANGES IN EARTH'S MAGNETIC FIELD

When delicate measurements are being attempted, it is found that the earth's magnetic field is continually changing by a considerable amount both in magnitude and direction. This change can, of course, be resolved into three mutually perpendicular components fixed in direction and changing only in magnitude. As will be subsequently explained, only variations in the E-W component cause difficulty in this experiment.

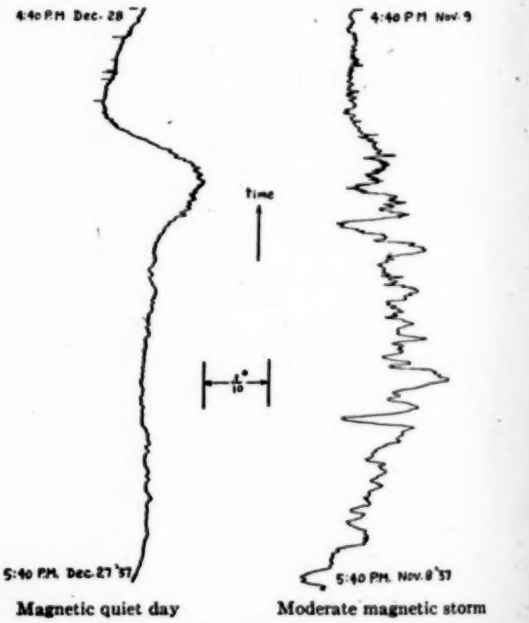

FIG. 3. Declination records of magnetic potentiometer.

[3] A. E. Ruark and M. F. Peters, J. Opt. Soc. Am. 13, 205 (1926).

In order to eliminate these E-W variations, an apparatus was designed which consists essentially of a solenoid with axis in the E-W direction, and a magnetized rod acting as a compass needle. The compass needle is located at the center of this solenoid, and the current is automatically adjusted so that the compass needle always points in the same direction. The E-W correcting coil in the instrument vault, 30 feet away, is placed in series with the above solenoid and shunted with a resistance of the proper value to obtain magnetic matching. The current traversing this coil, therefore, corrects for the E-W field variations.

The compass needle, consisting of a magnetized rod of hardened steel, supports a mirror and is suspended by a fine gold ribbon, the restoring force of which is negligible compared to that of the field. The needle is oil damped and enclosed in a housing to eliminate air currents.

An optical system projects a beam of light onto the mirror which after reflection forms a ribbon image on a light-splitting prism. The two halves of the light beam go to two Photox photoelectric cells. These cells are connected in parallel opposition and go to the galvanometer of a Leeds and Northrup Micromax recorder. The recorder operates a slide-wire which feeds current to the solenoid surrounding the compass needle.

Whenever a change in the field moves the compass needle off of center, the photo-cells become unbalanced. This puts a current through the galvanometer of the recording device and a current is immediately put through the coil system to bring the needle back to center. Figure 2 gives a schematic diagram of the system.

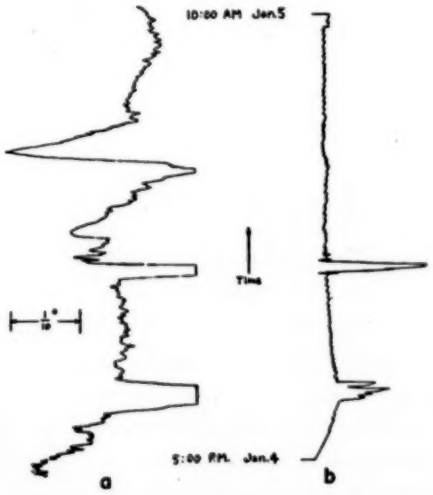

FIG. 4. (a) Angular change of the earth's magnetic field during a magnetic storm—January 4–5, 1938. (b) Same magnetic storm automatically compensated for changes in direction of the earth's field.

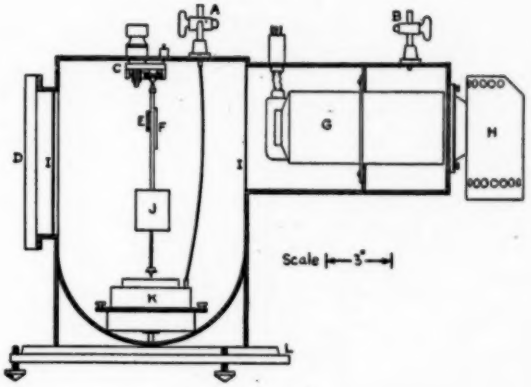

FIG. 5. Cross-sectional view of instrument. *A*—float control valve, *B*—evacuation valve, *C*—zero adjuster, *D*—glass entrance disk, *E*—calibrating mirror, *F*—amplifier mirror, *G*—photo-cell amplifier, *H*—lamp housing, *I*—removable conducting screen, *J*—inertia coil, *K*—float chamber, *L*—graduated turntable.

Figure 3 shows the changes which occur in the E-W component on a quiet day, and during a moderate magnetic storm. Figure 4 shows the correction of the instrument vault field during a magnetic storm. It can be seen by referring to the figure that the magnetic storm in the instrument vault field has been completely eliminated except in two places where the correcting device was driven beyond its limit. The two records shown in Fig. 4 were taken simultaneously on two separate recording systems. The small irregularities on the corrected field line are characteristic of the recorder used.

INERTIA INSTRUMENT AND AMPLIFICATION SYSTEM

Figure 5 shows a cross-sectional drawing of the primary instrument used in the experiment. This apparatus is located in the instrument vault at the center of the neutralizing coil system. The instrument is vacuum tight, is made of brass, and consists essentially of two intersecting cylinders. The vertical cylinder is the chamber in which the inertia coil is suspended; the horizontal cylinder holds a photo-cell amplifier designed to give an exceedingly high amplification of the motions of the inertia coil.

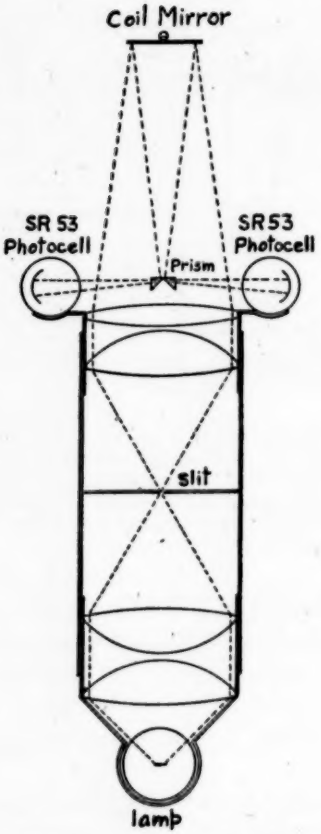

FIG. 6. Optical arrangement of photo-cell amplifier.

Entrance to the apparatus is made by means of an eight-inch glass disk lapped to another short intersecting cylinder opposite the amplifier. The apparatus when used is evacuated and all non-conducting surfaces are electrostatically shielded. The entire instrument is mounted on an accurately graduated turntable so that it can be set at any desired angular position. A zero adjuster is located on top of the instrument which gives a 1600 to 1 reduction and operates from the outside by means of a vacuum-tight knob. This large gear ratio enables the inertia coil to be readily brought to the balance position under the high amplification used.

A schematic diagram of the amplifier used to magnify the exceedingly minute deflections expected in this experiment is shown in Fig. 6. Light from a 6-volt ribbon filament lamp is condensed by means of a very fast lens onto a slit. The lamp is fed by a bank of eight storage batteries in parallel which gives a very constant voltage over a long period of time. The image of the slit is projected by another lens system via the coil mirror, onto a light-splitting prism. This prism divides the light, sending the two parts to two Westinghouse SR-53 vacuum type photo-cells. Any rotation of the mirror moves light from one photo-cell to the other. The output of these photo-cells is sent directly to the galvanometer system, no vacuum-tube amplification of the photo-cell output being used.

The amplifier circuit contains two galvanometers, one of which, shown at the center of Fig. 7, measures angular displacement of the primary coil, and the other, shown at the bottom of Fig. 7, measures the total amount of light falling on the two photo-cells. Both these galvanometers are specially constructed. The one for measuring the coil motion has a period of $\frac{1}{3}$ second. This rapid response is necessary to prevent phase shifting. The galvanometer for measuring light intensity has a double coil, both halves of which are identical.

It can be seen from Fig. 7 that the high speed

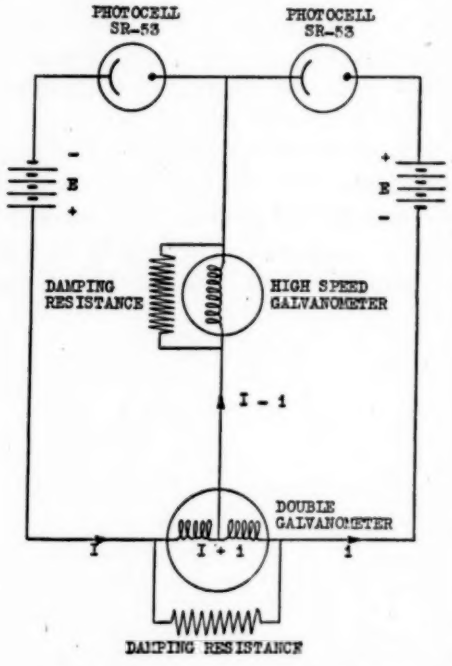

FIG. 7. Photo-cell amplifier circuit.

galvanometer reads the difference of the photo-cell currents and consequently gives readings proportional to the angular displacement of the primary coil. On the other hand, the double galvanometer reads the sum of the photo-cell

currents or a quantity proportional to the total amount of light falling on both photo-cells. The latter reading is important since the sensitivity of the deflection measuring system is proportional to this total amount of light.

These galvanometers are operated at five meters. Readings can be taken either on a scale or by means of a photographic recorder. Using this amplification system it is possible to obtain extremely stable results with amplifications giving equivalent coil pointers of several thousand meters. For the measurement of m/e of the electric carrier, the amplifier was set to give an equivalent pointer of about 1000 meters.

METHOD OF SUSPENDING INERTIA COILS

Practically all of the above-described apparatus is used either to give an amplification of the motion of the coil under test, or to provide a place to suspend it which can be evacuated and made free from any large magnetic fields. The coil is hung in this space by means of a gold ribbon of such a size as to give a period of about one minute.

When working with sensitivities of the order here used, a coil must be suspended so that it is immune to the naturally occurring disturbances which are almost continually present in the earth's crust. Fundamentally these disturbances in the earth do not make the coil rotate, but they do make it swing as a simple pendulum. The period of the coil as a simple pendulum is about 0.7 second. Since this period is of the order of magnitude of the natural microseisms, it is obvious that these disturbances will cause the coil to be continually agitated in this mode of vibration. If the coil is hanging freely without any restriction below the center of swing, this bobbing motion cannot couple with the torsional motion. Under the high amplification used in this experiment, it is practically impossible to find a point under the coil to fasten a spiral for the return current path, which would be on the axis of rotation. Hence, any restriction below the center of swing will cause bobbing to couple with torsion and the microseisms will consequently cause large changes in torsional amplitude. However, if the spiral is fastened at the point about which the coil swings as a simple pendulum, the above-mentioned difficulty will be eliminated.

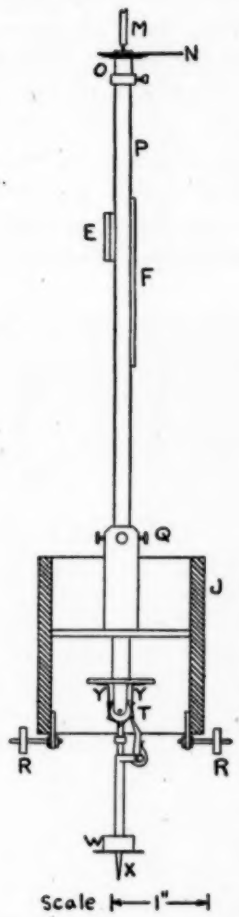

FIG. 8. Suspension system and coil reversing switch. *E*—calibrating mirror, *F*—amplifier mirror, *J*—inertia coil, *M*—supporting and lead-in rod, *N*—return current spiral, *O*—spiral adjusting collar, *P*—hollow tube surrounding supporting filament, *Q*—lateral adjusting screws for tube, *R*—weights for aligning magnetic moment with the vertical, *T*—commutator, *W*—counter-weight, *X*—rod for damping out lateral vibrations, *Y*—brush.

The method of accomplishing this is shown in Fig. 8. A very light conducting tube is attached to the top of the coil. This tube surrounds the supporting filament and has the return current spiral connected at its upper end. The tube is extensible so that the level of the spiral can be adjusted to the desired position. It is also adjustable laterally so that the tube can be made central with the supporting filament.

The importance of the proper positioning of the return current spiral is vividly demonstrated by the records shown in Fig. 9. These records are taken with a coil which is carrying no current. The two records on the left are taken with the

return spiral fastened under the coil with every reasonable effort made to locate the point of attachment on the axis of rotation. The record on the right is taken with this spiral removed and is identical with the records which are obtained when the spiral is properly located.

Another thing which is very important in suspending a coil for work under high amplification is that the supporting ribbon be fastened

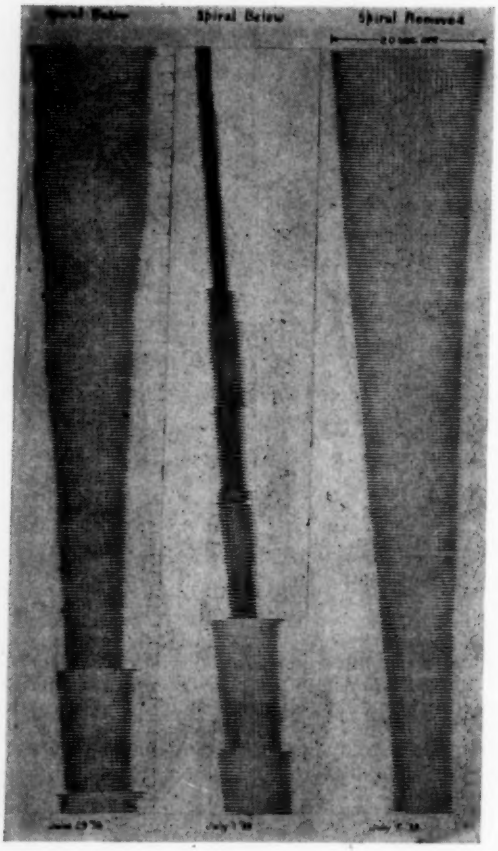

FIG. 9. Attenuation records showing effect of microseisms on coils with improperly placed lead-in spiral.

in such a manner that no force is taken up by a soldered connection. If this is not done, the coil will continually drift. In this work, the suspension ribbon was passed several times through a pair of small holes provided for the purpose at the end of the supporting rods. Solder was added to this joint only after the coil was hanging in position in the instrument.

The extremely small amount of drift present with this system of suspension can be seen by referring to Figs. 9 and 11. These records cover approximately three hours. Note magnitude of 20 seconds of arc.

METHOD OF LINING UP INERTIA COILS

After the coil on which readings are to be taken is suspended in the instrument, a measured current is allowed to flow until thermal equilibrium is established. This current value is then never changed throughout a set of data. All readings are obtained by operating a rapidly acting reversing switch. This switch interrupts the current for only about 1/1000 of a second in making a reversal.

When a coil is first hung in the apparatus, a reversal of the switch will in general give a steady deflection of several hundred centimeters even with the amplification much reduced. This is, of course, caused by a horizontal magnetic moment on the coil coupling with the earth's field. This force must be reduced to, and maintained at, zero before readings on electron inertia can be taken. Neutralization of the earth's field, which has been previously explained, is one of the things which is done to reduce this effect. If the magnetic moment of the inertia coil can also be brought very nearly into line with the axis of rotation, this effect will be still further reduced.

This is accomplished by adjusting some small weights, located under the coil (see Fig. 8), until the desired alignment is obtained. The entire apparatus is then rotated about the vertical so that any small remaining horizontal magnetic moment will be brought into a N-S line. Hence, only E-W fields are effective in turning the coil. Zero steady deflection is thus obtained under an amplification of about 1000 meters. The above steps are taken with the earth's field uncompensated. The neutralizing coils around the instrument are then turned on. When this is accomplished, a steady deflection of a few centimeters will, in general, return because of imperfect alignment of the neutralizing coils. A very small current in the E-W biasing coil again brings the steady deflection to zero. A steady deflection reading is taken before and after each electron inertia run and the current in the E-W coil is adjusted so that the deflection is zero at the beginning of each run. The magnetic poten-

tiometer for correcting E-W variations is, of course, operating throughout the experiment.

The experiment is performed by observing the change in amplitude of oscillation brought about by reversing the current in the inertia coil. An initial oscillation can be excited by sending a momentary current through a small auxiliary solenoid located outside the instrument. The double amplitude swing of the coil is adjusted to about 10 cm on the amplified scale which represents a coil motion of about 20 seconds of arc. The apparatus is then in condition for taking measurements on the inertia of the electric carrier.

METHOD OF MAKING MEASUREMENTS

In taking the actual measurements to determine the mass-charge ratio of the electric carrier, the operating reversing switch was thrown every time the coil crossed the center of its swing. This reversing switch was arranged under the galvanometer scale and when it was thrown in the direction in which the galvanometer spot was moving, the direction was called "with." When the switch was thrown opposite to the motion of the galvanometer, the direction was called "against." The direction chosen was such that the suspension phenomenon (explained under systematic errors) tended to build up the oscillations. In many cases, this very nearly balanced the frictional losses of the system, and without the electron inertia effect the amplitude would remain very nearly constant.

To obtain an inertia reading forty reversals of the current were made and the extremity of each swing was recorded. The value of amplitude change was obtained by an algebraic system of averaging all amplitude values and by assuming that the change was linear. The vacuum-operated coil switch (described later) was then thrown which reversed the current in the coil without reversing the current in the suspension. The readings were then repeated by throwing the operating reversing switch in the same direction as on the first run. The average amplitude change of these two runs, taking account of sign, gave one value for the electron inertia impulse. The beginning amplitude of the second run was adjusted so that at the end of 20 reversals it was approximately the same as the amplitude at the end of 20 reversals on the first run. The entire apparatus was next rotated through 180° and the process repeated giving another value for the electron inertia impulse. For each current value used in the various coils, eight values of double amplitude change per reversal were obtained.

A recording of one of these sets of data is shown in Fig. 10. This recording is the actual trace of the electron inertia amplitude change at

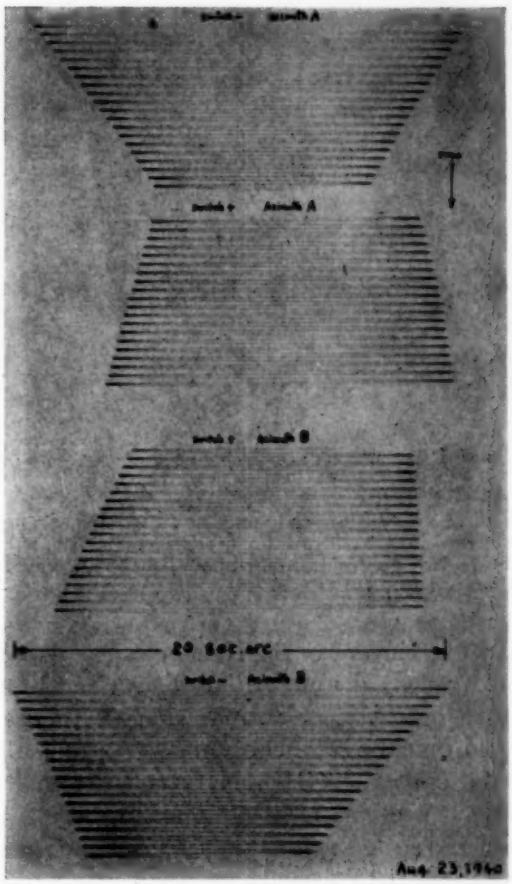

FIG. 10. Electron inertia amplitude changes.

the end of an equivalent pointer of 1000 meters.

At the end of each day's work, the photo-cell amplifier was calibrated to determine the relationship between equivalent pointer length and light intensity as recorded by the double galvanometer. This was done by rotating the instrument so that the residual horizontal magnetic moment of the inertia coil had maximum coupling with the horizontal Helmholtz coil. A deflection on the amplified scale for a given small

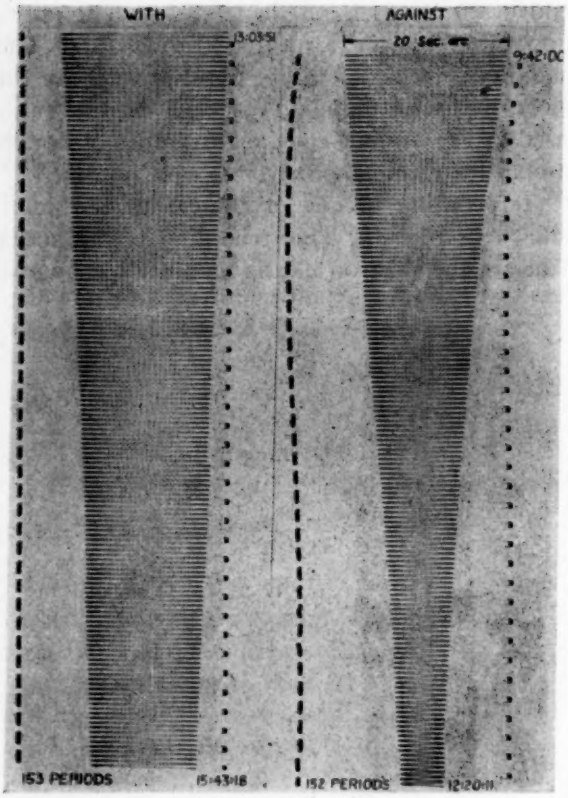

FIG. 11. Amplitude changes caused by suspension phenomenon. Coil with windings shorted. 0.0012"×0.018" ×4.5"—14K gold-platinum ribbon. Current reversed 20.3 milliamp. Sept. 8, 1938.

change in current in the Helmholtz coil was compared with a direct reading deflection obtained with a much larger current change. It was assumed that the coil deflections were proportional to the changes in Helmholtz coil current. The direct deflections were obtained by means of a lamp and scale mounted in the instrument vault. An appropriate secondary mirror was mounted on the inertia coil for this purpose.

SYSTEMATIC ERRORS AND THEIR ELIMINATION

Incomplete Elimination of Magnetic Coupling

Regardless of all the precautions which have been taken to keep the magnetic moment of the inertia coil from coupling with surrounding magnetic flux, it is found impossible to maintain this force at zero under the high amplification used. However, if the steady deflection is small compared to the amplitude of swing and if the current in the inertia coil is reversed very close to the center of the swing, the change in amplitude caused by this force will be very small compared to the change caused by the inertia of the electric carrier.

A dividing device is used on the scale. This device consists merely of three movable pointers arranged so that one of them is always halfway between the other two. The two outer pointers are set every time the galvanometer reaches the extremity of its swing. The third pointer, therefore, follows any change in center that might take place during the course of a run. Hence the current can be reversed very close to center.

The steady deflection is always set very close to zero at the beginning of an electron inertia run which requires about 20 minutes. At the end of a run, this deflection at 1000 meters amplification rarely exceeds 1 millimeter. These steady deflections were recorded and, since the correction factor can be readily measured, appropriate corrections can be made.

Suspension Phenomenon

As stated above, the steady deflection of these coils is always maintained very close to zero. If, however, this zero steady deflection is made up of two opposing forces, having different times of action, a large build-up of the coil might still take place. To illustrate, suppose that by some device on the coil system a steady deflection was caused by reversing the current, which acted slowly and did not reach its final value for 5 seconds. Since zero deflection is maintained, on a long period device, this force would be balanced by an equal force in the opposite direction caused by the magnetic moment of the coil. However, the force caused by the magnetic moment would act instantly. Thus, there would be five seconds elapsing when the forces on the coil would be unbalanced, which would, of course, cause an amplitude change.

It has been found during this investigation that when a suspension ribbon is carrying a current and this current is reversed but kept at exactly the same value, the suspension ribbon undergoes a slow distortion causing a force of the kind mentioned above to act on the coil. The hypothesis advanced to explain this characteristic

of the suspension assumes that because of non-uniformities in the structure of the filaments, the current follows slightly different paths in the two directions. Hence, reversing the current causes a slow distortion of the filament because of a redistribution of the generated heat between its various sections.

As far as is known, there is no reference in the literature to a suspension phenomenon of this kind. In some suspensions the effect will remain at a constant value almost indefinitely. In others, it has been observed to change slowly over a period of several weeks. There are never any rapid changes in the phenomenon unless the suspension system is removed from the instrument and replaced.

No suspension system that we have tried has been free from this effect. Regardless of how the current was led into the coils, a force of this kind was always present. A record of the amplitude change caused by the phenomenon is shown in Fig. 11. In obtaining these records the windings of the coil were short-circuited and the current in the suspension was reversed every time the system crossed the center of its swing. The broken lines are light intensity traces as recorded by the double galvanometer.

In order to eliminate the effects of the suspension phenomenon, a small reversing switch was designed which reversed the current in the coil without reversing the current in the suspension. This switch is, of course, fastened on the inertia coil and is operated by means of a small float located in the bottom of the instrument. The float is raised or lowered by means of varying the air pressure on a column of oil. A diagram of the float is shown in Fig. 12.

The operation of this switch can be seen by referring to Fig. 8. The float lifts the counterweight W. By means of a pawl and ratchet, the commutator T is thereby made to move over the brushes to which the coil leads are attached. The bearings of this commutator receive the current from the suspensions. The pointed rod X is used to damp out lateral vibrations caused by operating the switch. When the float is part way down, this rod extends into a small oil reservoir provided for the purpose. When all lateral vibrations have been damped out, the float is lowered to its proper level and all restriction below the coil is removed.

Effect of Leakage Currents

In certain coils it will be found that there exists a small fraction of the current that does not follow the wire. These leakage currents couple with any residual magnetic field that may be present around the coil. Since leakage currents can change slowly immediately after reversal, they can cause an amplitude change in the same manner as that caused by the suspension phenomenon. This effect is, however, very small when the field is properly neutralized and can be completely eliminated by taking readings at two 180° removed positions of the inertia apparatus.

THEORY AND RESULTS

Consider a quantity of electricity having a charge of e and a mass of m. This electricity is moving with an average angular velocity of ω in a circular loop of wire having a mean radius of r. The angular momentum Z of this moving electricity will be $Z=mr^2\omega$. The number of revolutions this charge makes in unit time is $\omega/2\pi$. It therefore represents an electric current of magnitude $i=e(\omega/2\pi)$. Therefore $\omega=2\pi i/e$ and $Z=2\pi r^2 im/e$. If a coil consists of N turns and if the average cross-sectional area of all the turns is A, then

$$Z=2AiNm/e. \tag{1}$$

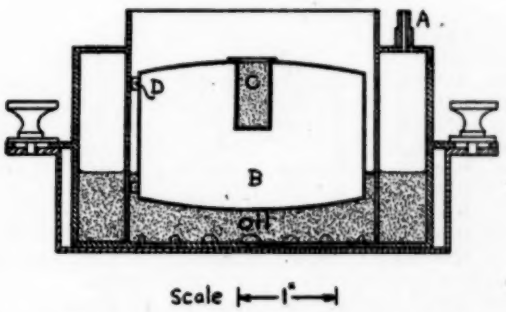

FIG. 12. Cross section of float system used to operate coil reversing switch. A—inlet from control valve, B—float, C—damping chamber, D—float guide.

Equation (1) gives the angular momentum of the moving electricity in a coil of wire. If the current is changed by an amount Δi, the change in angular momentum will be $\Delta Z=2A\Delta iNm/e$. If the angular momentum of an undamped tor-

TABLE I. Summary of data. S=change in double deflection per current reversal, d=change in double deflection per current reversal per milliamp.

Coil No. 1 Copper

i=6.21 milliamp.		i=12.08 milliamp.	
S	d	S	d
0.0580	0.00934	0.0965	0.00799
0.0547	0.00881	0.1095	0.00906
0.0550	0.00886	0.0885	0.00733
0.0591	0.00952	0.1116	0.00924
0.0597	0.00961	0.1125	0.00931
0.0525	0.00845	0.1191	0.00986
0.0554	0.00892	0.1130	0.00935
0.0520	0.00837	0.1109	0.00918
Av.	0.00898	Av.	0.00891

Av. d for both current values 0.00895
Calculated $m/e=5.64\times10^{-9}$ gram per coulomb

Coil No. 2 Copper

i=2.50 milliamp.		i=3.82 milliamp.	
0.0707	0.0283	0.1244	0.0326
0.0702	0.0281	0.1127	0.0295
0.0666	0.0266	0.1192	0.0312
0.0656	0.0262	0.1099	0.0288
0.0729	0.0292	0.0826	0.0216
0.0689	0.0276	0.0919	0.0241
0.0726	0.0290	0.0951	0.0249
0.0729	0.0292	0.0966	0.0253
Av.	0.0280	Av.	0.0273

Average d for both current values 0.0276
Calculated $m/e=5.67\times10^{-9}$ gram per coulomb

Coil No. 3 Aluminum

i=7.00 milliamp.		i=14.00 milliamp.	
0.0611	0.00873	0.1232	0.00880
0.0548	0.00783	0.1104	0.00789
0.0535	0.00764	0.1155	0.00825
0.0526	0.00751	0.1123	0.00802
0.0555	0.00793	0.1014	0.00724
0.0583	0.00833	0.1136	0.00811
0.0521	0.00744	0.1118	0.00799
0.0568	0.00811	0.1177	0.00841
Av.	0.00794	Av.	0.00809

Average d for both current values 0.00801
Calculated $m/e=5.66\times10^{-9}$ gram per coulomb

Coil No. 4 Copper

i=11.88 milliamp.		i=25.00 milliamp.		i=33.33 milliamp.	
0.0649	0.00546	0.1457	0.00583	0.1880	0.00564
0.0663	0.00558	0.1398	0.00559	0.1907	0.00572
0.0656	0.00552	0.1350	0.00540	0.1891	0.00576
0.0668	0.00562	0.1340	0.00536	0.1932	0.00580
0.0662	0.00557	0.1426	0.00570	0.1915	0.00574
0.0682	0.00574	0.1426	0.00570	0.1830	0.00549
0.0663	0.00558	0.1439	0.00576	0.1863	0.00559
0.0715	0.00602	0.1436	0.00574	0.1827	0.00548
Av.	0.00564	Av.	0.00564	Av.	0.00564

Average d for all three current values 0.00564
Calculated $m/e=5.79\times10^{-9}$ gram per coulomb

Average m/e for all coils, 5.69×10^{-9} gram per coulomb
Accepted[1] value, 5.68×10^{-9} gram per coulomb

[1] R. T. Birge, *Reports on Progress in Physics* 8, 121 (1941).

sional pendulum is changed by an amount ΔZ as the pendulum is crossing the center of its swing, it is easy to show that the change in amplitude will be $\Delta\theta=\Delta Z(P/2\pi I)$ where P = period of coil and I = moment of inertia of coil. Therefore $\Delta\theta=(\Delta iANP/\pi I)(m/e)$ is the amplitude change in radians owing to a current change of Δi.

In this experiment the current is always reversed; hence $\Delta i=2i$. Also $\Delta\theta$ is not observed directly; instead, the change d in double amplitude is observed at pointer length x. Hence $\Delta\theta=d/2x$. Therefore

$$d=(4ANiPx/\pi I)(m/e). \tag{2}$$

For convenience in computation, in the appended tables all the measured values of d are reduced to a double deflection per milliamp. per current reversal at a standard amplification of 1000 meters. Putting $i=10^{-3}$ amp. and $x=10^5$ cm and using πr^2 for A where r is the radius for the average area of the coils, we have

$$m/e=Id/400r^2NP. \tag{3}$$

If the ratio between the outer radius and the inner radius is close to unity, r in the above equation is the mean radius. If this is not true, it is easy to show that r^2 should be replaced by the following expression:

$$r^2=\frac{R_2^3-R_1^3}{3(R_2-R_1)},$$

where R_2=outer radius and R_1=inner radius. This expression gives the radius for the average cross-sectional area when the winding density is uniform.

From Eq. (3) it will be seen that by measuring d and the constants of the coil, the ratio of mass to charge of the carrier of electric current can be determined.

In three of the four coils on which measurements were made, the values obtained for m/e of the electric carrier checked very closely the accepted value for m/e of an electron. These three coils were very uniformly wound, each layer having the same number of turns. The windings on the fourth coil were not nearly as uniform. This coil was also wound in the form of a flat pancake with the outer radius being almost ten times the inner radius. In a coil of this shape non-uniformities in the winding would be very effective in producing error in the result. The value obtained for m/e using this coil departs

TABLE II. Coil data.

Wire in winding	Coil No. 1. No. 36 Silkenamel	Coil No. 2. No. 41 enameled	Coil No. 3. No. 34 enameled	Coil No. 4. No. 36 Silkenamel
Coil length	4.762 cm	4.762 cm	2.54 cm	0.254 cm
Outer radius	2.1195 cm	2.107 cm	2.756 cm	4.144 cm
Inner radius	1.811 cm	1.920 cm	2.555 cm	0.438 cm
r^2	3.8701 cm^2	4.057 cm^2	7.0551 cm^2	6.3923 cm^2
I	309.46 gram cm^2	248.81 gram cm^2	128.89 gram cm^2	524.70 gram cm^2
N	4663	11860	1231	3250
P	68.05 seconds	62.95 seconds	52.48 seconds	61.49 seconds

almost 2 percent from the accepted value. If the magnetic moment of this coil had been measured and its value used in place of ANi in Eq. (2), it is probable that much closer agreement with the accepted value would be obtained for this coil also.

In all coils the direction of the impulse indicated that the carrier was moving from negative to positive. The results of the electron inertia readings, together with the values used for computing m/e, are shown in Tables I and II.

ACKNOWLEDGMENTS

The authors wish to express their appreciation for the help given by the many members of the staff of the General Motors Research Laboratories in designing and fabricating the instruments used. Thanks are also due to Dr. G. M. Rassweiler and Mr. John Stone for their many excellent suggestions used in the preparation of the manuscript; and special thanks are due to Mr. J. F. Lash for valuable assistance in obtaining the experimental data.

PHYSICAL REVIEW VOLUME 66, NUMBERS 9 AND 10 NOVEMBER 1 AND 15, 1944

Static Isotropic Solutions of Einstein's Field Equations

MAX WYMAN
University of Alberta, Edmonton, Alberta, Canada
(Received April 10, 1944)

Line elements of the form $ds^2=V^2dt^2-(dl^2/W^2)$ are considered, where $V=V(x, y, z)$, $W=W(x, y, z)$. When the components of the energy momentum tensor T_j^i satisfy the equations $T_1^1=T_2^2=T_3^3$, $T_j^i=0$, $i\neq j$, it is shown that V, W are reducible to three basic forms. In empty space the basic solutions are determined. All isotropic solutions, in empty space, can be obtained from the basic solutions by means of transformations that are given.

INTRODUCTION

WHEN investigating a physical problem by means of the Einstein theory of gravitation, it is usual to consider the problem solved when the gravitational potentials g_{ij} appearing in the line element

$$ds^2=g_{ij}dx^idx^j$$

are obtained as solutions of the field equations. Because of their non-linear character it is difficult to obtain rigorous solutions of the field equations and at present no general solutions are known. The best we can do is to investigate solutions having some pre-assigned physical property. In choosing this property one must of course be guided by both the physical interest and the simplification it will make in the mathematical calculations.

The physical property we shall investigate is one of isotropy and the simplification in the form of the line element is obtained in the following way. Consider a frame of reference K with space-like coordinates x, y, z and time-like coordinate t. For the velocity of light, relative to K, to be independent of the direction of propagation, it has been shown[1] that the line element must have,

[1] See T. Levi-Civita, *Absolute Differential Calculus* (Blackie and Son, London, 1929), p. 338.

in this coordinate system, the form

$$ds^2 = V^2dt^2 - d\sigma^2,$$

where

$$d\sigma^2 = -\sum_{i,j=1}^{3} g_{ij}dx^i dx^j.$$

In the latter form the function $V = V(x, y, z, t)$ can be identified as the relativistic velocity of light. It should be emphasized that the velocity of light in this sense is not an invariant with respect to general transformations of coordinates. For this reason the isotropic property of light pertains only to a coordinate system and can be destroyed by a transformation of coordinates.

We shall in addition make the following assumption. In the same frame of reference K, the three-dimensional subspace t=constant is spatially isotropic. By this we mean that a small rigid rod (ds^2=a negative constant) joining the fixed point (x, y, z) to the variable point $(x+dx, y+dy, z+dz)$ traces out a sphere ($dx^2+dy^2+dz^2$ =constant) as the orientation of the rod is changed. This assumption implies that in the coordinate system K, the line element must have the form

$$ds^2 = V^2dt^2 - (dl^2/W^2), \qquad (1)$$

where

$$W = W(x, y, z, t) \quad \text{and} \quad dl^2 = dx^2+dy^2+dz^2.$$

Coordinate systems for which the line element takes the form (1) are called isotropic coordinates. If in addition it happens that in this coordinate system V, W are both independent of t, then we shall call the coordinates, static isotropic. Moreover, the solutions for V, W in these coordinate systems shall be called isotropic and static isotropic solutions, respectively. In experimental work we practically always assume these properties of isotropy for our coordinate systems.

The most general problem that can be considered along these lines is the determination of all the physical distributions of matter for which an isotropic coordinate system exists. Stated mathematically, we must find all the solutions for V and W by means of the field equations and then identify these solutions with some physical distribution of matter. The problem is complicated by the fact that two distinct solutions may be related by a coordinate transformation and hence will represent the same distribution of matter.

At present several particular isotropic solutions are known, but so far no attempt has been made to find all such solutions. In the present paper we shall deal only with the static isotropic solutions and shall assume throughout that V and W are independent of t. The following results are obtained: 1. When the energy-momentum tensor T_j^i satisfies the equations $T_1^1 = T_2^2 = T_3^3$, $T_j^i = 0$, $i \neq j$, the line element is reduced to three basic forms. These results apply to perfect fluids. 2. All the static isotropic solutions for empty space are obtained. When the cosmological constant Λ is taken to be zero, the result is negative. All the new solutions are shown to be reducible to the known solutions by means of coordinate transformations. In the more general case $\Lambda \neq 0$ three new solutions are found and in particular the isotropic form of the Schwarzschild exterior solution is obtained.

Our method of treating the non-linear differential equations involved seems to be quite powerful, and it is hoped that the method will serve as a guide to those seeking other types of solutions of the field equations.

I. TRANSFORMATIONS OF THE LINE ELEMENT

From any particular solution we can always, by means of coordinate transformations, generate an infinity of solutions. However, these formally different solutions are equivalent in that they describe the same physical situation from the point of view of different coordinate systems. For this reason we shall consider all solutions that are related by means of coordinate transformations as a single solution. We shall make use of the following transformations in reducing our solutions to their three basic forms.

T_1: Rotations and translations of the spatial axes x, y, z.

T_2: $x = \bar{x}/\bar{r}^2, \quad y = \bar{y}/\bar{r}^2, \quad z = \bar{z}/\bar{r}^2,$

$$\bar{r}^2 = \bar{x}^2+\bar{y}^2+\bar{z}^2.$$

T_3: $x = 2k\bar{x}/D_1, \quad y = k(1-\bar{r}^2)/D_1,$

$$z = 2k\bar{z}/D_1, \quad D_1 = \bar{x}^2+(\bar{y}-1)^2+\bar{z}^2.$$

T_4: $x = k(1-\bar{r}^2)/D_2, \quad y = 2k\bar{y}/D_2,$

$$z = 2k\bar{z}/D_2, \quad D_2 = (\bar{x}-1)^2+\bar{y}^2+\bar{z}^2.$$

For these transformations dl^2 transforms according to the following laws:

T_1: $dl^2=d\bar{l}^2=d\bar{x}^2+d\bar{y}^2+d\bar{z}^2$.

T_2: $dl^2=d\bar{l}^2/\bar{r}^4$.

T_3: $dl^2/x^2=d\bar{l}^2/\bar{x}^2$.

T_4: $dl^2/x^2=4d\bar{l}^2/(1-\bar{r}^2)^2$.

We thus see that these transformations preserve the isotropic form of the line element.

II. THE ENERGY-MOMENTUM TENSOR T_j^i

The components of the energy momentum tensor were calculated by means of Dingle's formulae.[2] If we use the notation $V_x=\partial V/\partial x$, $V_{xy}=\partial^2 V/\partial x\partial y$, etc., and let

$$H=\frac{(W_x^2+W_y^2+W_z^2+\Lambda)}{W^2},$$

we obtain the following results:

$$-\frac{8\pi T_1^1}{W^2}=-\frac{(W_{yy}+W_{zz})}{W}+\frac{(V_{yy}+V_{zz})}{V}-\frac{2W_xV_x}{WV}+H.$$

$$-\frac{8\pi T_2^2}{W^2}=-\frac{(W_{zz}+W_{xx})}{W}+\frac{(V_{zz}+V_{xx})}{V}-\frac{2W_yV_y}{WV}+H.$$

$$-\frac{8\pi T_3^3}{W^2}=-\frac{(W_{xx}+W_{yy})}{W}+\frac{(V_{xx}+V_{yy})}{V}-\frac{2W_zV_z}{WV}+H.$$

$$-\frac{8\pi T_4^4}{W^2}=-\frac{2}{W}(W_{xx}+W_{yy}+W_{zz})+3H-\frac{2\Lambda}{W^2}.$$

$$-\frac{8\pi T_2^1}{W^2}=\frac{W_{xy}}{W}-\frac{V_{xy}}{V}-\frac{(W_xV_y+W_yV_x)}{WV}.$$

$$-\frac{8\pi T_3^2}{W^2}=\frac{W_{yz}}{W}-\frac{V_{yz}}{V}-\frac{(W_yV_z+V_yW_z)}{WV}.$$

$$-\frac{8\pi T_3^1}{W^2}=\frac{W_{xz}}{W}-\frac{V_{xz}}{V}-\frac{(W_xV_z+W_zV_x)}{WV}.$$

[2] R. C. Tolman, *Relativity, Thermodynamics, and Cosmology* (Clarendon Press, Oxford, 1934), pp. 255–57.

III. FORM OF SOLUTIONS

The main result to be obtained in this section is as follows. If $T_1^1=T_2^2=T_3^3$ and $T_j^i=0$, $i\neq j$, then W, V can be reduced by means of rotations and translations to one of the following forms.

$$W=W(x),\quad V=V(x). \tag{3.1}$$

$$W=xf(u),\quad V=V(u),\quad u=y/x. \tag{3.2}$$

$$W=W(r),\quad V=V(r),\quad r^2=x^2+y^2+z^2. \tag{3.3}$$

$$W=xf(v)\quad V=V(v),\qquad v=\frac{r^2+k}{x},\quad k \text{ constant}. \tag{3.4}$$

These results will obviously apply to the empty space surrounding material bodies and also to perfect fluids.

The conditions imposed on T_j^i give us five equations. These become, on substituting $W=QV$, $V=e^{R/\sqrt{2}}$:

$$Q_{xx}-Q_{yy}=(R_x^2-R_y^2)Q, \tag{3.5}$$

$$Q_{yy}-Q_{zz}=(R_y^2-R_z^2)Q, \tag{3.6}$$

$$Q_{xy}=R_xR_yQ, \tag{3.7}$$

$$Q_{yz}=R_yR_zQ, \tag{3.8}$$

$$Q_{zx}=R_zR_xQ. \tag{3.9}$$

We can without loss of generality assume $Q_xQ_yQ_zR_xR_yR_z\neq 0$, for the following reason. Suppose Q were independent of x, then by a rotation of axes this letter can be supplied to Q. Hence all of these special solutions must come out of the more general case.

Calculating Q_{xyz} from each of (3.7), (3.8), (3.9) and equating the results, we find that Q must satisfy two first-order linear partial differential equations of the form

$$Q_x=AQ+BQ_z, \tag{3.10}$$

$$Q_y=\bar{A}Q+\bar{B}Q_z, \tag{3.11}$$

where

$$A=-\frac{R_z}{R_y}\frac{\partial}{\partial y}\left(\frac{R_x}{R_z}\right),\quad \bar{A}=-\frac{R_z}{R_x}\frac{\partial}{\partial x}\left(\frac{R_y}{R_z}\right); \tag{3.12}$$

$$B=R_x/R_z,\qquad \bar{B}=R_y/R_z. \tag{3.13}$$

From these equations we see that the determination of A, $\bar{A}$, B, $\bar{B}$ will determine the forms of

Q and R up to an arbitrary function. Clearly (3.12), (3.13) imply

$$B_y+A\bar{B}=0, \quad \bar{B}_x+\bar{A}B=0, \tag{3.14}$$

$$B_y-\bar{B}_x+B\bar{B}_z-\bar{B}B_z=0. \tag{3.15}$$

Calculating Q_{xy} from (3.10) and making use of (3.7), (3.8), and (3.14) we find that $A_y+A\bar{A}=0$. Similarly by means of (3.11) we find $\bar{A}_x+A\bar{A}=0$. Proceeding in this way and using all the integrability conditions that Eqs. (3.5)–(3.14) must satisfy, we can show that A, $\bar{A}$, B, $\bar{B}$ must be solutions of the following partial differential equations.

$$A_y+A\bar{A}=0, \quad \bar{A}_x+A\bar{A}=0, \tag{3.16}$$

$$A_x+A^2=\bar{A}_y+\bar{A}^2, \tag{3.17}$$

$$B_y+A\bar{B}=0, \quad \bar{B}_x+\bar{A}\bar{B}=0, \tag{3.18}$$

$$B_x+AB=\bar{B}_y+\bar{A}\bar{B}, \tag{3.19}$$

$$\bar{B}A_z=B\bar{A}_z, \tag{3.20}$$

$$B_y-\bar{B}_x+B\bar{B}_z-\bar{B}B_z=0, \tag{3.21}$$

$$B(\bar{B}_y+\bar{A}\bar{B})+B_z+A=0, \tag{3.22}$$

$$B(\bar{A}_y+\bar{A}^2)+A_z=0. \tag{3.23}$$

From their definitions neither B nor $\bar{B}$ can be zero. However, there is no such restriction on A or $\bar{A}$. It is advantageous to discuss the following cases separately.

(a) $A=\bar{A}=0.$

(b) $A\neq 0, \quad \bar{A}=0.$

(c) $A=0, \quad \bar{A}\neq 0.$

(d) $A\bar{A}\neq 0.$

When $A=\bar{A}=0$, the solutions for B, $\bar{B}$ are easy to determine. These are $B=(x+a)/(z+b)$, $\bar{B}=(y+c)/(z+b)$, or $B=k_1$, $\bar{B}=k_2$ where a, b, c, k_1, k_2 are constants. We may take $a=b=c=0$ because they can be removed by a translation of axes. For the first solution Eqs. (3.10), (3.11), (3.13) become

$$Q_x=(x/z)Q_z, \quad Q_y=(y/z)Q_z; \tag{3.24}$$

$$R_x=(x/z)R_z, \quad R_y=(y/z)R_z. \tag{3.25}$$

Solving (3.24), (3.25) we find $Q=Q(x^2+y^2+z^2)$, $R=R(x^2+y^2+z^2)$. Thus the line element is spherically symmetric. When $B=k_1$, $\bar{B}=k_2$, we find the solutions for W, V take the form of (3.1) after a suitable rotation of axes.

Since the method for solving cases (b), (c) is exactly the same as used in (d), we shall proceed immediately with the discussion of the last case.

When $A\bar{A}\neq 0$, $\bar{A}=-A_y/A$. Substituting into the second equation of (3.16), we find

$$\frac{A_{xy}}{A}-\frac{A_xA_y}{A^2}+A_y=0. \tag{3.26}$$

This may be integrated to give

$$A=\frac{F_x}{F(x,y)+\bar{F}(y,z)}, \tag{3.27}$$

where F, $\bar{F}$ are arbitrary functions of their arguments. Obviously

$$\bar{A}=\frac{\bar{F}_y}{F+\bar{F}}. \tag{3.28}$$

By means of (3.27), (3.28), and (3.17) we obtain $F_{xx}=\bar{F}_{yy}$. Since x, y are independent variables this implies $F_{xx}=F_{yy}=C(z)$. Carrying out the integration, we must have

$$A=\frac{C(z)x+H(z)}{C(z)\frac{1}{2}(x^2+y^2)+H(z)x+M(z)y+K(z)}, \tag{3.29}$$

$$\bar{A}=\frac{C(z)y+M(z)}{C(z)\frac{1}{2}(x^2+y^2)+H(z)x+M(z)y+K(z)}. \tag{3.30}$$

Again the proof divides into two parts according as $C(z)=0$ or $C(z)\neq 0$. Since the methods in both cases are the same, we shall omit the proof for the first case. When $C(z)=0$, the solutions can be reduced to one of forms (3.1), (3.2), (3.3). When $C(z)\neq 0$ we can divide numerator and denominator by $C(z)$, and the expressions for A, $\bar{A}$ take the form:

$$A=\frac{x+c_1(z)}{D}, \quad \bar{A}=\frac{y+c_2(z)}{D}, \tag{3.31}$$

where

$$D=\tfrac{1}{2}(x^2+y^2)+c_1(z)x+c_2(z)y+c_3(z).$$

In order to determine B, $\bar{B}$ we make the substitution $B=AZ$ into Eqs. (3.18), (3.19). By use

of (3.16), these become:

$$\bar{B}=\bar{A}Z-Z_y, \tag{3.32}$$

$$Z_{xy}=\bar{A}Z_x, \quad Z_{yy}=-AZ_x. \tag{3.33}$$

Since $\bar{A}=(\partial/\partial y)\log D$, we can integrate these equations to

$$Z=k_1\frac{[\frac{1}{2}(x^2-y^2)+c_1x-c_2y-c_3+c_1^2]}{x+c_1}+k_2y+k_3, \tag{3.34}$$

where k_1, k_2, k_3 are functions of z. Hence

$$B=k_1\frac{[\frac{1}{2}(x^2-y^2)+c_1x-c_2y-c_3+c_1^2]+(k_2y+k_3)(x+c_1)}{D}. \tag{3.35}$$

By means of (3.23) we find $k_1=c_1'$, $k_2=c_2'$, $k_3=c_3'-c_1c_1'$, where the primes denote total differentiation with respect to z. Thus

$$B=\frac{c_1'[\frac{1}{2}(x^2-y^2)-c_2y-c_3]+(c_2'y+c_3')(x+c_1)}{D}, \tag{3.36}$$

and

$$\bar{B}=\frac{-c_2'[\frac{1}{2}(x^2-y^2)+c_1x+c_3]+(c_1'x+c_3')(y+c_2)}{D}. \tag{3.37}$$

Substituting these values of A, $\bar{A}$, B, $\bar{B}$ into (3.22), we find that $c_1''=0$, $c_2''=0$, $c_3''=-1$. Hence $c_1=l_1z+l_2$, $c_2=l_3z+l_4$, $c_3=-\frac{1}{2}z^2+l_6z+l_5$, where the l's are constants. By a suitable translation of the x, y, z, axes we can make $l_2=l_4=l_6=0$. With these values of A, $\bar{A}$, B, $\bar{B}$, Eqs. (3.10), (3.11) become

$$Q_x=\frac{(x+l_1z)Q}{D}+\frac{[l_1[\frac{1}{2}(x^2-y^2+z^2)-l_3yz-l_5]+(x+l_1z)(l_3y-z)]Q_z}{D},$$

$$Q_y=\frac{(y+l_3z)Q}{D}+\frac{[-l_3[\frac{1}{2}(x^2-y^2-z^2)+l_1xz+l_5]+(y+l_3z)(l_1x-z)]Q_z}{D},$$

where

$$D=\tfrac{1}{2}(x^2+y^2-z^2)+l_1xz+l_3yz+l_5.$$

We have two similar equations to determine R from 3.13. The rotation of axes

$$\bar{x}=\frac{-l_1x-l_3y+z}{(1+l_1^2+l_3^2)^{\frac{1}{2}}},$$

$$\bar{y}=\frac{x+l_1z}{(1+l_1^2)^{\frac{1}{2}}},$$

$$\bar{z}=\frac{l_1l_3x-(1+l_1^2)y-l_3z}{(1+l_1^2+l_3^2)^{\frac{1}{2}}(1+l_1^2)^{\frac{1}{2}}},$$

reduces these equations to

$$Q_{\bar{x}}=\frac{Q}{\bar{x}}+\frac{(\bar{x}^2-\bar{y}^2-\bar{z}^2-2l_5)}{2\bar{x}\bar{z}}Q_{\bar{z}}, \tag{3.38}$$

$$Q_{\bar{y}}=(\bar{y}/\bar{z})Q_{\bar{z}}. \tag{3.39}$$

At the same time the equations for R become

$$R_{\bar{z}}=\frac{(\bar{x}^2-\bar{y}^2-\bar{z}^2-2l_5)}{2\bar{x}\bar{z}}R_{\bar{z}}, \tag{3.40}$$

$$R_{\bar{y}}=(\bar{y}/\bar{z})R_{\bar{z}}. \tag{3.41}$$

The general solutions of these equations are

$$Q=\bar{x}f\left\{\frac{\bar{x}^2+\bar{y}^2+\bar{z}^2+2l_5}{\bar{x}}\right\},$$

where f is an arbitrary function of its argument, and

$$R=R\left\{\frac{\bar{x}^2+\bar{y}^2+\bar{z}^2+2l_5}{\bar{x}}\right\}.$$

Thus W and V are of form (3.4).

IV. REDUCTION TO THREE BASIC FORMS

So far we have made use of only translations and rotations in order to reduce our solutions to

four forms. We now make use of transformations T_2, T_3, T_4 of Section I to show that there are only three basic forms.

The line element corresponding to (3.4) is

$$ds^2 = V^2(v)dt^2 - \frac{1}{f^2(v)}\frac{dl^2}{x^2}, \tag{4.1}$$

where

$$v = \frac{x^2+y^2+z^2+a}{x}.$$

When $a=0$, we use transformation T_2 of Section I. Then

$$v = \frac{1}{\bar{x}}, \quad \frac{dl^2}{x^2} = \frac{d\bar{l}^2}{\bar{x}^2}$$

and

$$ds^2 = \bar{V}^2(\bar{x})dt^2 - \frac{d\bar{l}^2}{\bar{W}^2(\bar{x})}.$$

If $a<0$, we let $a=-k^2$ and make use of T_3. Then $v=2k(\bar{y}/\bar{x})$ and $dl^2/x^2 = d\bar{l}^2/\bar{x}^2$. This reduces the line element (4.1) to the line element one would obtain by using (3.2). When $a>0$, we let $a=k^2$ and make use of T_4. The line element (4.1) then becomes spherically symmetric.

Thus, under the assumptions we have made, every isotropic solution can be reduced by transformations of coordinates to one of the forms (3.1), (3.2), (3.3).

V. SOLUTIONS IN EMPTY SPACE

When $\Lambda=0$, these three line elements have been discussed by others.[3] In empty space the basic solutions are as follows:

$ds^2 = dt^2 - dl^2$ (Special relativity),

$ds^2 = x^2dt^2 - dl^2$ (Special relativity),

$ds^2 = x^{-2}dt^2 - x^4dl^2$ (Infinite plane),

$$ds^2 = \left\{\frac{1-\frac{m}{2r}}{1+\frac{m}{2r}}\right\}^2 dt^2 - \left(1+\frac{m}{2r}\right)^4 dl^2$$ (Schwarzschild solution),

$$ds^2 = \frac{(x^2+y^2)^{\frac{1}{2}}-x}{(x^2+y^2)^{\frac{1}{2}}+x}dt^2 - \frac{A^2((x^2+y^2)^{\frac{1}{2}}+x)^2}{(x^2+y^2)^2}dl^2$$ (Semi-infinite plane of variable density).

From these we can generate, by means of the transformations[4] T_1, T_2, T_3, T_4, all possible static isotropic solutions in empty space for which $\Lambda=0$. For example, from the Schwarzschild solution we can obtain the line element.

$$ds^2 = \left\{\frac{1-\frac{m}{2}\frac{r_1}{r_2}}{1+\frac{m}{2}\frac{r_1}{r_2}}\right\}^2 dt^2 - 4k^2\left(\frac{1}{r_1}+\frac{m}{2r_2}\right)^4 dl^2,$$

where $r_1^2=(x+k)^2+y^2+z^2$, $r_2^2=(x-k)^2+y^2+z^2$. Excluding rotations and translations of axes, we can, in this way, generate twelve formally different solutions. They will, however, represent the same physical situations as above from the point of view of accelerated axes.

When $\Lambda\neq 0$ the general solutions can only be obtained by means of elliptic functions. We shall use the notation $P(x;\ g_2;\ g_3)$ to denote the Weierstrass elliptic function with invariants g_2, g_3. With this notation the three basic isotropic line elements for empty space are as follows.

$$ds^2 = \left[\frac{d}{dx}\log W\right]^2 dt^2 - \frac{dl^2}{W^2}, \tag{5.1}$$

where

$$W = \frac{4}{c}P\left(x;\ 0;\ \frac{\Lambda c^2}{48}\right).$$

$$ds^2 = \left[\frac{d}{d\theta}\log W\right]^2 dt^2 - \frac{dl^2}{\rho^2 W^2}, \tag{5.2}$$

where

$$W = \frac{4}{c}\left[P\left(\theta;\ \frac{1}{12};\ \frac{\Lambda c^2}{48}+\frac{1}{216}\right)+\frac{1}{12}\right]$$

and ρ, θ, z are cylindrical coordinates.

$$ds^2 = \left[r\frac{d}{dr}\log u\right]^2 dt^2 - \frac{dl^2}{r^2u^2}, \tag{5.3}$$

[3] P. Y. Chou, Am. J. Math. 59, 754–763 (1937) and Am. J. Math. 62, 43–48 (1940).

[4] Since T_1, T_2, T_3, T_4 were used to reduce the line elements to their simplest form, we use the inverse transformations to generate new solutions from the basic solutions.

where

$$u=\frac{4}{c}\left[P\left(\log r;\frac{1}{12};\frac{\Lambda c^2}{48}-\frac{1}{216}\right)-\frac{1}{12}\right].$$

In each case c is an arbitrary constant. It might be pointed out that for certain values of c the elliptic function will degenerate into elementary functions. However, all the basic solutions are contained in the above three line elements. We shall outline the method by which the spherically symmetric line element (5.3) was obtained. The method of obtaining the others is much the same.

For a spherically symmetric line element the equations $T_j^i=0$ lead to the following three equations.

$$\frac{1}{W}\left[W_{rr}+\frac{W_r}{r}\right]-\frac{1}{V}\left[V_{rr}+\frac{V_r}{r}\right]-\frac{[W_r^2+\Lambda]}{W^2}=0, \quad (5.4)$$

$$\frac{1}{W}\left[W_{rr}-\frac{W_r}{r}\right]-\frac{1}{V}\left[V_{rr}-\frac{V_r}{r}\right]-2\frac{W_rV_r}{WV}=0, \quad (5.5)$$

$$\frac{2}{W}\left[W_{rr}+\frac{2W_r}{r}\right]-\frac{[3W_r^2+\Lambda]}{W^2}=0. \quad (5.6)$$

Adding (5.5), (5.6) and subtracting (5.4) we find

$$\frac{V_r}{V}\left[r\frac{W_r}{W}-1\right]=r\frac{W_{rr}}{W}+\frac{W_r}{W}-r\frac{W_r^2}{W^2}=\frac{d}{dr}\left[r\frac{W_r}{W}-1\right]. \quad (5.7)$$

This can be integrated to give

$$V=A\left[r\frac{W_r}{W}-1\right],$$

where A is a constant of integration. We may take $A=1$ since this involves only a change of the time scale. Thus the equation

$$V=r(W_r/W)-1 \quad (5.8)$$

will determine V once W is known. To determine W we make the substitutions $W=ru$, $s=\log r$ in (5.6). This becomes

$$\frac{2d^2u}{ds^2}-\frac{3}{u}\left(\frac{du}{ds}\right)^2=\frac{\Lambda}{u}-u. \quad (5.9)$$

Since (5.9) does not contain s explicitly, we can integrate with respect to u, and (5.9) becomes

$$\left(\frac{du}{ds}\right)^2=cu^3+u^2-\frac{\Lambda}{3}. \quad (5.10)$$

The general solution of (5.10) is

$$u=\frac{4}{c}\left[P\left(s+a;\frac{1}{12};\frac{\Lambda c^2}{48}-\frac{1}{216}\right)-\frac{1}{12}\right], \quad (5.11)$$

where a is an arbitrary constant. However, by a suitable change in the length scale of r we may take $a=0$. Equations (5.11), (5.8) lead to

$$W=ru, \quad V=r(d/dr)\log u, \quad (5.12)$$

$$u=\frac{4}{c}\left[P\left(\log r;\frac{1}{12};\frac{\Lambda c^2}{48}-\frac{1}{216}\right)-\frac{1}{12}\right]. \quad (5.13)$$

Thus we obtain the line element (5.3). It is not difficult to show that (5.3) is the isotropic form of the Schwarzschild exterior solution.

The line elements (5.1), (5.2) are obtained in a similar manner. From the three basic line elements (5.1), (5.2), (5.3) we can generate all the static isotropic solutions ($\Lambda\neq 0$) by means of the transformations of Section I.

VI. CONCLUSION

When the components of the energy momentum tensor T_j^i satisfy the conditions $T_1^1=T_2^2=T_3^3$, $T_j^i=0$, $i\neq j$ it has been shown that the line element can be reduced to three basic forms. These results may be used to determine isotropic solutions valid inside matter. The author has obtained several such solutions and will publish these results in a later paper.

In empty space we have seen that the condition $\Lambda=0$ implies that the known physical distributions of matter are the only ones for which static isotropic coordinate systems exist. We feel that the new forms of line element found for these known physical distributions may be of interest. Oftentimes certain physical properties are more readily discernible in one system of coordinates than in another. However, no detailed study of these line elements has as yet been made.

In the more general case ($\Lambda\neq 0$), three new

line elements were found. The line element (5.3) is the isotropic form of the Schwarzschild exterior solution ($\Lambda \neq 0$). As yet the author has not succeeded in identifying the other two. The solutions of this type were included in this paper for two reasons. First, for completeness, to show the problem is soluble even when the more general field equations are used. Second, and more important, is the fact that the type of equation one must solve, when seeking non-static isotropic solutions, is exactly the same type as is solved in this part of the paper. The only difference is that Λ is replaced by a function of t.

In a later paper the results for non-static isotropic solutions will be given. By similar methods all these solutions are found, one of which may be identified as the relativistic solution for the field owing to an expanding spherical mass of gas.

PHYSICAL REVIEW VOLUME 66, NUMBERS 9 AND 10 NOVEMBER 1 AND 15, 1944

The Electrical Resistivity of Copper-Zinc and Copper-Tin Alloys at Low Temperatures*

HENRY A. FAIRBANK
Sloane Physics Laboratory, Yale University, New Haven, Connecticut

(Received August 22, 1944)

A systematic investigation of the resistivity ρ of the copper-zinc and copper-tin alpha-phase solid solution systems has been made in the temperature range 14.3°K to room temperature. Measurements were taken on both annealed and hard-drawn specimens. For the annealed set, the resistivity varied linearly with the temperature above 70°K and with a higher power of T at low temperatures, approaching a constant value below 20°K. Above 70°K the value of $(d\rho/dT)$ was found to increase linearly with atomic percent solute in variance with Matthiessen's rule. The residual resistivity increased with percent of added solute for both alloy systems, but not in agreement with Nordheim's theory, unless it be assumed that the effective number of free electrons per atom increases with added solute atoms or that the specimens were not true random solid solutions. The cold work produced some unexpected effects. Although the expected increase of resistivity with residual strain occurred in the Cu-Zn alloys, the specimens of zero to three atomic percent tin, which were hard-drawn through a 75 percent reduction and left in the strained state, showed a lower resistivity at low temperatures than did the corresponding annealed, quenched specimens. Possible explanations of this anomolous behavior are discussed.

I. INTRODUCTION

L. NORDHEIM[1] has predicted on the basis of a quantum mechanical treatment that the residual resistivity of a disordered binary substitutional alloy free from strains should be a parabolic function of the atomic percent of solute. Although room temperature data on several binary alloys have been obtained by Linde[2] and others,[3] extrapolations to absolute zero must be made to provide any comparison with the theory, and there is insufficient evidence to allow reliance on these large extrapolations.

A few results, however, have been found at temperatures near the absolute zero. Pospisil[4] has investigated rather thoroughly the resistivity of the Cu-Au alloy system down to 20°K. Krupkowski and de Haas[5] carried out similar measurements for the Cu-Ni system down to 14.8°K. Giauque and Stout[6] have made resistance measurements for six Au-Ag alloys from 1.6°K to 0°C, and Lane[7] has obtained similar

* This is part of a dissertation presented to the Faculty of the Graduate School of Yale University in candidacy for the Degree of Doctor of Philosophy, June, 1944.

[1] L. Nordheim, Ann. d. Physik **9**, 664 (1931).

[2] J. O. Linde, Ann. d. Physik **10**, 52 (1931); **14**, 353 (1932); **15**, 219 (1932). C. H. Johansson and J. O. Linde, Ann. d. Physik **25**, 1 (1936).

[3] B. Svensson, Ann. d. Physik **14**, 699 (1932). W. Geibel, Zeits f. angew. Chemie **70**, 240 (1911). A. L. Norbury and K. Kuwada, Phil. Mag. **4**, 1338 (1927).

[4] V. Pospisil, Ann. d. Physik **18**, 497 (1933).

[5] A. Krupkowski and W. J. de Haas, Leiden Communications **194a**, 3 (1928).

[6] W. F. Giauque and J. W. Stout, J. Am. Chem. Soc. **60**, 388 (1938).

[7] C. T. Lane and W. Dodd, Phys. Rev. **61**, 183 (1942).

measurements from 4.2°K to room temperature for several single crystals of antimony containing small amounts of tin in solid solution. The results for the first three alloy systems are in fair agreement with Nordheim's theory. For Sb-Sn the agreement is poor. It appeared highly desirable that further experimental data on other alloy systems be taken at temperatures near absolute zero as a basis upon which to test and extend the present theory.

Hence the purpose of this investigation was to study in a systematic fashion the electrical resistivity of a series of copper alloys in the alpha-solid solution range at low temperatures. Results have been obtained for copper alloyed with zinc, and copper alloyed with tin from 14.3°K to room temperature. Two complete sets of data on each group were taken; one set on annealed quenched specimens which theoretically should have been strain-free and completely disordered, and the other on specimens hard-drawn by a specified amount and left in the strained condition. Thus it was possible to test for these copper alloy systems: 1. the dependence of the electrical resistivity of alpha-phase copper alloys on temperature; 2. Matthiessen's rule which states that the change in resistance owing to a small addition of another metal in solid solution is independent of temperature; 3. Nordheim's prediction for the variation of residual resistance with percent solute; 4. the effect of strain on the resistivity at high and low temperatures.

II. PREPARATION OF THE SPECIMENS

Both the copper-tin and copper-zinc alloys were furnished by the American Brass Company of Waterbury, Connecticut, through the kindness of Dr. C. S. Smith and Mr. E. W. Palmer, who have made a systematic study[8] of the electrical and thermal conductivities of these and several other copper-alloy systems at 20°C and above.

The copper-zinc wires were prepared from the $\frac{3}{4}$-inch rods used by Dr. Smith in his thermal conductivity measurements. Each rod was hot-rolled flat to a strip 0.200 inch thick at a temperature of 800°C and a square section 0.2 inch ×0.2 inch was sawed out, swaged round, and drawn in round dies to wires of 0.04-inch diameter. This was accomplished by first drawing the wires in four steps to 0.162 inch in diameter, followed by a one-hour anneal at 750°C and air cooling to room temperature. The wires were then drawn in 6 steps to 0.080 inch and again annealed for one hour at 750°C and air cooled. In both anneals the wire in the form of a coil was sealed from the air by tightly wrapping in a sheet of copper 0.005 inch thick. The last drawing was from 0.080-inch to 0.040-inch diameter (a 75 percent reduction), leaving the wires 6 numbers hard. The treatment of the specimens up to this point was performed by the American Brass Company.

From these wires two sets of specimens 3 inches long were prepared. The first set was annealed at 700°C for one hour in a graphite mold and then rapidly quenched by immersing the graphite mold containing the specimens in cold water. This treatment should have sufficed to remove all residual strains and leave the specimens in a disordered state.

An adjacent section 3 inches long of each alloy wire was snipped off and left in the hard-drawn state. To determine the effect of residual strains on the resistivity, measurements on both the unannealed and annealed specimens were taken for each alloy.

To remove the thin oxide film that formed during annealing, the specimens were lightly etched in a dilute H_2SO_4 solution. The cleaning was finished by lightly polishing each wire with fine steel wool.

The copper-tin specimens were prepared from $\frac{3}{4}$-inch rods in the same way as were the copper-zinc alloys with a few minor variations. The $\frac{3}{4}$-inch rods were cold-rolled instead of hot-rolled, to a strip 0.200 inch thick, annealed one hour at 750°C, and air cooled. The succeeding cold drawing followed the same pattern as for the copper-zinc alloys. Again two sets of specimens were prepared from the hard-drawn 0.040-inch wires; the first set was left in the hard-drawn condition and the second set was sealed in a copper tube, annealed at 700°C for an hour, and quenched in cold water. In pickling the specimens following each anneal, the H_2SO_4 etch was followed by a cleaning in a sodium bichromate cleaning solution and a dip in a 50 percent solu-

[8] C. S. Smith, Trans. A. I. M. E., Inst. Met. Div. **89**, 84 (1930); **91**, 354 (1931). C. S. Smith and E. W. Palmer, Trans. A. I. M. E., Inst. Met. Div. **117**, 225 (1935).

tion of HCl. The drawing, annealing, and pickling of this set of specimens were performed entirely by the American Brass Company.

The purity of both sets of alloys was reasonably good. In the copper-zinc alloys there were traces of iron and lead but in no case did the weight percentage of either impurity exceed 0.03 percent. In the copper-tin alloys traces of phosphorous were present in addition to small amounts of iron and lead. In the 2.70 atomic percent tin specimen (4.92 weight percent), the most unfavorable case, there were present 0.06 weight percent phosphorous, 0.01 weight percent iron, and 0.05 weight percent lead.[9]

III. THE RESISTIVITY MEASUREMENTS

Current and potential leads of No. 36 copper wire were either spot-welded or soldered to each specimen. The spot welding was done with a conventional apparatus using copper electrodes. Observation under a low powered microscope revealed a clean weld with no apparent disturbance of the specimen. It was found that an equally satisfactory junction could be made by soldering the copper leads on with a low melting eutectic solder.[10] By tinning the lead wires first a clean connection could be made with no observable disturbance of the specimen.

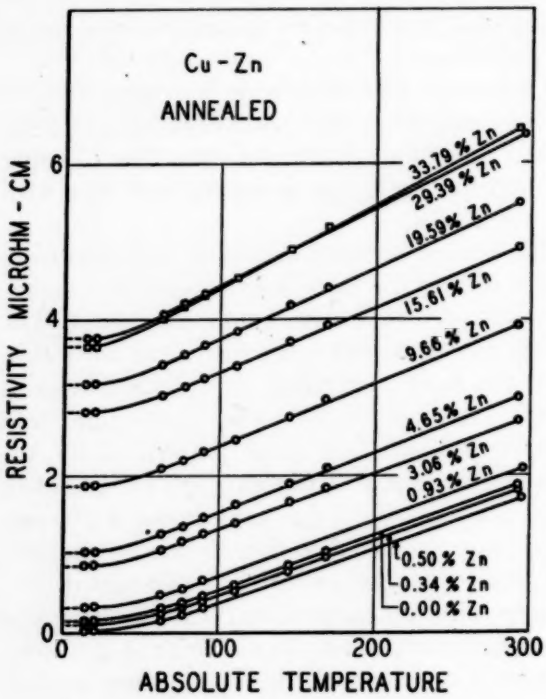

FIG. 1. Dependence of the resistivity on temperature for the annealed, quenched Cu-Zn specimens.

The resistance of the specimens was measured by comparison with a standard resistance of about two-thousandth ohm by means of a type K Leeds and Northrup potentiometer. The modified circuit described by Kapitza and Milner[11] was used in order to nullify the effect of any thermal e.m.f.'s in the specimens or lead wires. The latter become important when parts of the apparatus are at widely different temperatures.

In order that the resistance of a number of specimens could be measured in the same run, the specimens were mounted in groups of twelve on a fiber holder and placed in the bottom of a long narrow Dewar flask (2.6-cm inside diameter and 30 cm long). In addition to measurements at room temperature, resistivity values were determined at the following fixed points: freezing point of water, boiling point of ethylene (169.5°K), liquid ethylene under reduced pressure (*ca.* 146°K), boiling point of methane (111.6°K), boiling point of oxygen (90.2°K), boiling point of nitrogen (77.3°K), near the triple point of nitrogen (*ca.* 63.5°K), boiling point of hydrogen (20.4°K), and near the triple point of hydrogen (*ca.* 14.3°K). Each of the above gases was liquefied by the use of liquid air with the exception of hydrogen, which was liquefied with a small-scale Hampson-type liquefier.[12] In the case of the boiling liquids the vapor pressure served to determine the temperature,[13] and for the room temperature measurements a calibrated copper-constantan thermocouple[14] was used.

The distance between the potential leads on the specimens was measured with a sensitive comparator. Since the wires were drawn through accurate dies, the cross-sectional area was

[9] The author is indebted to the American Brass Company for performing the analyses on these specimens.

[10] The solder was 63 percent tin, 37 percent lead and was produced by the Belmont Smelting and Refining Company, Brooklyn.

[11] P. Kapitza and C. Milner, J. Sci. Inst. **14**, 165 (1937).

[12] A description of the design and operation details of this liquefier will be published soon in another journal by the author.

[13] F. Henning and J. Otto, Physik. Zeits. **37**, 633 (1936).

[14] W. F. Roeser and A. I. Dahl, J. Research Nat. Bur. Stand. **20**, 337 (1938).

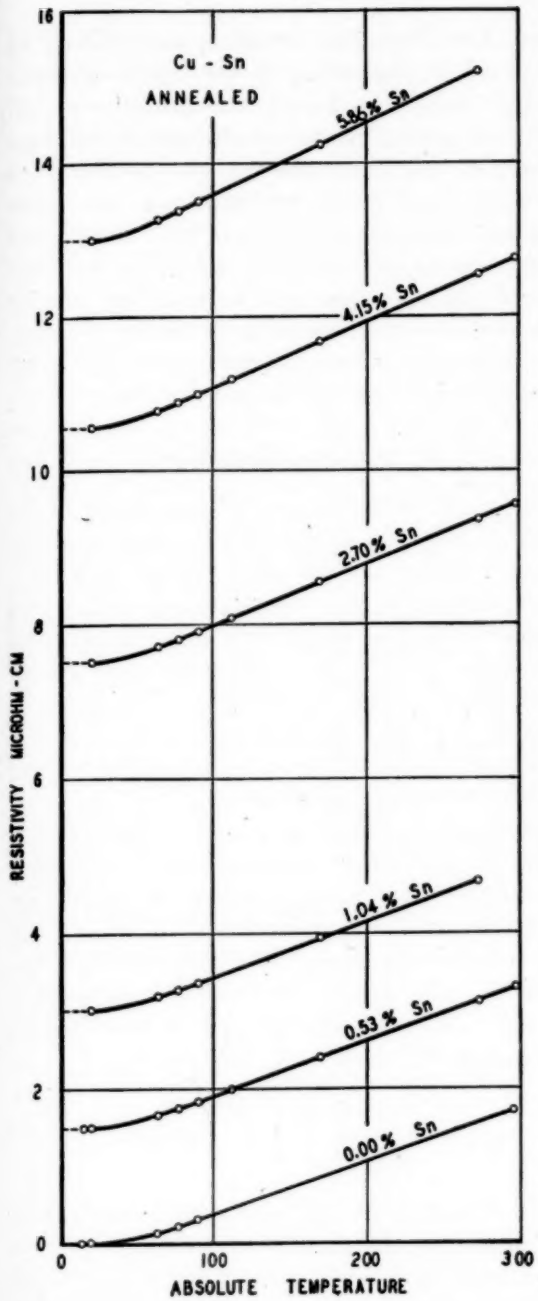

FIG. 2. Dependence of the resistivity on temperature for the annealed, quenched Cu-Sn specimens.

measured with an ordinary sensitive micrometer caliper.

The temperature and resistance measurements are probably accurate to within one percent, but the resistivity measurements may be in error by 2 percent.

IV. RESULTS AND DISCUSSIONS FOR THE ANNEALED SPECIMENS

A. Temperature Dependence

The dependence of resistivity on temperature is shown in Figs. 1 and 2 for the copper-zinc and copper-tin alloys, respectively. In the temperature range above 70°K the resistivity for all the alloys in both systems is clearly a linear function of the temperature, in agreement with the Bloch theory.[15]

At low temperatures the temperature dependent part of the resistivity is definitely proportional to a higher power of the absolute temperature, but whether it varies as the fifth power of T in agreement with the prediction of the theory of Bloch and Bardeen[15] is impossible to determine without more data in the low temperature region.

The slopes of the curves between 20.4°K and 14.3°K are practically zero in every case investigated, indicating that the extrapolated value of the resistivity at absolute zero is not appreciably different from that at 20°K. In the case of two of the specimens (15.61 atomic percent Zn and 19.59 atomic percent Zn) the value of the resistivity at 14.3°K appeared to be slightly higher than at 20.4°K. However, it is unlikely that this is significant inasmuch as the difference in the values is of the same order of magnitude as the possible error of measurement.

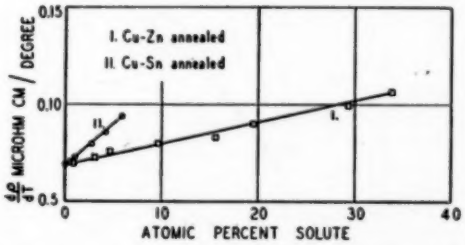

FIG. 3. Temperature rate of change of resistance above 70°K for the annealed, quenched specimens of both alloy systems.

B. Matthiessen's Rule

A close inspection of Figs. 1 and 2 reveals that Matthiessen's rule is not closely obeyed for these

[15] An excellent summary of the quantum theories of electrical resistance is given by Seitz, *The Modern Theory of Solids* (McGraw-Hill Book Company, Inc., New York, 1940). F. Bloch, Zeits f. Physik **59**, 208 (1930). J. Bardeen, Phys. Rev. **52**, 688 (1937).

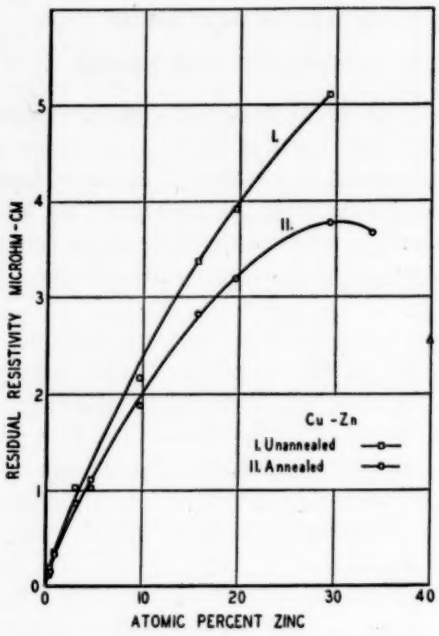

FIG. 4. Dependence of the resistivity at 14.3°K on the percentage of zinc atoms. Curve *I* is for the hard-drawn specimens and curve *II* for the annealed quenched specimens.

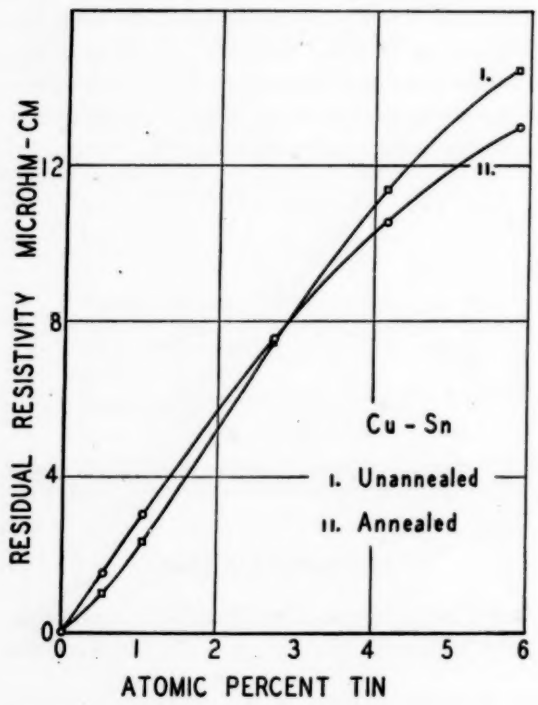

FIG. 5. Dependence of the resistivity at 20.4°K on the percentage of tin atoms. Curve *I* is for the hard-drawn specimens and curve *II* for the annealed, quenched specimens.

alloys. The divergence is shown more clearly in Fig. 3 where the slope of the resistivity-temperature curves in the high temperature region is plotted against percent added solute. If Matthiessen's rule were obeyed, the temperature dependent part of the resistance of each alloy should be identical with that of pure copper and $d\rho/dT$ should be the same for all specimens. Instead we find that $d\rho/dT$ increases linearly with atomic percent solute for both sets of alloys. This is in agreement with the results found by Borelius[16] on several gold alloy systems.

C. Residual Resistivity

In Figs. 4 and 5 is shown the dependence of the residual resistivity of the two systems of alloys on the percent added solute. The resistivity values are those for the lowest temperatures attained, 14.3°K for the Cu-Zn group and 20.4°K for the Cu-Sn group, but these values should not deviate appreciably from those at absolute zero as explained previously. For the present let us consider only the curves for the annealed quenched specimens.

When foreign atoms are added in solid solution to the lattice of a pure metal, the slightly different field of the solute atom destroys the periodicity of the lattice and thus increases the probability that an electron wave will be scattered. Nordheim[1] has shown that the residual resistivity of a binary substitutional alloy, free from strains and completely disordered, is given by

$$\rho_0 = \frac{h}{4e^2N^{\frac{1}{3}}}\left(\frac{3n}{\pi}\right)^{\frac{1}{3}}(1-x)xQ_{12},$$

where N is the effective number of free electrons per atom, n is the number of atoms per cc, x is the atomic fraction of solute, and Q_{12} is the effective scattering cross section of each solute atom. Provided N, n, and Q_{12} are not functions of x, a plot of ρ_0 *versus* $(1-x)x$ should be a straight line curve through the origin. That this is not the case for the alpha-phase Cu-Zn and Cu-Sn alloys is seen in Figs. 6 and 7. Curve *I* in each figure is the straight line extension of the experimental curve for small values of x and represents the theoretical curve expected if the

[16] G. Borelius, Metallwirts. **12**, 173 (1933).

residual resistivity were proportional to $(1-x)x$. Curve *II* in each figure is the experimental curve and is seen to be far from linear.

A small part of this discrepancy could be attributed to the decrease in n; the number of atoms per cc as either zinc or tin atoms are added in solid solution to the copper lattice. The decrease in n can be calculated from the density of the alloys and the atomic masses of the constituent atoms. In the Cu-Zn alloy system n decreases only slightly with increasing percentage zinc, the decrease in n being only 6 percent below the value for pure copper for a specimen of 35 atomic percent zinc. Since n appears in Nordheim's formula to the one-third power this would account for a 2 percent discrepancy between the experimental and theoretical curves for this alloy. In the copper-tin system the decrease in n is more rapid as tin atoms are added, the decrease being 5 percent for the alloy of 6 atomic percent tin. Likewise, this would account for a discrepancy of only one-third of 5 percent between the two curves in Fig. 7 for this composition alloy.

To account for the remainder of the discrepancy two possibilities suggest themselves: Either the specimens used were not true random solid solutions or the effective number of free

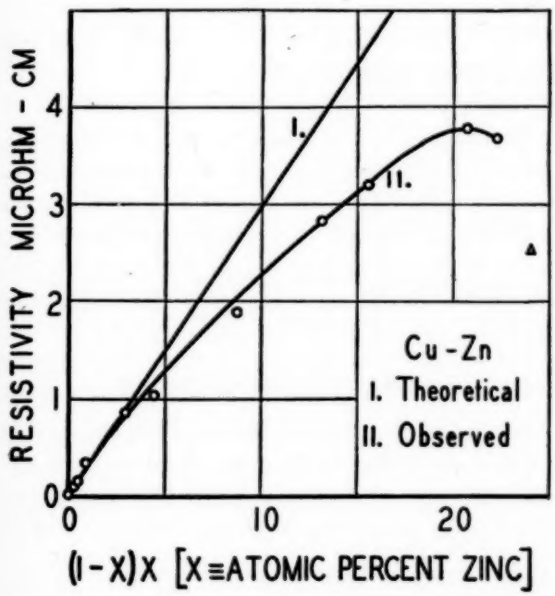

FIG. 6. Curve *I* is the straight line extension of the experimental curve, curve *II*, for small values of x. The resistivity values are for the annealed, quenched Cu-Zn specimens at 14.3°K.

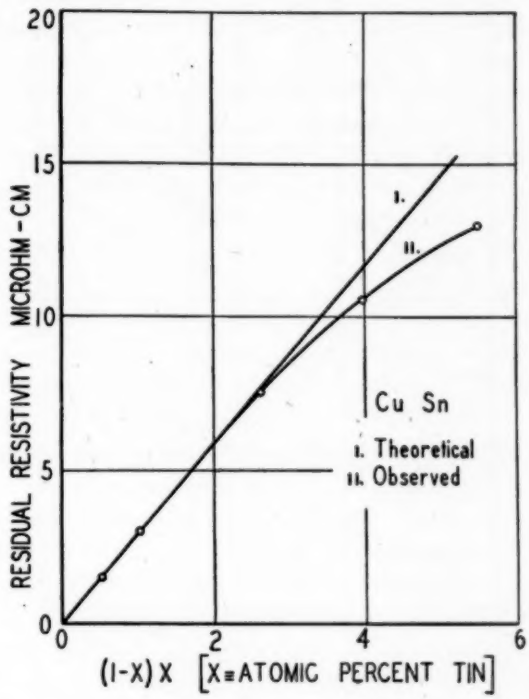

FIG. 7. Curve *I* is the straight line extension of the experimental curve, curve *II*, for small values of x. The resistivity values are for the annealed, quenched Cu-Sn specimens at 20.4°K.

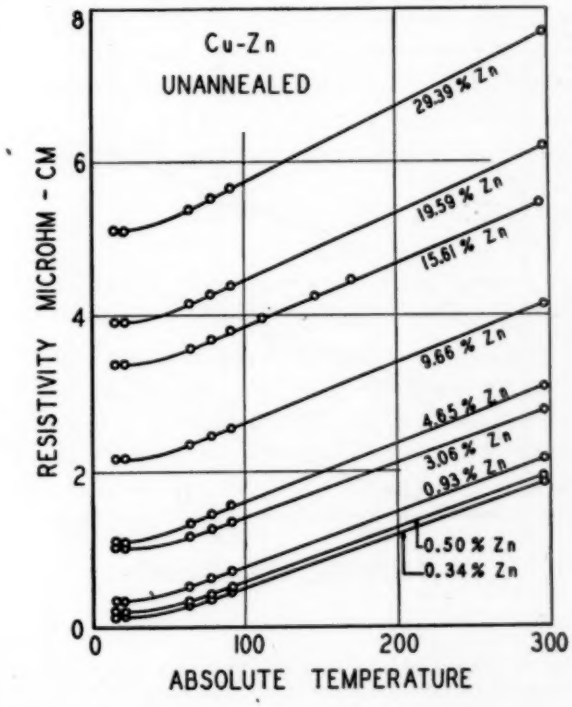

FIG. 8. Dependence of the resistivity on temperature for the hard-drawn Cu-Zn specimens.

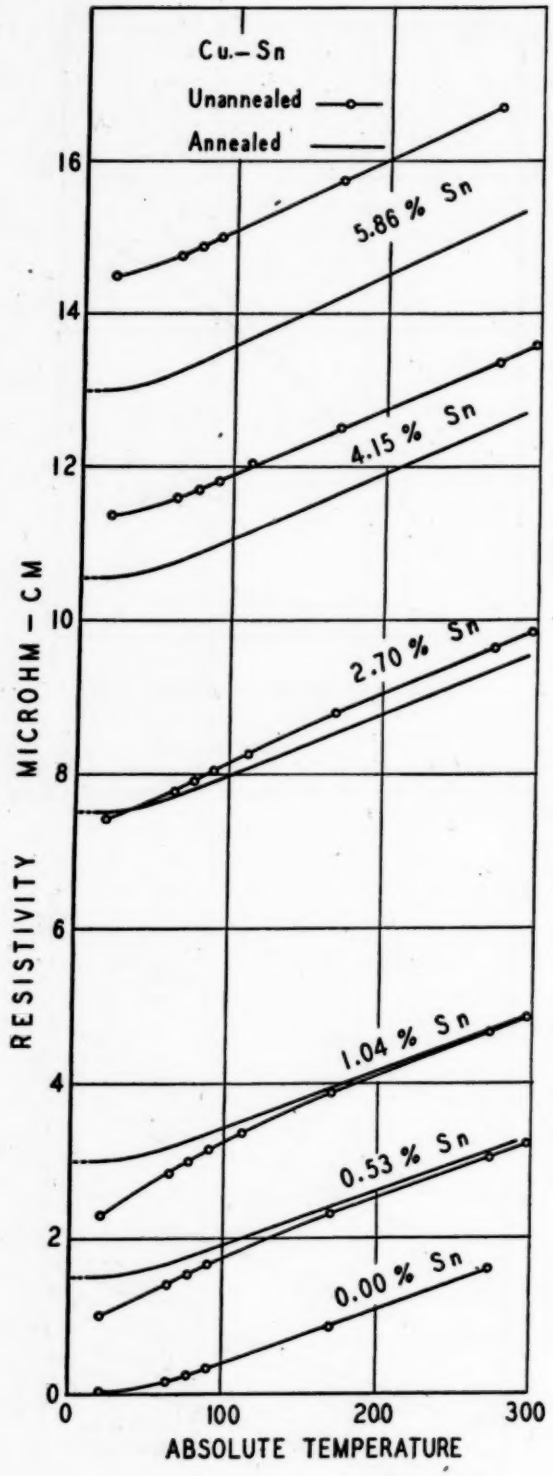

FIG. 9. Dependence of the resistivity on temperature for the hard-drawn Cu-Sn specimens. For ready comparison the curves for the corresponding annealed, quenched specimens are also shown.

electrons increases with increasing percent solute in both alloy systems. The first possibility seems unlikely. The work of many investigators[17] is in agreement that zinc forms a solid solution with copper up to about 36 atomic percent zinc at 700°C and to an even higher value at room temperature. The copper-tin system[17] has an alpha-phase limit of about 8 atomic percent tin at 700°C. Haase and Pawlek[18] did find that the alpha-phase limit for the Cu-Sn system may be as small as one percent tin or less at room temperature, but these results were obtained on specimens put through large amounts of cold work followed by long time anneals at temperatures from 200 to 400°C. Inasmuch as all the Cu-Zn and Cu-Sn alloys in the annealed group were annealed at 700°C for 1 hour and then quenched, one should expect a true solid solution for all the specimens. An exception to this statement is the Cu-Zn alloy of 40.07 atomic percent zinc. It clearly is beyond the alpha-phase limit and its low resistivity attests to this fact. A point for this specimen is included in Figs. 4 and 6 merely to show the effect expected if the other specimens were not true solid solutions.

There is the possibility that the distribution of solute atoms is not entirely random even though the specimens were quenched from 700°C. If any order were present at this annealing temperature, it would be preserved in the quench and would produce a lower resistivity than would occur for a completely random solid solution.

A more likely explanation of the behavior of the curves in Figs. 6 and 7 is that the effective number of free electrons per atom may change as zinc or tin atoms are added in solid solution to the copper lattice. It might be well, however, to reserve final judgment on the theoretical interpretation of these curves until the theory of Nordheim has been refined and extended.

V. EFFECT OF COLD WORK

The temperature dependence of the resistivity for the copper-zinc specimens which were hard-drawn through a 75 percent reduction and left in the strained condition is shown in Fig. 8. The

[17] *International Critical Tables* (1927), Vol. II, pp. 433, 435. J. L. Haughton, Inst. Met. Monograph and Report Series, No. 2, 79, 81 (1942).

[18] C. Haase and F. Pawlek, Zeits. f. Metallkunde 28, 73 (1936).

expected increase in resistivity caused by residual strains was found, the increase being larger for the higher composition specimens. This is seen more easily in Fig. 4 where the resistivity at 14.3°K is plotted against atomic percent zinc for both the annealed and unannealed group. The temperature dependence of the specimens is seen to be changed very little as can be seen by comparing Figs. 1 and 8.

The results for the unannealed group of copper-tin alloys is much more interesting as is immediately evident on inspection of Figs. 5 and 9. For the higher percentage tin specimens (4.15 percent Sn and 5.86 percent Sn) a regular increase in resistance owing to strains is found throughout the temperature range investigated, in agreement with results on the copper-zinc system. However, in the region between 0 and 3 atomic percent tin the annealed specimens are seen to have a higher resistivity than the unannealed. Furthermore, the decrease in resistance of the hard-drawn specimens below that of the annealed specimens increases as the temperature is lowered. In fact, it appears from the trend of the curves in Fig. 9 that the resistivity of the 1.04 percent Sn unannealed specimen might drop to a much lower value at temperatures nearer absolute zero in complete disagreement with the trend of the curves for the annealed specimens.

Several possible explanations of this anomolous behavior suggest themselves. First, it may in some way be caused by the impurities in the specimens or a surface effect introduced in pickling or spot welding or in some other phase of preparation. This possibility has been thoroughly investigated and it seems very unlikely, as the anomalies in the curves for the unannealed specimens occur for several specimens in a regular manner. Furthermore, the preparation of both unannealed and annealed specimens was parallel in every detail except for the final anneal of the latter group, and no such effects occur among the annealed specimens.

A second possibility is seen on reviewing the preliminary treatment of the unannealed group of specimens. The last anneal prior to the reduction from 0.080-inch to 0.040-inch diameter was followed by an air cooling. The work of Haase and Pawlek,[18] mentioned previously, showed that extensive cold work, followed by long-time anneals at temperatures from 200 to 400°C, resulted in a marked reduction of the alpha-phase solid solution limit. This would suggest that some phase separation may have occurred even though the treatment was only remotely similar to that of Haase and Pawlek. Why this should cause the anomalous behavior at low temperatures is hard to see, however.

It seems more likely that the effect is one of order. This may have occurred during the air quench or it may well have been produced in some manner by the cold work. The former point can be tested by repeating the measurements with two sets of specimens—one set annealed at a high temperature and quenched before the reduction, the other set annealed and very slowly cooled to room temperature before reduction.

The question of whether any irreversible changes occurred at low temperatures for this group of specimens naturally arises. Since the data at the lowest temperatures were taken first, this point was not directly tested on the set of specimens used. However, a check measurement was made on another group of specimens, taken from the same alloy wires, at high temperatures, and reasonable agreement in the resistivity values was found, indicating no irreversible effect.

The author wishes to express his appreciation to Professor C. T. Lane, under whose direction this research was begun, for suggesting the problem and offering many helpful suggestions. He is much indebted to Dr. C. S. Smith and Mr. E. W. Palmer of the American Brass Company for their advice and many services.

The Quantum Mechanical Hamiltonian for the Linear Polyatomic Molecule Treated as a Limiting Case of the Non-Linear Polyatomic Molecule

HARALD H. NIELSEN
Mendenhall Laboratory of Physics, Ohio State University, Columbus, Ohio

(Received August 3, 1944)

The quantum mechanical Hamiltonian for a general triatomic molecule is derived by the method of Wilson and Howard. It is pointed out that the corresponding wave equation does not lend itself to an exact solution and that the actual Hamiltonian must be replaced by its expansion. When the Hamiltonian is expanded on the basis that the displacement of the particles from equilibrium is small compared to the equilibrium positions of the particles (as is legitimate in the non-linear case) the results of Shaffer and Nielsen are obtained. In the case of linear XY_2 molecules the equilibrium value of the moment of inertia $I_{zz}^{(e)}=0$ so that the displacements of the particles normal to the axis z must be considered large compared to the values of equilibrium coordinates x_i^0 and y_i^0 of the nuclei. If the molecule is considered as very nearly linear indeed and the Hamiltonian is expanded on the hypothesis that $\mu q^2 \gg I_{zz}^{(e)}$, μ being the reduced mass and q being the normal coordinate, the results of Dennison for the linear XY_2 molecular model are approached asymptotically as $I_{zz}^{(e)}$ approaches zero.

I. INTRODUCTION

THE correct form for the quantum mechanical Hamiltonian for a vibrating and rotating polyatomic molecule has been shown by Wilson and Howard[1] to be the following:

$$H=(1/2)\sum_{\alpha\beta}\mu_{\alpha\beta}P_\alpha P_\beta-\sum_\alpha h_\alpha P_\alpha+(\mu^{\frac{1}{4}}/2)\sum_{\alpha\beta}p_\alpha\mu_{\alpha\beta}\mu^{-\frac{1}{2}}p_\beta+(1/2)\sum_s\mu^{\frac{1}{4}}p_s\mu^{-\frac{1}{2}}p_s+V, \tag{1}$$

where

$$h_\alpha=(1/2)\sum_\beta\{2\mu_{\alpha\beta}p_\alpha+(p_\beta\mu_{\alpha\beta})+\mu_{\alpha\beta}\mu^{\frac{1}{4}}(p_\beta\mu^{-\frac{1}{4}})\}, \tag{2}$$

α and β being summed over x, y, and z. The P_α are the operators corresponding to the components of the angular momentum along the body fixed axes x, y, and z; i.e.,

$$\begin{aligned}P_x&=(-ih)[(-\cos\varphi/\sin\theta)(\partial/\partial\psi-\cos\theta\partial/\partial\varphi)+\sin\varphi\partial/\partial\theta],\\ P_y&=(-ih)[(\sin\varphi/\sin\theta)(\partial/\partial\psi-\cos\theta\partial/\partial\varphi)+\cos\varphi\partial/\partial\theta],\\ P_z&=(-ih)\partial/\partial\varphi,\end{aligned} \tag{3}$$

θ, ψ, and φ being so defined that θ is the angle between the space fixed z' axis and the axis z; ψ, the angle between the nodal line and the x' axis, and φ the angle between the x axis and the nodal line. The quantities $\mu_{\alpha\beta}$ are defined as $\Delta_{\alpha\beta}/\Delta$ where $\Delta_{\alpha\beta}$ is the $\alpha\beta$th cofactor of the determinant Δ which is:

$$\Delta=\begin{vmatrix} I'_{xx} & -I'_{xy} & -I'_{xz}\\ -I'_{yx} & I'_{yy} & -I'_{yz}\\ -I'_{zx} & -I'_{zy} & I'_{zz}\end{vmatrix}=\mu^{-1}. \tag{4}$$

The $I'_{\alpha\alpha}$ and $I'_{\alpha\beta}$ are defined as follows:

$$I'_{\alpha\alpha}=I_{\alpha\alpha}-(\textstyle\sum_s(h/\lambda_s^{\frac{1}{4}})\xi_{\alpha s}q_s)^2,\quad I'_{\alpha\beta}=I_{\alpha\beta}-\textstyle\sum_s(h/\lambda_s^{\frac{1}{4}})\xi_{\alpha s}\eta_{\beta s}q_s^2, \tag{5}$$

in which $I_{\alpha\alpha}$ and $I_{\alpha\beta}$ are, respectively, the moments and products of inertia, q_s are dimensionless normal coordinates, and the $\xi_{\alpha s}$, $\eta_{\alpha s}$, and $\zeta_{\alpha s}$ ($\xi_{\alpha s}$, $\eta_{\alpha s}$, and $\zeta_{\alpha s}$ are, respectively, associated with the axes x, y, and z) are what may be termed Coriolis coupling coefficients which depend upon the nature of the normal oscillations. The p_β are the components of the internal angular momentum of

[1] E. B. Wilson, Jr., and J. B. Howard, J. Chem. Phys. 42, 262 (1936).

oscillation in the coordinates moving with the molecule. They are known to be the following:

$$p_x=\sum_s \sum_{s'>s'} \xi_{ss'}[(\lambda_s/\lambda_{s'})^{\frac{1}{2}}q_s p_{s'}-(\lambda_{s'}/\lambda_s)^{\frac{1}{2}}q_{s'}p_s], \quad (\lambda_s=(2\pi c\omega_s)^2), \tag{6}$$

p_y and p_z being obtained from (6) by permutation of $\xi_{ss'}$, $\eta_{ss'}$, and $\zeta_{ss'}$. The p_s occurring in the above relation are the momenta $p_s=-ih(\partial/\partial q_s)$ conjugate to the coordinates q_s. The method of Wilson and Howard has been applied by various authors to many molecular models to obtain explicit relations for their vibration-rotation energies.

The method of Wilson and Howard was formulated for non-linear molecules and it was not at once apparent how it might be applied in the case of linear polyatomic molecules. This problem has been dealt with by Sayvetz[2] who has treated the linear molecule as a special case of the axially symmetric molecule where the equilibrium value of one of the moments of inertia reduces to zero. In such molecules certain of the oscillations will be perpendicular to the internuclear axis z (the axis of symmetry). Since the force fields about the z axis will be cylindrically symmetric, oscillations of the molecule along the x axis will have the same frequencies as the corresponding oscillations along the y axis. Such frequencies are evidently twofold degenerate and require two coordinates, q_{s1} and q_{s2} to describe them. It is frequently convenient in such cases to replace these coordinates by their equivalents $q_{s1}=\rho_s \sin\chi_s$ and $q_{s2}=\rho_s\cos\chi_s$ in polar coordinates. ρ_s may be interpreted as the radius vector of the displacement and χ_s is the angle between ρ_s and the body fixed x axis. It is readily shown that in such cases $p_s=-ih\sum_s \zeta_{ss}\partial/\partial\chi_s$. Sayvetz has pointed out that in linear molecules the Eulerian angle φ enters only as a constant parameter and may therefore be given any convenient arbitrary value. It follows that $p_z=P_z$ so that all terms in (1) which contain (p_z-P_z) will vanish. As a consequence the third row and column of the determinant (4) will disappear and the Wilson and Howard method may be applied as before.

A problem which is intimately related to what has gone before is that of the quantum mechanical equations for the vibration-rotation energies of the non-linear XY_2 molecular model and of the linear XY_2 model. The former has been obtained by Shaffer and Nielsen[3] and by Darling and Dennison using the Wilson and Howard method in its original form; the latter has been arrived at by Dennison[4] using the Sayvetz modification. The two equations for the two models in the explicit forms in which they are given appear quite different and indeed the energy values finally obtained have certain fundamental differences, i.e., one cannot obtain either the quantum mechanical equation for the linear model or the corresponding energies for the linear case simply by letting $I_{zz}\to 0$ in the non-linear case. This fact has led to the belief that there is something fundamentally different between the two models rather than that the one simply is a special case of the other. This is, of course, disturbing since the wave equation in the non-linear case was derived quite generally for any shape of the model. In this paper we shall investigate the wave equation for the non-linear triatomic molecule and show that as the model straightens out the equation becomes asymptotically of the same form as the equation derived for the linear triatomic molecule by the Sayvetz method.

II. THE LINEAR XY_2 MODEL

The linear XY_2 molecular model has been treated by Dennison,[4] who has chosen the equilibrium positions of the three particles in the body fixed axes x, y, and z to be $(0, 0, -a)$; $(0, 0, 0)$; $(0, 0, +a)$. The displacements δx_i, δy_i, etc., of the particles from their equilibrium positions when expressed in terms of the normal coordinates are readily shown to be:

$$\begin{aligned}
&\delta x_1=(\sqrt{\mu}/M)q_{21}, \quad \delta x_2=\delta x_3=(-\sqrt{\mu}/2m)q_{21},\\
&\delta y_1=(\sqrt{\mu}/M)q_{22}, \quad \delta y_2=\delta y_3=(-\sqrt{\mu}/2m)q_{22},\\
&\delta z_1=(\sqrt{\mu}/M)q_3, \quad \delta z_2=(-\sqrt{\mu}/2m)q_3-(1/2m)^{\frac{1}{2}}q_1, \quad \delta z_3=(-\sqrt{\mu}/2m)q_3+(1/2m)^{\frac{1}{2}}q_1,
\end{aligned} \tag{7}$$

[2] A. Sayvetz, J. Chem. Phys. **7**, 383 (1939).
[3] W. H. Shaffer and H. H. Nielsen, Phys. Rev. **56**, 188 (1939). B. T. Darling and D. M. Dennison, Phys. Rev. **57**, 128 (1940).
[4] D. M. Dennison, Rev. Mod. Phys. **12**, 175 (1940).

where $\mu=(2mM/2m+M)$, m and M being the masses of the Y and X particles, respectively. The quantum mechanical Hamiltonian operator may be obtained by the Wilson-Howard method directly, with the modification of Sayvetz, or perhaps a little more easily from Eqs. 17-a, b, and c in Nielsen's[6] discussion of the vibration-rotation energies of the general polyatomic molecule. The only non-vanishing constants a_s, A_{sssr}, etc., which appear in these relations are the following:

$$a_1=b_1=-2(I_e)^{\frac{1}{2}}, \quad A_{1111}=B_{1111}=1, \tag{8}$$

where I_e is the equilibrium value of the moment of inertia, $2ma^2$. This leads at once to the following as the Hamiltonian, expressed in orders of magnitude, for the linear XY_2 molecule:

$$H^0=(\hbar/2)\{\lambda_1^{\frac{1}{2}}(p_1^2/\hbar^2+q_1^2)+\lambda_2^{\frac{1}{2}}(p_{21}^2/\hbar^2+p_{22}^2/\hbar^2+q_{21}^2+q_{22}^2)+\lambda_3^{\frac{1}{2}}(p_3^2/\hbar^2+q_3^2)\}+(P_x^2+P_y^2)/2I_e, \tag{9-a}$$

$$H^{(1)}=(-i\hbar^{\frac{1}{2}}\lambda_1^{\frac{1}{4}}p_1/I_e^{\frac{1}{2}})-(p_xP_x+p_yP_y)/I_e-(\hbar^2/\lambda_1)^{\frac{1}{2}}(q_1/I_e^{\frac{1}{2}})(P_x^2+P_y^2)+V_1, \tag{9-b}$$

$$H^{(2)}=(-i\hbar/I_e\lambda_1^{\frac{1}{2}})q_1p_1+(p_x^2+p_y^2)/2I_e+(3\hbar/2\lambda_1^{\frac{1}{2}})q_1^2(P_x^2+P_y^2)/I_e$$
$$+2(\hbar^2/\lambda_1)^{\frac{1}{2}}(q_1/I_e^{\frac{1}{2}})(p_xP_x+p_yP_y)+V_2, \tag{9-c}$$

where

$$p_x=[(\lambda_3/\lambda_2)^{\frac{1}{2}}q_{22}p_3-(\lambda_2/\lambda_3)^{\frac{1}{2}}q_3p_{22}]$$

and

$$p_y=[(\lambda_2/\lambda_3)^{\frac{1}{2}}q_3p_{21}-(\lambda_3/\lambda_2)^{\frac{1}{2}}q_{21}p_3],$$

$$V_1=hc\{k_{111}q_1^3+k_{122}q_1(q_{21}^2+q_{22}^2)+k_{133}q_1q_3^2\}$$

and

$$V_2=hc\{k_{1111}q_1^4+k_{2222}(q_{21}^2+q_{22}^2)^2+k_{3333}q_3^4+k_{1122}q_1^2(q_{21}^2+q_{22}^2)+k_{1133}q_1^2q_3^2+k_{2233}q_2^2q_3^2\}.$$

This will be seen to be equivalent to the Hamiltonian given by Dennison.[4]

We shall now replace q_{21} and q_{22}, respectively, by $\rho_2\cos\chi_2$ and $\rho_2\sin\chi_2$ and p_{21} and p_{22}, respectively, by $(-i\hbar)[\cos\chi_2\partial/\partial\rho-(\sin\chi_2/\rho_2)\partial/\partial\chi_2]$ and $(-i\hbar)[\sin\chi_2\partial/\partial\rho_2+(\cos\chi_2/\rho_2)\partial/\partial\chi_2]$. According to Sayvetz the angle φ occurs only as a constant parameter and may therefore be replaced by some convenient arbitrary value. For φ we shall choose the value $\varphi=\pi/2$. The operators (3) will then simply become:

$$\begin{aligned}P_x&=(-i\hbar)\partial/\partial\theta,\\ P_y&=(-i\hbar)[(\sin\theta)^{-1}(\partial/\partial\psi-\cos\theta\partial/\partial\chi_2)],\\ P_z&=(-i\hbar)\partial/\partial\chi_2.\end{aligned} \tag{10}$$

When we make these substitutions in (9), remembering that

$$P_x^2=-\hbar^2\{(\sin\theta)^{-1}\partial/\partial\theta(\sin\theta)\partial/\partial\theta\}$$

we have the following:

$$H^0=(\hbar/2)\{\lambda_1^{\frac{1}{2}}(p_1^2/\hbar^2+q_1^2)+\lambda_2^{\frac{1}{2}}(p_{\rho_2}^2/\hbar^2-(i/\rho_2)(p_{\rho_2}/\hbar)+(1/\rho_2^2)p_{\chi_2}^2/\hbar^2+\rho_2^2)$$
$$+\lambda_3^{\frac{1}{2}}(p_3^2/\hbar^2+q_3^2)\}+(P_x'^2+P_y'^2)/2I_e, \tag{11-a}$$

$$H^{(1)}=(-i\hbar\lambda_1^{\frac{1}{2}}/I_e)p_1-(\hbar/I_e\lambda_1^{\frac{1}{2}})^{\frac{1}{2}}q_1(P_x'^2+P_y'^2)/I_e+(\lambda_2/\lambda_3)^{\frac{1}{2}}(q_3/\rho_2)P_y'p_{\chi_2}$$
$$-\{(\lambda_3/\lambda_2)^{\frac{1}{2}}\rho_2p_3-(\lambda_2/\lambda_3)^{\frac{1}{2}}q_3p_{\rho_2}\}P_x'+V_1, \tag{11-b}$$

$$H^{(2)}=(-i\hbar/I_e)q_1p_1+(3\hbar/2\lambda_1^{\frac{1}{2}})q_1^2(P_x'^2+P_y'^2)/I_e+2(\hbar^2/\lambda_1)^{\frac{1}{2}}(q_1/I_e^{\frac{1}{2}})\{[(\lambda_3/\lambda_2)^{\frac{1}{2}}\rho_2p_3$$
$$-(\lambda_2/\lambda_3)^{\frac{1}{2}}q_3p_{\rho_2}]P_x'-(\lambda_2/\lambda_3)^{\frac{1}{2}}(q_3/\rho_2)P_y'p_{\chi_2}\}+\{(\lambda_3/\lambda_2)^{\frac{1}{2}}\rho_2^2p_3^2-\rho_2p_{\rho_2}p_3q_3$$
$$-q_3p_3p_{\rho_2}\rho_2+(\lambda_2/\lambda_3)^{\frac{1}{2}}q_3^2p_{\rho_2}^2\}/2I_e+(\lambda_2/\lambda_3)^{\frac{1}{2}}(q_3/\rho_2)^2p_{\chi_2}^2/I_{zz}^{(e)}+V_2, \tag{11-c}$$

in which

$$(P_x'^2+P_y'^2)=(P_x^2+P_y^2)=-\hbar^2\{(\sin\theta)^{-1}\partial/\partial\theta(\sin\theta\,\partial/\partial\theta)+(\sin\theta)^{-1}(\partial/\partial\psi-\cos\theta\,\partial/\partial\chi_2)^2\},$$

[6] H. H. Nielsen, Phys. Rev. 60, 794 (1941).

and P_x', P_y', and P_z' are identical in form with the operators (3), φ having everywhere been replaced by χ_2. Equations (11-a, b, c) may be regarded as the quantum mechanical Hamiltonian for the linear triatomic molecule accurate to second order of approximation.

III. THE GENERAL XY_2 MOLECULE

In our discussion of the quantum mechanical Hamiltonian for the general XY_2 molecular model we shall follow, except for minor details, the work of Shaffer and Nielsen.[6] The base of the triangle will here be oriented so that it will be parallel to the body fixed z axis rather than the axis x. If we denote the particles of masses M, m, and m by the numbers 1, 2, and 3, respectively, their equilibrium positions in the body fixed coordinates will be:

$$x_1^0=x_2^0=x_3^0=0, \quad y_1^0=(\mu a/M)\cot\alpha, \quad y_2^0=y_3^0=(\mu a/2m)\cot\alpha, \quad z_1^0=0, \quad z_2^0=-z_3^0=a, \tag{12}$$

where μ is the reduced mass $2mM/(2m+M)$ and 2α is the vertex angle. In their work[6] they have used the perfectly general quadratic potential energy function:

$$V^0=(1/2)\{K_1(\delta s_2^2+\delta s_3^2)+K_2\delta s_1^2+K_3\delta s_1(\delta s_2+\delta s_3)+K_4\delta s_2\delta s_3\}, \tag{13}$$

in which the K_i are constants and the δs_i are the relative displacements of the particles j and k (i, j, and k taking the values 1, 2, and 3; $i\neq k$). Expressed in terms of the intermediate coordinates:

$$\begin{gathered} q_1'=(m/2)^{\frac{1}{2}}(\delta z_3-\delta z_2), \quad q_2'=\sqrt{\mu}[\delta y_1-(1/2)(\delta y_2+\delta y_3)], \\ q_3'=(\mu I_{zz}^{(e)}/I_{yy}^{(e)})^{\frac{1}{2}}(\delta z_1-(1/2)(\delta z_2+\delta z_3)), \end{gathered} \tag{14}$$

the function becomes:

$$V^0=(1/2)(k_1q_1'^2+k_2q_2'^2+k_3q_3'^2+2k_4q_1'q_2'), \tag{15}$$

in which:

$$\begin{aligned} k_1&=(2/m)\{(K_1/2)\sin^2\alpha+K_2+K_3\sin\alpha+(K_4/2)\sin^2\alpha\}, \\ k_2&=\mu^{-1}(2K_1+K_4)\cos^2\alpha, \\ k_3&=\mu^{-1}(2K_1-K_4)\cos^2\alpha, \\ k_4&=(1/2m\mu)^{\frac{1}{2}}(K_1+K_3/\sin\alpha+K_4/2)\sin\alpha\cos\alpha. \end{aligned} \tag{16}$$

Transformation to normal coordinates is effected by introducing for q_1' and q_2' the following linear combinations:

$$q_1'=q_1\cos\gamma-q_2\sin\gamma, \quad q_2'=q_1\sin\gamma+q_2\cos\gamma, \tag{17}$$

where

$$\begin{aligned} \sin\gamma&=(1/2)^{\frac{1}{2}}\{1-[(k_2-k_1)^2/(k_4^2+(k_2-k_1)^2)]^{\frac{1}{2}}\}^{\frac{1}{2}}, \\ \cos\gamma&=(1/2)^{\frac{1}{2}}\{1+[(k_2-k_1)^2/(k_4^2+(k_2-k_1)^2)]^{\frac{1}{2}}\}^{\frac{1}{2}}. \end{aligned} \tag{18}$$

The final form of the potential energy will then be:

$$V^0=2\pi^2c^2(\omega_1^2q_1^2+\omega_2^2q_2^2+\omega_3^2q_3^2), \tag{19}$$

where

$$\begin{aligned} \omega_1&=(1/2\pi c)\{k_1\cos^2\gamma+k_2\sin^2\gamma+k_4\sin\gamma\cos\gamma\}^{\frac{1}{2}}, \\ \omega_2&=(1/2\pi c)\{k_1\sin^2\gamma+k_2\cos^2\gamma-k_4\sin\gamma\cos\gamma\}^{\frac{1}{2}}, \\ \omega_3&=(1/2\pi c)k_3^{\frac{1}{2}}. \end{aligned} \tag{20}$$

The quantities $I'_{\alpha\beta}$ required to set up the quantum mechanical Hamiltonian have been determined by Shaffer and Nielsen. In our slightly different notation they will be:

$$\begin{aligned} I'_{zz}&=I_{zz}^{(e)}\{1+(2\xi_{32}/(I_{zz}^{(e)})^{\frac{1}{2}})q_1+(\xi_{32}^2/I_{zz}^{(e)})q_1^2+(2\xi_{31}/(I_{zz}^{(e)})^{\frac{1}{2}})q_2+(\xi_{31}^2/I_{zz}^{(e)})q_2^2\}, \\ I'_{yy}&=I_{yy}^{(e)}\{1+(2\cos\gamma/(I_{yy}^{(e)})^{\frac{1}{2}})q_1+(\cos^2\gamma/I_{yy}^{(e)})q_1^2+(q_3^2/I_{zz}^{(e)})-(2\sin\gamma/(I_{yy}^{(e)})^{\frac{1}{2}})q_2 \\ &\qquad +(\sin^2\gamma/I_{yy}^{(e)})q_2^2-(2\sin\gamma\cos\gamma/I_{yy}^{(e)})q_1q_2\}, \end{aligned}$$

[6] W. H. Shaffer and H. H. Nielsen, Phys. Rev. **56**, 188 (1939).

$$I'_{zz}=q_2^2\cos^2\gamma+q_1^2\sin^2\gamma+2q_1q_2\sin\gamma\cos\gamma+I_{zz}^{(e)}\{1+(2\sin\gamma/(I_{zz}^{(e)})^{\frac{1}{2}})q_1 +(2\cos\gamma/(I_{zz}^{(e)})^{\frac{1}{2}})q_2+(q_3^2/I_{zz}^{(e)})\}, \quad (21)$$

$$I'_{yz}=\{[(I_{yy}^{(e)}/I_{zz}^{(e)})^{\frac{1}{2}}\cos\gamma-(I_{zz}^{(e)}/I_{zz}^{(e)})^{\frac{1}{2}}\sin\gamma]q_2q_3+2(I_{zz}^{(e)}I_{yy}^{(e)}/I_{zz}^{(e)})^{\frac{1}{2}}q_3 +[(I_{yy}^{(e)}/I_{zz}^{(e)})^{\frac{1}{2}}\sin\gamma+(I_{zz}^{(e)}/I_{zz}^{(e)})^{\frac{1}{2}}\cos\gamma]q_1q_3\},$$

$$I'_{xy}=I'_{xz}\equiv 0, \quad \xi_{31}=[(I_{yy}^{(e)}/I_{zz}^{(e)})^{\frac{1}{2}}\sin\gamma-(I_{zz}^{(e)}/I_{zz}^{(e)})^{\frac{1}{2}}\cos\gamma], \quad \xi_{32}=[(I_{yy}^{(e)}/I_{zz}^{(e)})^{\frac{1}{2}}\cos\gamma+(I_{zz}^{(e)}/I_{zz}^{(e)})^{\frac{1}{2}}\sin\gamma]$$

and the anharmonic portions of the potential energy are the following:

$$V^{(1)}=hc\{k_{111}q_1^3+k_{222}q_2^3+k_{133}q_1q_3^2+k_{233}q_2q_3^2+k_{122}q_1q_2^2+k_{112}q_1^2q_2\},$$
$$V^{(2)}=hc\{k_{1111}q_1^4+k_{2222}q_2^4+k_{3333}q_3^4+k_{1133}q_1^2q_3^2+k_{2233}q_2^2q_3^2+k_{1122}q_1^2q_2^2+k_{1233}q_1q_2q_3^2\}. \quad (22)$$

With this information at hand the quantum mechanical Hamiltonian (1) is now formally determined. The resulting wave equation does not lend itself to an exact solution and Eq. (1) must be replaced by its expansion and a solution arrived at by successive approximations. Shaffer and Nielsen carried out their expansion on the hypothesis that the displacements of the particles from their positions of equilibrium are small compared to the equilibrium values of the coordinates themselves (i.e., $\delta x_i/x_i^0\ll 1$). This expansion yields expressions for H^0, $H^{(1)}$, and $H^{(2)}$ which are materially different from the relations (11) in Section II of this paper and is evidently not a suitable one. This becomes apparent when we stop to consider that in the case of a linear molecule $x_i^0=y_i^0=0$, but δx_i and δy_i may be different from zero. In this paper we shall want to consider an expansion appropriate for a non-linear triatomic molecule which is so nearly linear that we may consider $I_{zz}^{(e)}\ll\mu q_2^2$. Equation (1) may now be expanded much as before after the coordinates q_s have, for convenience, been replaced by $(h/4\pi^2c\omega_s)^{\frac{1}{2}}q_s$. Certain differences will be observed, however, peculiar to the frequency ω_2. For example, the quantity $\mu^{\frac{1}{2}}p_2\mu^{-\frac{1}{2}}p_2$ will contain a second *zero-order* term, $(-ihc\omega_2/q_2)(p_2/h)$, in addition to the usual term $hc\omega_2(p_2/h)^2$; the term h_z will contain a second *first-order* term, $(ih/2)(\omega_2/\omega_3)^{\frac{1}{2}}(q_3/q_2)$, in addition to the usual term $[(\omega_2/\omega_3)^{\frac{1}{2}}q_3p_2-(\omega_3/\omega_2)^{\frac{1}{2}}q_2p_3]$, and so on. When the expansion has been completed and the terms collected in orders of magnitude, one obtains:

$$H^0=(hc/2)\{\omega_1[(p_1/h)^2+q_1^2]+\omega_2[(p_2/h)^2-(i/q_2)(p_2/h)+(1/q_2)^2P_z^2/h^2+q_2^2] +\omega_3[(p_3/h)^2+q_3^2]\}+(P_x^2/2I_{xx}^{(e)})+(P_y^2/2I_{yy}^{(e)}), \quad (23\text{-a})$$

$$H^{(1)}=(1/2)\{-ih^{\frac{1}{2}}(2\pi c\omega_1)^{\frac{1}{2}}[(\cos\gamma/(I_{yy}^{(e)})^{\frac{1}{2}})+(\xi_{32}/(I_{zz}^{(e)})^{\frac{1}{2}}](p_1/h) -2(h/I_{zz}^{(e)3})^{\frac{1}{2}}(\xi_{32}q_1/(2\pi c\omega_1)^{\frac{1}{2}})P_x^2-2(h/I_{yy}^{(e)3})^{\frac{1}{2}}(\cos\gamma q_1/(2\pi c\omega_1)^{\frac{1}{2}})P_y^2 +(2\xi_{32}/I_{zz}^{(e)})([(\omega_2/\omega_3)^{\frac{1}{2}}q_3p_2-(\omega_3/\omega_2)^{\frac{1}{2}}q_2p_3]-(ih/2)(\omega_2/\omega_3)^{\frac{1}{2}}(q_3/q_2))P_x +(\omega_2/\omega_3)^{\frac{1}{2}}(q_3/q_2)(P_yP_z+P_zP_y)+\epsilon_1\}+V^{(1)}, \quad (23\text{-b})$$

$$H^{(2)}=(1/2)\{(-ih^2)[(\cos/(I_{yy}^{(e)})^{\frac{1}{2}})+(\xi_{32}/(I_{zz}^{(e)})^{\frac{1}{2}})]^2(q_1p_1/h)+(3\xi_{32}^2h/2\pi c\omega_1I_{zz}^{(e)})q_1^2P_x^2 +(3\cos^2\gamma h/2\pi c\omega_1I_{yy}^{(e)})q_1^2P_y^2+(\omega_2/\omega_3)(q_3/q_2)^2(P_z^2/I_{zz}^{(e)})+4(h/I_{zz}^{(e)3})^{\frac{1}{2}}(\xi_{32}q_1/(2\pi c\omega_1)^{\frac{1}{2}}) \times([(\omega_3/\omega_2)^{\frac{1}{2}}q_2p_3-(\omega_2/\omega_3)^{\frac{1}{2}}q_3p_2]-(ih/2)(\omega_2/\omega_3)^{\frac{1}{2}}(q_3/q_2))P_x -2(h/I_{yy}^{(e)3})^{\frac{1}{2}}(\omega_2/\omega_3)^{\frac{1}{2}}(q_3/q_2)(\cos\gamma q_1/(2\pi c\omega_1)^{\frac{1}{2}})(P_yP_z+P_zP_y) +(I_{zz}^{(e)})^{-1}(\xi_{32}[(\omega_2/\omega_3)q_3^2p_2^2-q_3p_3p_2q_2-q_2p_2p_3q_3+(\omega_3/\omega_2)q_2^2p_3^2])+\epsilon_2\}+V^{(2)}, \quad (23\text{-c})$$

in which

$$\epsilon_1=(1/2)\{[-ih^{\frac{1}{2}}\xi_{31}(2\pi c\omega_2)^{\frac{1}{2}}/(I_{zz}^{(e)})^{\frac{1}{2}}](p_2/h)-2(h/I_{zz}^{(e)3})[\xi_{31}q_2/(2\pi c\omega_2)^{\frac{1}{2}}]P_x^2 +(2\xi_{31}/I_{zz}^{(e)})[(\omega_1/\omega_3)^{\frac{1}{2}}q_3p_1-(\omega_3/\omega_1)^{\frac{1}{2}}q_1p_3)]P_x \quad (24)$$

and

$$\epsilon_2=(1/2)\{-i\hbar^2(-(\xi_{31}^2/I_{xx}^{(e)})(q_2p_2/\hbar)-[(I_{zz}^{(e)})^{\frac{1}{2}}\sin\gamma/I_{zz}^{(e)}I_{yy}^{(e)}]$$
$$\times[(I_{yy}^{(e)})^{\frac{1}{2}}\cos\gamma-(I_{zz}^{(e)})^{\frac{1}{2}}\sin\gamma](q_3p_3/\hbar))+(3\xi_{31}^2\hbar/2\pi c\omega_2 I_{xx}^{(e)})q_2^2P_z^2$$
$$+[3\hbar(I_{zz}^{(e)})\sin\gamma/2\pi c\omega_3 I_{xx}^{(e)}I_{yy}^{(e)}][(I_{zz}^{(e)})^{\frac{1}{2}}\sin\gamma-(I_{yy}^{(e)})^{\frac{1}{2}}\cos\gamma]q_3^2P_y^2+((2\pi c\omega_2/\hbar)\sin^2\gamma$$
$$+[(I_{zz}^{(e)}/I_{yy}^{(e)})\sin^2\gamma-(I_{zz}^{(e)}/I_{yy}^{(e)})^{\frac{1}{2}}\sin\gamma\cos\gamma](\hbar/2\pi c\omega_3 I_{xx}^{(e)})q_3^2)(1/q_2)^2P_z^2$$
$$+(I_{xx}^{(e)})^{-1}(\xi_{31}[(\omega_1/\omega_3)q_3^2p_1^2-q_3p_3p_1q_1-q_1p_1p_3q_3+(\omega_3/\omega_1)q_1^2p_3^2])\}. \quad (25)$$

We have now only to compare the relations (23) to (25) as the molecule straightens out with the relations (11) for the linear molecule. First, the function (15) for V^0 will go over into the relation V^0 in (11-a), i.e., k_4 goes to zero. This is obvious except for the term $K_3\cos\alpha$ which, however, has no meaning for a linear molecule, i.e., K_3 must be equal to zero. Evidently then $\sin\gamma\to 0$ and $\cos\gamma\to 1$. Moreover, symmetry conditions demand that the coefficients k_{222}, k_{233}, k_{112}, and k_{1233} must vanish. As a consequence of the foregoing ξ_{31}, ϵ_1, ϵ_2, and $I_{zz}^{(e)}$ all approach zero while ξ_{32} will approach unity and $I_{yy}^{(e)}\to I_{xx}^{(e)}$. Comparison now shows that the two sets of relations (11) and (23) are alike in form except for the terms $(p_zP_z/I_{xx}^{(e)})$ and $(q_3/q_2)(P_yP_z+P_zP_y)$.

The commutation relations for the rotator have been investigated by Klein[7] who has found that:

$$P_\alpha P_\beta-P_\beta P_\alpha=-i\hbar P_\gamma, \quad (26)$$

where α, β, and γ take the values x, y, and z in cyclic rotation ($\alpha\neq\beta\neq\gamma$). With the aid of the commutation relations (26) the term $(\omega_2/\omega_3)^{\frac{1}{2}}(q_3/q_2)(P_yP_z+P_zP_y)/I_{xx}^{(e)}$ may be written as $2(\omega_2/\omega_3)^{\frac{1}{2}}\times(q_3/q_2)(P_yP_z+(i\hbar/2)P_z)/I_{xx}^{(e)}$. The last component of the foregoing term will just cancel a similar term in $(p_zP_z/I_{xx}^{(e)})$. The agreement is now complete except, of course, the angle φ and the operator P_z occur everywhere in our case instead of χ_2 and $p\chi_2$, respectively, in the former case. Thus we have demonstrated that the quantum mechanical Hamiltonian for the non-linear triatomic molecule derived by the usual Wilson-Howard way will asymptotically assume the same form exactly as the quantum mechanical Hamiltonian for the linear triatomic molecule derived using the Sayvetz modification. In the Sayvetz modification the Eulerian angle φ occurs as an arbitrary constant. In our example the angle χ occurs as an arbitrary constant, namely, $\chi=0$. The above discussion could, of course, as readily be applied to a general non-linear molecule as to the non-linear XY_2 molecule.

[7] O. Klein, Zeits. f. Physik **58**, 730 (1929).

Letters to the Editor

PROMPT publication of brief reports of important discoveries in physics may be secured by addressing them to this department. The closing date for this department is the third of the month. Because of the late closing date for the section no proof can be shown to authors. The Board of Editors does not hold itself responsible for the opinions expressed by the correspondents. Communications should not in general exceed 600 words in length.

High Energy Gamma-Ray from Radio-Yttrium (100d)

G. R. GAMERTSFELDER*
Department of Physics, University of Illinois, Urbana, Illinois
September 18, 1944

BOMBARDMENT of strontium by either protons or deuterons produces a radioactive yttrium isotope of about 100 days half-life time. An yttrium source of several millicuries intensity produced by deuteron bombardment in the 60-inch cyclotron in Berkeley, and chemically separated from the strontium target,[1] was available for experiments here. The gamma-rays of this isotope, which decays by K-electron capture, have been investigated previously by various methods. Detecting the recoil protons produced by photo-neutrons from RdY+Be, Scharff-Goldhaber[2] obtained a value of 1.87 Mev for the energy of the intense hard gamma-ray component. Richardson,[3] measuring the momentum distribution of secondary electrons ejected from a thin radiator in a cloud chamber, found the spectrum to consist of two lines of energies 1.92 and 0.95 Mev, the intensities being approximately equal. Downing, Deutsch, and Roberts,[4] using a magnetic lens spectrometer, found 1.89 and 0.908 Mev for the energies of the gamma-rays and also established coincidences between them, indicating that the gamma-rays are emitted from an excited state of about 2.8 Mev in cascade. It seemed worth while, therefore, to make a search for a high energy gamma-ray which would correspond to the apparently highly forbidden transition from the 2.8-Mev state to the ground state.[5] If this 2.8-Mev gamma-ray were emitted, one should be able to produce with a RdY source photo-neutrons in deuterium (threshold = 2.17 Mev).

To study this question the RdY source was placed either within a toroidal soft glass vessel containing D_2O, or within a similarly shaped Be block, submersed in the center of a large water tank. Neutrons were detected with a boron-lined ionization chamber at a distance of 4 cm from the source. The background count of the ionization chamber was 0.3 count/min. With RdY+D_2O, $N^D = 1.3$ counts/min. (above background) were recorded, and with RdY+Be, $N^{Be} = 240$ counts/min., indicating that a high energy γ-ray, presumably of 2.8 Mev, is indeed emitted by the RdY. The experiment was repeated after an interval of five months (1.5 half-life times of RdY) and essentially the same ratio of counts was obtained, thus making it appear improbable that the high energy γ-ray was caused by an impurity. The intensity of the RdY+D_2O photo-neutrons was unfortunately too small to allow a determination of their energy.

It is of interest to know the relative probability p of emission of the 2.8-Mev and 1.9-Mev γ-rays in the decay of RdY. To estimate this quantity the following procedure was adopted. The relative yield (η) of photo-neutrons from the D_2O vessel and the Be block used was measured for the γ-rays of RdTh of 2.62-Mev energy. The result was $\eta_{2.6} = 1.5$. Here and in the following, the subscript refers to the γ-ray energy in Mev. If ϵ is the relative efficiency with which neutrons from RdY+D (which should have an energy of $\sim$300 kev) and RdY+Be ($\sim$220 kev)[3] were detected in the arrangement described, and σ^D and σ^{Be} the cross sections for photo-disintegration of the D and Be nucleus, respectively, we can write

$$p = \frac{N^D}{N^{Be}} \frac{1}{\epsilon} \frac{1}{\eta_{2.6}} \frac{\sigma^D_{2.6}}{\sigma^D_{2.6}} \frac{\sigma^{Be}_{1.9}}{\sigma^{Be}_{2.6}}.$$

This expression neglects the absorption of the γ-rays in the D_2O and Be, and the relative contribution of the 2.8-Mev γ-ray as compared to the 1.9-Mev γ-ray to the neutron yield from RdY+Be. ϵ was estimated empirically to be about 8/9. From the theory of the photo-disintegration of the deuteron,[6] one can calculate $\sigma^D_{2.6}/\sigma^D_{2.6} = 0.8$. The least known of the quantities involved is the ratio $\sigma^{Be}_{1.9}/\sigma^{Be}_{2.6}$. Though there is some experimental and theoretical[7] evidence which indicates that the Be photo-cross section decreases with increasing γ-ray energy in the region which is of interest here, the exact value of the ratio $\sigma^{Be}_{1.9}/\sigma^{Be}_{2.6}$ is not known. If it is assumed to be 3 ± 1, one obtains $p = 0.01 \pm 0.005$.

* Now at Radiation Laboratory, Massachusetts Institute of Technology, Cambridge, Massachusetts.
[1] C. Pecher, Phys. Rev. 58, 843 (1940).
[2] G. Scharff-Goldhaber, Phys. Rev. 59, 937A (1941).
[3] J. R. Richardson, Phys. Rev. 60, 188 (1941).
[4] J. R. Downing, M. Deutsch, and A. Roberts, Phys. Rev. 60, 470 (1941).
[5] G. R. Gamertsfelder, Phys. Rev. 63, 60A (1943).
[6] H. A. Bethe and R. F. Bacher, Rev. Mod. Phys. 8, 122 (1936).
[7] V. I. Mamasachlisow, Physik. Zeits. Sowjetunion 10, 214 (1936).

The Effect of Order-Disorder on the Thermoelectric Properties of Ni_3Mn

R. I. JAFFEE
Department of Mining and Metallurgy, University of California, Berkeley, California
August 24, 1944

FROM measurements of physical properties it has been concluded that Ni_3Mn (23.78 weight percent Mn) undergoes an order-disorder transformation at about 500°C.[1] The ordered structure obtained by annealing below 500°C or by cooling through the transformation range very slowly is ferromagnetic with a Curie point at about 450°C. This present work reports the difference in the thermoelectric properties of the disordered and the well-ordered states at temperatures from 300°C to 530°C.

Some thermoelectric work was done previously by Kaya and Nakayama[2] who annealed Ni_2Mn at various temperatures, quenched to preserve the high temperature condition, and measured the thermoelectric force between 0°C and 100°C of a couple made up of the annealed alloy and a specimen of disordered alloy (as could be obtained by quenching from 700–800°C). They found measurable e.m.f.'s set up by the couple when the specimen had been annealed below about 600°C. The thermoelectric force leveled off at about 500°C, reaching a value of about 0.7 millivolt. Their data showed considerable scatter and no particular critical points could be detected below 600°C.

The specimen of Ni_2Mn used in the present work was a length of 22-gauge nickel-manganese wire prepared at the Salt Lake City station of the Bureau of Mines from a 7-inch length of swaged rod by alternate cold drawing and annealing at 900°C. The chemical analysis of the original rod was 23.2 percent Mn and 76.9 percent Ni. The wire, in the non-magnetic disordered condition, was brazed to the junction of a National Bureau of Standards standard Chromel-Alumel thermocouple, whose calibration against Pt(27) was known.

This thermal junction was heated in air to 540°C at a rate of about 2°C per minute, and then cooled very slowly at about 1°C per hour, and the thermoelectric data between 0°C and T were obtained. It took 168 hours to cool from 532°C to 300°C, which is an average rate of 1.38°C per hour. The thermal e.m.f.'s during heating were measured with two portable potentiometers and during cooling with a type K potentiometer.

The thermoelectric force against National Bureau of Standards standard platinum, Pt(27), is shown in Fig. 1, and the derived thermoelectric power data are also plotted in Fig. 1. The heating curve of the disordered alloy is quite straight, with an average thermoelectric power of 0.0125 millivolt per degree C. It is possible, however, that some ordering of the originally disordered alloy took place during heating to 530°C. The cooling data coincided with the heating data down to 490°C where they diverged gradually, apparently because of the onset of ordering.

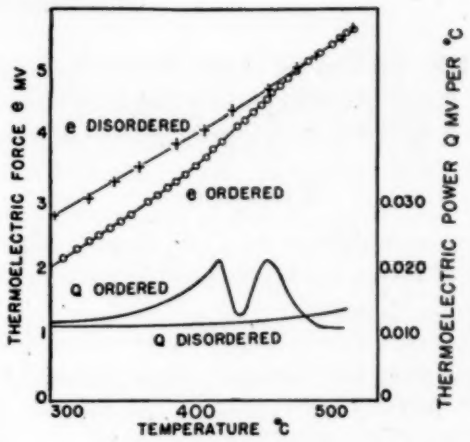

FIG. 1. Thermoelectric properties of Ni_2Mn against platinum in the disordered and ordered states.

There appears to be a slight discontinuity in the cooling curve at 430–440°C; this may be an effect at the Curie point, which from magnetic measurements was found to occur at about this temperature. The two curves have about the same thermoelectric power at lower temperatures, but with 0.7 millivolt between the thermoelectric force curves.

This work was part of a research carried out at the Bureau of Mines Eastern Experiment Station, College Park, Maryland, under a University of Maryland research fellowship.

[1] S. Kaya and A. Kussmann, Zeits. f. Physik 72, 293–309 (1931); N. Thompson, Proc. Phys. Soc. London 52, 217–228 (1940).
[2] S. Kaya and H. Nakayama, Proc. Phys. Math. Soc. Japan 22, 126–141 (1940).

Information For Contributors

THE Editors of THE PHYSICAL REVIEW would be aided in their task if the following items were used as a guide by all contributors.

MANUSCRIPTS

Send manuscripts to J. W. Buchta, Department of Physics, University of Minnesota, Minneapolis, Minnesota.

Papers must be in English, typewritten double-spaced with wide margins on a durable white paper, preferably lettersize. The original copy, not the carbon, should be submitted.

For general style, spellings, abbreviations, and form, recent issues of this journal should be consulted.

ABSTRACTS

An abstract must accompany each article. It should be adequate as an *index* and as a *summary*. As an index it should give all subjects, major and minor, concerning which new information is presented. As a summary it should give the conclusions of the article and all numerical results of general interest.

MATHEMATICAL EXPRESSIONS

Make all expressions clear to the typesetter. Identify in the margin of the manuscript Greek letters and unusual symbols.

Use fractional exponents instead of root signs.

Avoid complicated exponents and subscripts. Should it be necessary to repeat a complicated expression a number of times it should be represented by some convenient symbol.

The solidus (/) should be used wherever possible for fractions.

REFERENCES

References should appear as footnotes, numbered consecutively, and arranged thus:

[1] A. B. Smith, Phys. Rev. 41, 852 (1932).
[2] G. R. Harrison, *Atoms in Action* (William Morrow & Company, New York, 1939), first edition, p. 30.

FIGURES AND TABLES

Legends for figures must accompany manuscript. Each table should have a caption. These in all cases should be complete in themselves so as to make the data intelligible to the reader without reference to the text. Each figure and table should be cited in sequence in the text.

LINE DRAWINGS AND PHOTOGRAPHS

Plan figures for reduction to one-third or one-fourth the original size. Wherever possible arrange figures so that after reduction they will not be wider than three inches. Lettering must be large enough to be readable (about 3 mm high) after reduction. The figures should be so arranged that the space is used efficiently.

Line drawings must be made with India ink on white paper or tracing cloth. Coordinate paper is not desirable, but if used must be blue-lined and all coordinates to be reproduced drawn with India ink.

Drawings which cannot be used will be returned to the author.

Photographs of drawings seldom are satisfactory. They often do not show clear black and white contrasts and are not suitable for relettering which is sometimes necessary. Photographs of apparatus seldom give as much information as drawings.

Please avoid round or oval photographs.

ALTERATIONS

Take great care that each manuscript is typographically accurate. A limited number of alterations in proof are unavoidable, but the cost of making extensive alterations after the article has been set in type will be charged to the author.

Proof and all correspondence concerning papers in the process of publication should be addressed to the Publications Manager, American Institute of Physics, 57 East 55 Street, New York 22, New York.